

Diol Oxidation to Diacids over Supported Metal Catalysts

---

A Dissertation

Presented to  
the faculty of the School of Engineering and Applied Science  
University of Virginia

---

in partial fulfillment  
of the requirements for the degree

Doctor of Philosophy

by

Matthew Ide

December

2013

APPROVAL SHEET

The dissertation  
is submitted in partial fulfillment of the requirements  
for the degree of  
Doctor of Philosophy

  
AUTHOR

The dissertation has been read and approved by the examining committee:

Robert J. Davis

---

Advisor

Roseanne Ford

---

Ian Harrison

---

Matthew Neurock

---

John O'Connell

---

Accepted for the School of Engineering and Applied Science:



Dean, School of Engineering and Applied Science

December  
2013

## Abstract

Oxidation is a key reaction in organic synthesis and will likely play a significant role in the development of value-added chemicals from biomass. The application of heterogeneous catalysis and molecular oxygen to oxidation reactions offers a green alternative to traditional, toxic chemical oxidants. An example of a biorenewable substrate that can be derived from fructose is 1,6-hexanediol. Adipic acid can be produced by the selective oxidation of 1,6-hexanediol and is a monomer for the production of nylon-6,6, which is a widely used polymer in the textiles, plastics, and automotive industries. The current production of adipic acid from fossil resources contributes considerably to greenhouse gas emissions. Thus, the production of adipic acid from biorenewable feedstocks with an environmentally friendly chemistry is an attractive target. In addition, so-called green oxidation could be applied to many other multi-functional alcohols whose acid products are valuable chemicals.

In this work, the selective catalytic oxidation of a variety of terminal alcohols was performed over Pt/C with 10 bar dioxygen at 343 K in aqueous solvent at low pH. The influences of Pt particle size, carbon support, alcohol structure, and start-up conditions were explored. Although the turnover frequency was not affected by particle size or the carbon support, the structure of the alcohols affected their initial rate of conversion. Both the rate of oxidation of  $\alpha,\omega$ -diols and selectivity of the diols to the diacids increased with increasing carbon chain length. Although the rate of 1,6-hexanediol oxidation was independent of dioxygen pressure, the order of reaction with respect to diol concentration depended on the start-up conditions. A kinetic model involving two types of metal sites was proposed to account for the experimental observations. The mechanism of alcohol oxidation over supported metal catalysts was discussed in light of these new results and prior published works.

The oxidation of alcohols with O<sub>2</sub> at 343 K over Pt was explored to determine the origin of catalyst deactivation. The catalyst deactivation was observed during the oxidation of a variety of terminal alcohols over platinum supported on C, BN, SiO<sub>2</sub>, TiO<sub>2</sub>, and Al<sub>2</sub>O<sub>3</sub>. A decrease in TOF for 1,6-hexanediol oxidation after the exposure of Pt/C to dioxygen was easily reversed by reduction with the alcohol substrate. However, Pt that had been deactivated during alcohol oxidation could not be regenerated in a similar manner, suggesting that over-oxidation of Pt was not the cause of deactivation. The sintering of Pt nanoparticles, dissolution of Pt, and strong adsorption of chelating species also did not contribute significantly to the observed deactivation. In-situ ATR-IR spectroscopy of the Pt surface determined that CO was produced before alcohol oxidation, but was easily oxidized by O<sub>2</sub> to CO<sub>2</sub>. A strongly adsorbed species was observed during a temperature programmed desorption reaction experiment on a recycled Pt/BN catalyst recovered after ethanol oxidation.

Bimetallic Pt and Au nanoparticles were prepared by sol-immobilization synthesis and subsequently supported on carbon, titania, and silica prior to evaluation in the aqueous oxidation of 1,6-hexanediol with 10 bar O<sub>2</sub> at 343 K and a low pH. The removal of the polymer stabilizer (polyvinyl alcohol) increased the TOF of 1,6-hexanediol oxidation. Although the initial TOF of 1,6-hexanediol oxidation over the monometallic Pt/C was 0.20 s<sup>-1</sup>, the initial TOF over the bimetallic AuPt/C catalyst was substantially greater at 0.68 s<sup>-1</sup>. Interestingly, a Au/C catalyst was inert at these reaction conditions. The bimetallic AuPt/C catalyst was characterized by hydrogen chemisorption, XRD, and TEM with EDS. The EDS of single nanoparticles indicated that they contained both Au and Pt. The AuPt/TiO<sub>2</sub> and AuPt/SiO<sub>2</sub> catalysts had significantly lower TOF's than AuPt/C.

## Acknowledgements

I thank my advisor, Robert J. Davis, for his guidance and insight during my studies at the University of Virginia. I thank all of the present and past Davis group members whose interactions were invaluable. A special thanks to: Yuanzhou Xi, Bhushan Zope, Joseph Kozlowski, Sara Davis, Juan Ruiz-Lopez, Derek Falcone, Sabra Hanspal, Kehua Yin, and Ben Huang. I would also like to thank Professor Matthew Neurock and his research group for many helpful discussions, in particular: Bing Hao, David Hibbits, and Eric Dybeck. Thanks also goes to the staff of the Chemical Engineering Department: Ricky Buchanan, Vickie Faulconer, and Teresa Morris.

I gratefully acknowledge funding support from the National Science Foundation under Award Nos. EEC-0813570 and OISE 0730277. A big thank you to the Center for Biorenewable Chemicals and all of the wonderful people I met through both CBiRC and the SLC, in particular: Chris Leber, Shivani Garg, Javier Cardenas, Mike Nolan, Liam Royce, Peter Keeling, Brent Shenks, Raj Raman, and Marna Nelson.

Loving thanks to my family and friends for their support to pursue my graduate studies.

## Table of Contents

<b>Chapter 1: Introduction .....</b>	<b>1</b>
Biorenewable Chemical Production from Biomass .....	1
Polyol Oxidation over Pt.....	4
Glucose Oxidation over Pt.....	7
Diol Oxidation over Pt, Pd, and Au .....	7
Alcohol Oxidation Mechanism .....	10
Focus of this work.....	12
References.....	13
<b>Chapter 2: Aqueous Alcohol Oxidation over Supported Pt, Pd, and Au Catalysts.....</b>	<b>17</b>
Introduction.....	17
Experimental Methods .....	19
Catalyst preparation .....	19
Catalyst characterization.....	20
Alcohol oxidation.....	21
Results and Discussion .....	22
Catalyst characterization.....	22
Alcohol oxidation at low pH.....	24
Diol oxidation at acidic and basic conditions over Pt, Pd, and Au.....	29
Effect of carbon support and Pt particle size .....	31
Effect of alcohol structure on the oxidation rate over Pt .....	32
Conclusions.....	37
Acknowledgements.....	38
References.....	38
<b>Chapter 3: Kinetics and Mechanism of Aqueous Alcohol Oxidation over Supported Pt at Acidic Conditions .....</b>	<b>41</b>
Introduction.....	41
Experimental Methods .....	44
Catalyst preparation .....	44
Catalyst characterization.....	44
Alcohol oxidation.....	44

Results and Discussion .....	46
Kinetics of alcohol oxidation to an aldehyde over Pt at acidic conditions .....	46
Influence of reactor startup conditions .....	49
Proposed kinetic model and kinetic isotope effect .....	52
Rate equation after inert startup conditions .....	56
Rate equation after oxidative startup conditions.....	57
Conclusions.....	58
Acknowledgements.....	58
References.....	58
<b>Chapter 4: Deactivation of Supported Pt Catalysts during Alcohol Oxidation.....</b>	<b>62</b>
Introduction.....	62
Experimental Methods .....	64
Catalyst preparation .....	64
Catalyst characterization.....	64
Alcohol oxidation.....	65
Results and Discussion .....	67
Catalyst characterization.....	67
Deactivation of Pt during alcohol oxidation .....	68
Investigation of leaching and sintering .....	71
Effect of startup conditions.....	73
Influence of chemical additives .....	75
Detection of byproducts in the gas phase .....	78
Conclusions.....	81
Acknowledgements.....	81
References.....	81
<b>Chapter 5: In-situ ATR-IR Spectroscopy on Pt.....</b>	<b>86</b>
Introduction.....	86
Experimental Methods .....	88
In-situ ATR-IR spectroscopy .....	88
TGA-MS .....	89
Results and Discussion .....	90

Catalyst stability.....	90
Benzyl alcohol oxidation .....	92
Ethanol oxidation .....	95
TGA-MS of ethanol oxidation over Pt/BN.....	99
Conclusions.....	101
Acknowledgements.....	102
References.....	102
<b>Chapter 6: Bimetallic Nanoparticles for Alcohol Oxidation.....</b>	<b>104</b>
Introduction.....	104
Experimental Methods .....	106
Catalyst preparation .....	106
Catalyst characterization.....	107
Alcohol oxidation.....	108
Results and Discussion .....	110
Catalyst characterization.....	110
Alcohol oxidation.....	116
Conclusions.....	122
Acknowledgements.....	123
References.....	123
<b>Chapter 7: Concluding Remarks.....</b>	<b>126</b>
Conclusions.....	126
Future Direction .....	129
Bimetallic catalyst synthesis .....	129
Influence of solvent on alcohol oxidation rate.....	130
Oxidation of 1,6-hexanediol in a continuous flow reactor .....	130
<b>Appendix A: HPLC Analysis.....</b>	<b>132</b>
Sample Chromatograms.....	132
Sample Calibrations .....	133
<b>Appendix B: Rate Equation Derivation.....</b>	<b>134</b>
Inert startup .....	134
Oxidative startup.....	135



<b>Appendix C: Promotional Effect of Water on Liquid Phase Alcohol Dehydrogenation ...</b>	<b>136</b>
Literature Review.....	136
References.....	138
<b>Appendix D: The Important Role of Hydroxyl on Oxidation Catalysis by Gold .....</b>	<b>140</b>
Introduction.....	140
Catalysis by gold and oxidation activity.....	142
Mechanism of selective oxidation over gold catalysts .....	147
Analogy to electrochemistry.....	153
Conclusions and outlook.....	155
Acknowledgements.....	156
References.....	156
<b>Appendix E: Effect of Oxygen Pressure .....</b>	<b>160</b>
TOF of 1,6-Hexanediol at Low Oxygen Pressure .....	160

## List of Figures

<b>Figure 1.1.</b> The CBiRC strategy for the production of bio-renewable chemicals from biomass...	3
<b>Figure 1.2.</b> Commonly observed glycerol oxidation products.....	4
<b>Figure 1.3.</b> Summary of literature trends for the oxidation of 1,2-ethanediol.....	9
<b>Figure 1.4.</b> The general scheme for primary alcohol oxidation to an aldehyde.....	11
<b>Figure 1.5.</b> The general scheme for aldehyde oxidation to an acid.....	12
<b>Figure 2.1.</b> Reaction pathway for the biorenewable production of adipic acid.....	18
<b>Figure 2.2.</b> Bright field and corresponding dark field TEM image of 2.69% Pt/C catalyst reduced at 473 K.....	23
<b>Figure 2.3.</b> High angle annular dark-field TEM image of 2.69% Pt/C catalyst.....	24
<b>Figure 2.4.</b> Influence of acetic acid on the initial turnover frequency (TOF) of 1,6-hexanediol oxidation and initial pH of solution over 2.69% Pt/C with 0.1 M 1,6-hexanediol at 343 K and 10 bar O <sub>2</sub> .....	27
<b>Figure 2.5.</b> The general reaction path for the sequential oxidation of an $\alpha,\omega$ -diol. The oxidation of the diol first produces an aldehyde-alcohol (ALD) and then an $\omega$ -hydroxy acid (HA). Further oxidation of the $\omega$ -hydroxy acid (HA) generates an acid-aldehyde (AA) and then the final oxidation product, a diacid (DA).....	28
<b>Figure 2.6.</b> Reaction profile for 1,6-hexanediol oxidation with 10 bar dioxygen at 343 K over 2.69% Pt/C. The solid line is the conversion of 1,6-hexanediol. The dotted lines are the product selectivities of 6-hydroxyhexanal (ALD), 6-hydroxyhexanoic acid (HA), 6-oxohexanoic acid (AA), and adipic acid (DA).....	29
<b>Figure 2.7.</b> Product selectivities from the oxidation of various $\alpha,\omega$ -diols at approximately 90% conversion over 2.69% Pt/C at 343 K, 10 bar O <sub>2</sub> , 0.1 M substrate, and 100:1 substrate:Pt (mol:mol), 0.35 M acetic acid. All carbon balances were greater than 85%.....	34
<b>Figure 3.1.</b> Influence of dioxygen pressure on the turnover frequency of 1,6-hexanediol (HDO) and ethanol (EtOH) oxidation after inert startup over 2.69% Pt/C from 303 to 343 K at 0.1 M 1,6-hexanediol, 1,6-hexanediol:Pt = 500:1 (mol:mol), 0.35 M acetic acid, pH = 2.5.....	47
<b>Figure 3.2.</b> Influence of substrate concentration on the turnover frequency for 1,6-hexanediol (HDO), 1,3-propanediol (PDO), and ethanol (EtOH) oxidation after inert startup over 2.69% Pt/C from 303 to 343 K at pO <sub>2</sub> = 10 bar, 0.35 M acetic acid, pH = 2.5.....	48

- Figure 3.3.** Arrhenius-type plot from oxidation of 1,6-hexanediol, 1,3-propanediol, and 6-hydroxyhexanoic acid after inert startup over 2.69% Pt/C at 0.1 M substrate, substrate:Pt = 500:1 (mol:mol),  $pO_2 = 10$  bar, 0.35 M acetic acid, pH = 2.5. .... 49
- Figure 3.4.** Influence of substrate concentration on turnover frequency for 1,6-hexanediol oxidation over 2.69% Pt/C after inert or oxidative startup conditions at  $pO_2 = 10$  bar,  $T = 343$  K, pH = 2.5. .... 50
- Figure 3.5.** Influence of dioxygen pressure on the turnover frequency of 1,6-hexanediol (HDO) and ethanol (EtOH) oxidation after oxidative startup over 2.69% Pt/C for 343 K at 0.1 M 1,6-hexanediol, 1,6-hexanediol:Pt = 500:1 (mol:mol), 0.35 M acetic acid, pH = 2.5. .... 51
- Figure 3.6.** Influence of substrate concentration on the turnover frequency for 1,6-hexanediol oxidation after oxidative startup over 2.69% Pt/C from 303 K to 343 K at  $pO_2 = 10$  bar, pH = 2.5. .... 52
- Figure 4.1.** Comparison of (a) fresh and (b) deactivated 2.69% Pt/C catalyst with bright field TEM images. .... 68
- Figure 4.2.** Reaction profile of benzyl alcohol, 1,6-hexanediol, ethanol, 1,2-ethanediol, and 1,3-propanediol oxidation over 2.69% Pt/C with 0.1 M substrate, substrate:Pt = 500:1 (mol:mol), and 0.35 M acetic acid at 10 bar  $O_2$  and 343 K. .... 69
- Figure 4.3.** Reaction profile of 1,6-hexanediol oxidation over Pt/ $Al_2O_3$ , Pt/BN, Pt/C, Pt/ $TiO_2$ , and Pt/ $SiO_2$  with 0.1 M 1,6-hexanediol, 1,6-hexanediol:Pt = 500:1 (mol:mol), and 0.35 M acetic acid at 10 bar  $O_2$  and 343 K. .... 70
- Figure 5.1.** Attenuated total reflectance IR spectroscopy of a thin catalyst layer on an internal reflectance element crystal. Modified and reprinted from reference [8]. .... 87
- Figure 5.2.** In-situ ATR-IR spectroscopy of a catalyst film on an IRE. The penetration depth (dp) probes the surface of the IRE. Modified and reprinted from reference [3]. .... 88
- Figure 5.3.** ATR-IR spectra of silica dip coated onto the IRE and after treatment with  $N_2$  gas, liquid  $H_2O/N_2$ , still  $H_2O$ , and benzyl alcohol oxidation. .... 91
- Figure 5.4.** In-situ ATR-IR spectra of aqueous benzyl alcohol (a) saturated with  $N_2$  flowing over Pt/ $SiO_2$  and the production of CO adsorbed on Pt (b) over 20 min at 5 bar and 298 K. The water background has been removed. .... 93
- Figure 5.5.** In-situ ATR-IR spectra of the disappearance of benzyl alcohol (a) with  $H_2O$  saturated  $N_2$  flowing over Pt/ $SiO_2$  and the strong adsorption of CO on Pt (b) over 45 min at 5 bar and 298 K. The water background has been removed. .... 94
- Figure 5.6.** In-situ ATR-IR spectra of the rapid disappearance of CO after flowing  $H_2O$  saturated  $O_2$  flowing over Pt/ $SiO_2$  at 5 bar and 298 K. The water background has been removed. .... 94

- Figure 5.7.** In-situ ATR-IR spectra of aqueous benzyl alcohol (a) saturated with O<sub>2</sub> flowing over Pt/SiO<sub>2</sub> and the lack of CO (b) over 45 min at 5 bar and 298 K. The water background has been removed..... 95
- Figure 5.8.** In-situ ATR-IR spectra of aqueous ethanol (a) saturated with N<sub>2</sub> flowing over Pt/BN and the production of CO adsorbed on Pt (b) over 20 min at 5 bar and 298 K. The water background has been removed..... 96
- Figure 5.9.** In-situ ATR-IR spectra of the disappearance of ethanol (a) with H<sub>2</sub>O saturated N<sub>2</sub> flowing over Pt/BN and the strong adsorption of CO on Pt (b) over 45 min at 5 bar and 298 K. 97
- Figure 5.10.** In-situ ATR-IR spectra of the disappearance of CO after flowing H<sub>2</sub>O saturated with air flowing over Pt/BN for 10 min at 5 bar and 298 K. The water background has been removed..... 97
- Figure 5.11.** In-situ ATR-IR spectra of the negative peaks observed after flowing H<sub>2</sub>O saturated with H<sub>2</sub> flowing over Pt/BN for 360 min at 5 bar and 298 K. Spectra obtained at 5, 15, 30, 60, 180, and 360 min. The water background has been removed..... 98
- Figure 5.12.** TGA profile of weight loss (%) and derivative of weight loss (%/°C) of Pt/BN after ethanol oxidation for 24 h. .... 99
- Figure 5.13.** Mass spectrum corresponding to TGA profile of m/z = 14 and 16 after Pt/BN ethanol oxidation for 24 h. .... 101
- Figure 6.1.** TEM dark field images of 1.1% PtAu/C. .... 112
- Figure 6.2.** TEM dark field image (a) and corresponding energy dispersive X-ray spectroscopy (EDS) (b) of a single nanoparticle for the fresh 1.1% PtAu/C catalyst. The orange box identifies the area probed by EDS. .... 113
- Figure 6.3.** TEM dark field image (a) and corresponding energy dispersive X-ray spectroscopy (b) of approximately one hundred particles for the used 1.1% PtAu/C catalyst..... 114
- Figure 6.4.** XRD patterns of Pt/C, Au/C, and PtAu/C Catalysts. The dashed lines represent the (111) faces of the monometallic and bimetallic nanoparticles. .... 115
- Figure 6.5.** Influence of acetic acid on the initial turnover frequency (TOF) of 1,6-hexanediol oxidation over 1.1% Pt-Au/C with 0.1 M 1,6-hexanediol at 343 K and 10 bar O<sub>2</sub>. .... 120
- Figure 6.6.** Reaction profile for the oxidation of 1,6-hexanediol over Pt/C and Pt-Au/C. Reaction conditions: 0.1 M 1,6-hexanediol (HDO), HDO.:Met. ~ 500, pO<sub>2</sub> = 10 bar, T = 343 K, 0.35 M Acetic Acid, pH = 2.5. .... 121
- Figure A.1.** Sample HPLC chromatogram with RI (refractive index) dectector for 1,6-hexanediol oxidation using Bio-Rad Aminex column. .... 132

<b>Figure A.2.</b> Sample HPLC chromatogram with UV-VIS detector at 290 nm for 1,6-hexanediol oxidation using Bio-Rad Aminex column. ....	132
<b>Figure A.3.</b> Sample calibration for (a) 1,6-hexanediol, (b) 6-hydroxyhexanoic acid, and (c) adipic acid with the refractive index detector. ....	133
<b>Figure D.1.</b> Reaction network for the aqueous-phase oxidation of glycerol over Au catalysts at basic conditions. Proposed intermediates are shown in dotted boxes. Reproduced with permission from ref 20. Copyright 2007 Elsevier Inc. ....	146
<b>Figure D.2.</b> Reaction scheme for the aqueous-phase oxidation of an alcohol to an acid over Au at basic conditions. Reproduced with permission from ref 22. Copyright 2010 Science. ....	149
<b>Figure D.3.</b> Proposed reaction and regeneration/deactivation pathway for CO oxidation involving cationic gold. Reproduced with permission from ref 27. Copyright 2007 American Chemical Society. ....	151
<b>Figure D.4.</b> DFT calculations for the reaction coordination of CO oxidation. The reaction scheme is (a) adsorption of CO* and OH*, (b) nucleophilic addition of OH* to CO* to form COOH**, (c) cleavage of O-H bond, and (d) formation of CO <sub>2</sub> and H <sub>3</sub> O <sup>+</sup> . Reproduced with permission from ref 36. ....	154
<b>Figure E.1.</b> TOF of 1,6-hexanediol oxidation at low oxygen pressure. ....	160

## List of Tables

<b>Table 1.1.</b> Literature review of TOF and reaction conditions during glycerol oxidation .....	5
<b>Table 2.1.</b> Catalyst characterization results.....	23
<b>Table 2.2.</b> Results from 1,6-hexanediol oxidation over 2.69% Pt/C in the presence of organic and mineral acids. ....	25
<b>Table 2.3.</b> Turnover frequencies and product selectivities of $\alpha,\omega$ -diol oxidation with and without base over Pt/C, Pd/C, and Au/TiO <sub>2</sub> .....	30
<b>Table 2.4.</b> Results from the oxidation of C2 through C6 $\alpha,\omega$ -diols over 2.69% Pt/C. ....	33
<b>Table 2.5.</b> Turnover frequencies for the oxidation of various alcohols over 2.69% Pt/C.....	36
<b>Table 3.1.</b> Reaction orders for 1,6-hexanediol oxidation over 2.69% Pt/C at acidic conditions after inert or oxidative startup conditions. ....	52
<b>Table 3.2.</b> Proposed two site mechanism for alcohol oxidation over supported Pt at acidic conditions.....	53
<b>Table 3.3.</b> Kinetic isotope effect of deuterated ethanol and deuterated oxide over 2.69% Pt/C at acidic conditions after inert startup conditions. ....	54
<b>Table 4.1.</b> Summary of catalyst characterization results.....	67
<b>Table 4.2.</b> Results from the oxidation of 1,6-hexanediol. ....	71
<b>Table 4.3.</b> Elemental analysis of filtrate after 24 h of 1,6-hexanediol oxidation. ....	71
<b>Table 4.4.</b> Influence of Pt/C treatment before and after Pt/C recycle for 1,6-hexanediol oxidation. ....	74
<b>Table 4.5.</b> Influence of additives on the rate of 1,6-hexanediol oxidation over Pt/C. ....	76
<b>Table 4.6.</b> Amount of CO <sub>2</sub> produced after 20 h for substrate oxidation over Pt/C.....	79
<b>Table 5.1.</b> Results from the oxidation of ethanol and benzyl alcohol.....	93
<b>Table 6.1.</b> Characterization of catalysts prepared by sol-immobilization.....	111
<b>Table 6.2.</b> Elemental composition of nanoparticles determined by energy dispersive X-ray spectroscopy.....	114
<b>Table 6.3.</b> Characterization of catalysts prepared by incipient wetness co-impregnation. ....	116

<b>Table 6.4.</b> Oxidation activity of 1,6-hexanediol over catalysts synthesized by the sol-immobilization technique.....	118
<b>Table 6.5.</b> Oxidation activity of 1,6-hexanediol over catalysts synthesized by co-precipitation incipient wetness.....	122
<b>Table D.1.</b> DFT results for reaction energies ( $\text{kJ mol}^{-1}$ ) and activation energies ( $\text{kJ mol}^{-1}$ ) for the oxidation of ethanol and reduction of oxygen on Au(111) in a water solvent. <sup>22</sup> .....	150

## **Chapter 1: Introduction**

### **Biorenewable Chemical Production from Biomass**

The world has recognized the need to decrease its dependence on non-renewable resources. The earth's fossil fuels are being exhausted at an incredible rate and while forecasts for when the resource will be too expensive to effectively utilize for energy vary, at some point the consumption of the non-renewable resources will be greater than its production [1]. Although, in the general public, the most popular sources of renewable energy are solar, wind, geothermal, and hydroelectric power, none of these can satisfy all of the fuel or chemical manufacturing needs of the world [2]. In particular, technology is needed to replace basic and intermediate chemicals from fossil fuels that make up the building blocks of most consumer products with those from a bio-renewable source.

The chemical industry produced 63 million metric tonnes of basic and intermediate chemicals in 2010 valued at over \$2 trillion [3]. The vast majority of chemicals were produced from fossil fuel feedstocks, such as petroleum, coal, and natural gas. The decline in easily obtainable fossil fuel and increase in price have peaked interest in the production of more sustainable chemicals both in industry and government. While a significant amount of research and policy has concentrated on the production of bio-renewable fuels and energy from biomass, such as bio-ethanol, approximately 50% of the value of a barrel of oil comes from only 5% of the mass of the barrel that is used to produce chemicals. [4].

Chemical production from biomass offers an environmentally friendly and sustainable route to continue to provide basic materials and products demanded by society. The replacement of petrochemical building blocks, intermediate compounds, and advanced materials is not trivial. The research and development of key biorenewable platform chemicals and associated



technology is nascent compared to the petrochemical industry. The U.S. Department of Energy has identified numerous molecules derived from biomass that have a high potential value [5]. While the key platform intermediates needed for a successful biorefinery have yet to be decided, common catalytic reactions, such as reduction, oxidation, and dehydration will most likely play a role. The typical heterogeneous catalysts employed for these reactions in the petrochemical industry, however, will not always be optimal because of the vastly different feedstocks and reaction conditions. New catalytic processes are needed to produce these products and ensure the economic success of a refinery that utilizes carbohydrates instead of fossil fuels [6]. The oxidation of alcohols and aldehydes to higher value acid products will undoubtedly play a role in a biorefinery because biomass is already a highly oxygenated feedstock.

The federal government heavily supports the development of technology that improves the capability of a biorefinery to produce high value fuels and chemicals. The NSF Engineering Research Center for Biorenewable Chemicals (CBiRC) has been funded to develop the tools needed to transform the chemical industry. CBiRC focuses on advancing both biological and chemical transformations that support a more sustainable chemical industry. The production of bi-functional compounds using biological and chemical catalytic expertise is one concentration of CBiRC as shown in Figure 1.1. Bio-renewable sugars are diversified into a wide range of products with multiple functional groups using enzyme and microbial metabolic bioengineering. The highly functional intermediate products are then converted to valuable chemicals by chemical catalysis.

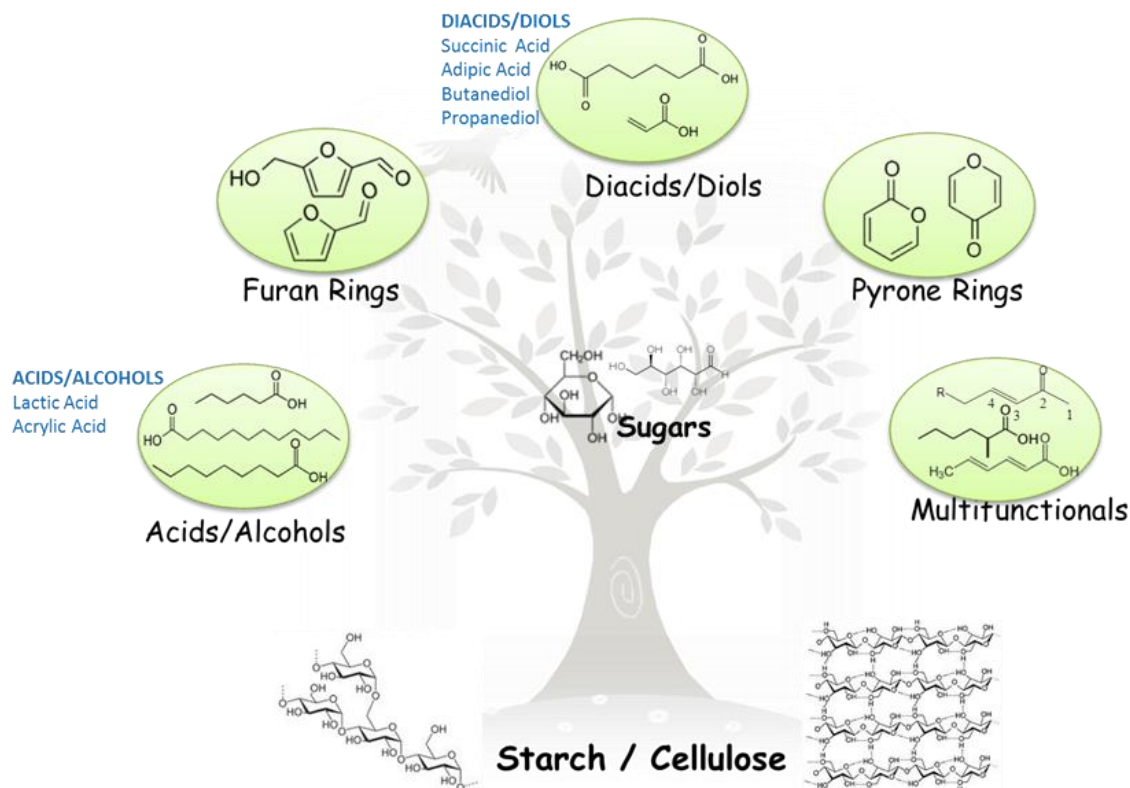


**Figure 1.1.** The CBIIRC strategy for the production of bio-renewable chemicals from biomass.

A significant portion of the intermediate products contain alcohol or aldehyde groups. The oxidation of these oxygenated intermediates, such as  $\alpha,\omega$ -diols to diacids, can produce both drop-in replacements for non-renewable chemicals and unique platform chemicals. The oxidation of chemical intermediates from sugars, however, demands unique catalytic solutions. For instance, the elimination of water from the biorenewable substrate is both technically difficult and costly, thus an aqueous oxidation is advantageous. The demand for green chemistry in industrial processes makes aqueous alcohol oxidation with molecular oxygen as the oxidant and with an easily recycled heterogeneous catalyst alluring. Furthermore, the addition of inorganic additives, such as sodium hydroxide, should be avoided to prevent waste from neutralization of the product stream after oxidation. Also, since small impurities from such a diverse biomass feedstock are common and can easily poison the catalyst surface, a robust and

stable catalyst is needed. Obviously, a significant amount of research is required to determine other challenges and discover solutions for the application of aqueous alcohol oxidation in a sustainable biorefinery.

## Polyol Oxidation over Pt

The oxidation of glycerol with dioxygen as the oxidant is a commonly investigated alcohol oxidation reaction over Pt in an aqueous solvent that is investigated in the literature. The oxidation of glycerol by heterogeneous catalysts has both economic and academic appeal. Glycerol is a major byproduct of biodiesel synthesis via transesterification of triglycerides with alcohols. Glycerol oxidation to high value fine chemicals, such as glyceric acid, tartronic acid, or dihydroxyacetone as shown in Figure 1.2, could help bio-diesel economics become more competitive compared to diesel produced from non-renewable resources. Academic interest in oxidative upgrading of glycerol stems from glycerol being a model polyol with three hydroxyl groups, two primary and one secondary. Thus, for our interests, it is reasonable to use as background information for multi-functional alcohol oxidation.

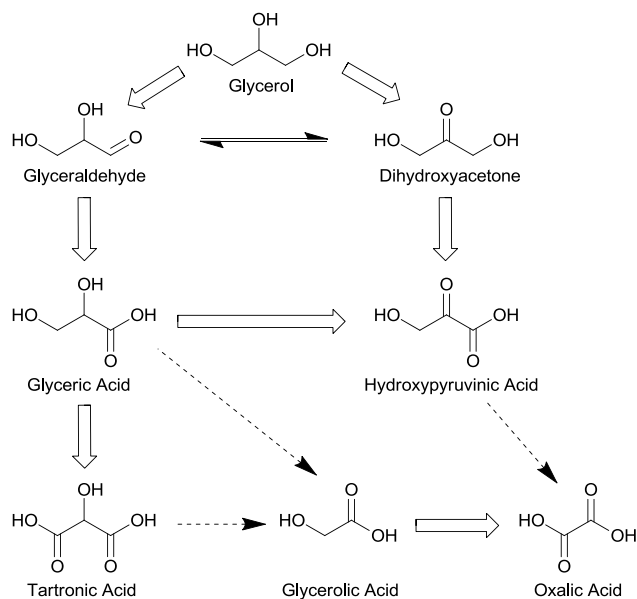


**Figure 1.2.** Commonly observed glycerol oxidation products.

Table 1.1 provides the initial TOF for a few examples of Pt catalyzed glycerol oxidation. Carrettin et al. investigated the role of the type of basic promoter on glycerol oxidation with a 5% Pt/C catalyst [7]. Sodium hydroxide (NaOH) was determined to promote the highest conversion when compared to other alkali metal hydroxides. One major advantage of using supported Pt catalysts is that oxidation is possible even without base, unlike Au catalysts. However, a major disadvantage of Pt catalysts is that they can deactivate quickly under certain reaction conditions. Deactivation of the Pt catalysts can be caused by over-oxidation of the metal to form oxides on the surface and by poisoning of the surface with acid products, byproducts, or cleavage products [8].

**Table 1.1.** Literature review of TOF and reaction conditions during glycerol oxidation

Catalyst	Size (nm)	T (K)	pO <sub>2</sub> (kPa)	NaOH:Glycerol (mol:mol)	TOF (s <sup>-1</sup> )	Reference
3% Pt/C	2.3	333	1100	2	1.6	9
0.5% Pt/C	5	343	1000	0.8	1.2 <sup>a</sup>	10
1% Pt/TiO <sub>2</sub>	2.5	363	100	4	0.3 <sup>a</sup>	11
0.5% Pt/C	3.8	333	300	2	0.3 <sup>a</sup>	12
1% Pt/C	2.5	323	300	4	0.3 <sup>a</sup>	13
5% Pt/C	2.3	333	300	2	0.06 <sup>a</sup>	7
5% Pt/MWNTs	6.7	333	Flow	0	0.6 <sup>a</sup>	15
5% Pt/MWNTs	2.1	333	Flow	0	0.5 <sup>a</sup>	14
5% Pt/C	3.6	398	Flow	pH = 4	0.2 <sup>a</sup>	16
5% Pt/C	3.2	333	Flow	0	0.2 <sup>a</sup>	17
3% Pt/C	3.2	333	Flow	0	0.1 <sup>a</sup>	14
3% Pt/C	2.3	333	1100	0	0.06	9
5% Pt/C	5	343	500	pH = 7	0.05	18

<sup>a</sup> TOF calculated or re-calculated on based on available surface metal.

The initial rate of reaction for supported Pt catalyst in the presence of base was observed both by Zope et al. [9] at 333 K and Huang et al. [10] at 343 K to be on the order of  $\sim 1 \text{ s}^{-1}$ . Huang et al. noted that the TOF was sensitive to the dioxygen pressure, decreasing to about  $0.4 \text{ s}^{-1}$  at a pressure of 300 kPa. The majority of examples cited in Table 1.1, however, have initial

rates significantly below  $\sim 1 \text{ s}^{-1}$ . A TOF of  $0.3 \text{ s}^{-1}$  was calculated over a 1% Pt/TiO<sub>2</sub> catalyst, a 0.5% Pt/C catalyst, and a 1% Pt/C catalyst [11-13]. It is possible that rapid deactivation could play a role in the low initial rate, but a second reason might be mass transfer limitations of O<sub>2</sub> at low pressure and high catalyst loading used in the study.

In the absence of base, the TOF for glycerol oxidation is about  $\sim 0.5 \text{ s}^{-1}$  as observed by Liang et al. over 5% Pt/MWNT [14]. Again, this value could be influenced by rapid deactivation. It has been suggested that over-oxidation can form metal oxides on the surface that are not active for oxidation and that byproducts, intermediates, or acids can strongly adsorb on the metal surface. Gao et al. observed quick deactivation with the rate of reaction dropping in half from  $0.6 \text{ s}^{-1}$  at 20 min to approximately  $0.3 \text{ s}^{-1}$  at 60 min in the absence of base over 5% Pt/MWNT [15]. Both Brandner et al. and Liang et al. determined TOF's of about  $0.2 \text{ s}^{-1}$  despite their significantly different temperatures with Pt nanoparticles of about the same size [16, 17]. The TOF of  $0.06 \text{ s}^{-1}$  reported by Zope et al. at 5 h over 1% Pt/C, even at the low conversion of 5%, is probably measured after too long to accurately gauge the initial rate of reaction without interference from deactivation [9], which also maybe have affected the TOF measured by Hu et al. [18]. Villa et al. tested both 1% Pt/C and 1% Pt/H-mordenite, but did not report the reaction profile or an estimation of particle size, thus no TOF could be calculated [19]. Villa did note that the Pt/H-mordenite catalyst had a lower selectivity to one-carbon products. However, the conversion was significantly higher for the Pt/C catalyst, 78% compared to 20% for the Pt/H-mordenite; thus the difference in selectivity could just be a result of over-oxidation of the glyceric and tartronic acid at higher conversions.

## Glucose Oxidation over Pt

In addition to glycerol, the oxidation of glucose can also be used to gain insight into multi-functional alcohol oxidation. Glucose is a six carbon monosaccharide sugar that can be oxidized to a sugar acid or a diacid. A major barrier in glucose oxidation with supported Pt is the rapid deactivation of the catalyst over a wide range of reaction conditions. Reaction rate profiles for carbohydrate oxidation over Pt are relatively rare, which is surprising given the problem of deactivation. Single point evaluations of conversion and selectivity may be misleading because of rapid deactivation of the catalyst. Biella et al. determined that glucose oxidation almost always had a 99% selectivity to gluconic acid at 323 K from a pH of 7 to 9, but did not fully characterize the 5% Pt/C catalyst making it difficult to compare rates [20, 21]. One study that reported sufficient information to calculate a TOF was performed by Delidovich et al. who measured a TOF for glucose oxidation of  $0.05 \text{ s}^{-1}$  for a 5% Pt/C catalyst at 333 K and pH of 9 and the TOF was independent of the Pt particle size between 1.1 and 4.5 nm [22]. Abbadi et al. showed that the pH had a significant effect on rate of reaction and rate of deactivation [23]. At acidic conditions (i.e. no control of pH) a 5% Pt/C quickly deactivated during oxidation of 0.05 M glucose at 333 K, while a pH of 9 prevented complete catalyst deactivation. While attempts to reactivate the catalyst by dihydrogen flow for 30 minutes were not successful, addition of KOH did reactivate the Pt catalyst.

## Diol Oxidation over Pt, Pd, and Au

The field of  $\alpha,\omega$ -diol oxidation by heterogeneous catalysis with  $\text{O}_2$  as the oxidant has not been extensively explored. The literature has in it a few attempts at the oxidation of  $\alpha,\omega$ -diols with base in an aqueous solution, in organic solvents, and in the absence of base in aqueous solutions. The absence of base is of both industrial and academic importance as the effective

oxidation of diols to diacids over heterogeneous catalysts without the addition of a homogeneous base would allow the development of a cleaner and more economical process.

The catalytic oxidation of  $\alpha,\omega$ -diols with base in an aqueous solution has been reported over supported Au, Pt, and Pd. The oxidation of 1,3-propanediol with 1% Au/C and 1% Au/TiO<sub>2</sub> was reported by Biella et al. with 100% and 95% selectivity, respectively, to the  $\omega$ -hydroxy acid product (3-hydroxypropionic acid) [21]. Supported gold catalysts appear to be very selective towards the  $\omega$ -hydroxy acid product as the use of a 1% Au/C catalyst for the oxidation of 1,2-ethanediol had a 90% selectivity to glycolic acid [24]. While Au rapidly converted 1,2-ethanediol to glycolic acid, Prati et al. showed no catalytic activity for glycolic acid oxidation over the 1% Au/C catalyst. However, 5% Pt/C had a 40% selectivity to oxalic acid (diacid product) at 18% conversion and 5% Pd/C had a 50% selectivity to oxalic acid at 40% conversion at the same conditions as 1% Au/C [25]. Both the Pt/C and Pd/C catalysts were less selective to the  $\omega$ -hydroxy acid with 50% and 57% selectivity, respectively, for 1,2-ethanediol oxidation, but both had a low selectivity to the diacid product (6%) [24]. The production of C<sub>1</sub> products was mentioned, presumably by C-C bond cleavage, but both Pt and Pd were more selective than Au at  $\alpha,\omega$ -diol oxidation to the diacid. Recycle experiments for 1,2-ethanediol oxidation in the presence of base found that the initial rate of the Pt/C catalyst did not change after four recycles, but the Pd/C catalyst had deactivated by 50% after the fourth run because of Pd metal leaching into solution [26].

The oxidation of an  $\alpha,\omega$ -diol in an organic solvent can significantly change the reaction products and selectivity. A 3% Au/TiO<sub>2</sub> catalyst with 5 nm particles oxidized 1,4-butanediol to  $\gamma$ -butyrolactone with 99% conversion and 99% selectivity in a tributyl phosphate (TBP) solvent [27]. Oxidative esterification of 1,3-propanediol in a methanol solvent has been reported over

1% Au/CeO<sub>2</sub> with 78.8% selectivity to methyl 3-hydroxypropionate at 98.1% conversion in the absence of base [28]. A similarly high selectivity of 83% to methyl glycolate was reported at 63% conversion of 1,2-ethanediol over 4.6% Au/Al<sub>2</sub>O<sub>3</sub> in a methanol solvent in the absence of base. A 1% Pd/Al<sub>2</sub>O<sub>3</sub> catalyst only had a 54% selectivity to methyl glycolate at 50% conversion at the same conditions [29]. In a 10% NaOCH<sub>3</sub> solution relative to 1,3-propanediol, Taarning et al. found a 90% selectivity to methyl 3-hydroxypropionate at 84% conversion over 1% Au/TiO<sub>2</sub> [30].

Despite high selectivity toward the methyl ester (or lactone), oxidative esterification of diols over supported gold catalysts has low activity both with and without base. The oxidation of 1,3-propanediol had a TOF of 0.013 s<sup>-1</sup> over 1% Au/TiO<sub>2</sub> (3.5 nm) with base at 373 K and a TOF of 0.015 s<sup>-1</sup> over 1% Au/CeO<sub>2</sub> (3 nm) without base at 398 K [28, 30]. The rate is an order of magnitude slower than the TOF of 0.14 s<sup>-1</sup> for 1,3-propanediol oxidation over 1% Au/TiO<sub>2</sub> at 343 K with base [21]. In addition, the 1% Au/TiO<sub>2</sub> catalyst (5.4 nm) had a TOF of 0.006 s<sup>-1</sup> for 1,4-butanediol oxidation without base at 393 K [27]. Thus, even at high temperatures, the rate of oxidative esterification over supported gold catalysts is low both with and without base. The use of water as a solvent clearly has a tremendous impact on the rate of alcohol oxidation over Au.

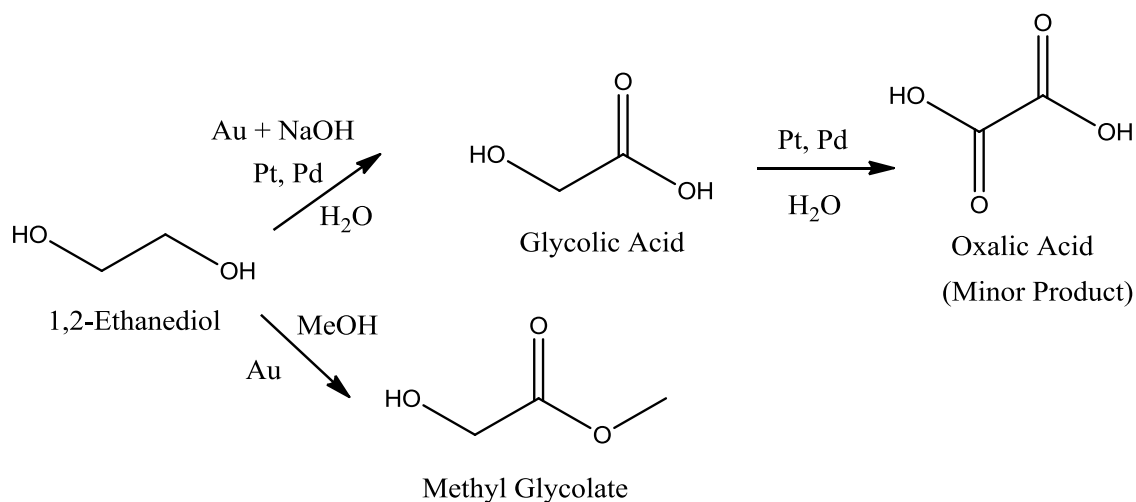


**Figure 1.3.** Summary of literature trends for the oxidation of 1,2-ethanediol.



Recent literature has demonstrated that some heterogeneous catalysts can oxidize diols in the absence of base. For example, the oxidation of 1,2-ethanediol was run using a 1% 1:3 Au-Pt/MgO catalyst with 25% selectivity to oxalic acid (di-acid) at 40.6% conversion, [31] but Mg can sometimes leach into solution under these experimental conditions and most likely acts as a homogeneous base. Prati et al. has performed the oxidation of 1,3-propanediol with a 1% 6:4 Au-Pt/H-mordenite and found an 85% selectivity to the hydroxy-monoacid (3-hydroxypropionic acid) at 41% conversion [32]. There is no mention of any diacid being produced. Thus, the only success at  $\alpha,\omega$ -diol and polyol oxidation has been reported over supported Pt catalysts. A pictorial summary of the  $\alpha,\omega$ -diol oxidation field over Pt, Pd, and Au is collected in Figure 1.3. While the literature offered no concrete explanation on the selectivity, activity, or deactivation of Pt during diol oxidation at acidic aqueous conditions, this work intends to study alcohol oxidation at a low pH over Pt and comment on its possibility for use in the production of bio-renewable chemicals.

## Alcohol Oxidation Mechanism

A brief overview of the generally accepted mechanism of alcohol oxidation is described below while a more in depth discussion focused on comparing experimental results in this work to the literature can be found in Chapter 3. The dehydrogenation of an alcohol first produces an aldehyde or a ketone. In solution, the first step would be a reversible deprotonation of the alcohol to form an alkoxide anion. The extent of deprotonation of an alcohol in water can be determined by its  $pK_a$ . A typical primary alcohol is a weak Brønsted acid with a  $pK_a$  of approximately 14-16. In a basic solution, a significant increase in the concentration of deprotonated alcohol species in solution would be observed. On a catalytic surface, an adsorbed metal alkoxide most likely forms

after deprotonation of the weakly acidic alcohol [33]. Whether the O-H bond cleavage happens in solution or at the metal surface depends upon the catalytic surface and the pH of solution [9]. A byproduct of alcohol deprotonation is a hydrogen ion in solution or metal-hydride species adsorbed to the catalyst surface.

The second step of alcohol dehydrogenation to an aldehyde is the  $\beta$ -hydride elimination or the C-H bond cleavage of the alkoxide species [34]. This oxidative dehydrogenation can be undertaken in solution by an oxidant or on a catalytic surface. The bond breaking reaction forms an adsorbed aldehyde or ketone and hydrogen as a byproduct. The aldehyde or ketone can desorb from the catalytic surface after  $\beta$ -hydride elimination. On a catalyst surface the C-H cleavage could form a metal-hydride [9]. An oxidant, such as dioxygen, can then oxidize the hydrogen produced by deprotonation. The oxidative dehydrogenation of a primary alcohol is summarized in

Figure 1.4.

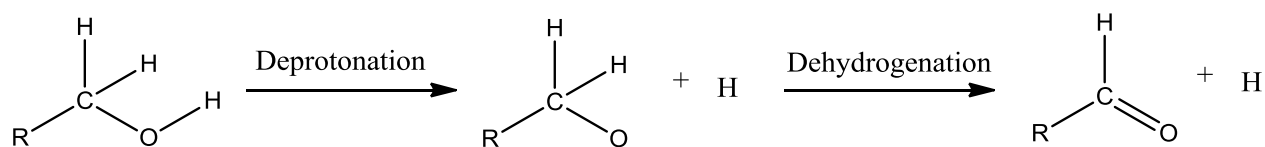


**Figure 1.4.** The general scheme for primary alcohol oxidation to an aldehyde.

The aldehyde hydration and geminal diol dehydrogenation to an acid is shown in Figure 1.5. In an aqueous solution, a carbonyl group can be hydrated via nucleophilic addition to form a geminal diol. The carbonyl group hydration is generally a reversible reaction where water can be eliminated by dehydration. The ratio of carbonyl to geminal diol in an aqueous solution depends on its chemical equilibrium. Aldehydes that do not have steric hindrance tend to favor hydration (formaldehyde has a  $K_{\text{eq}} \sim 2000$ ), while aldehydes that are more sterically hindered do not

(acetaldehyde has a  $K_{\text{eq}} \sim 1$ ) [35]. A solution that is basic or acidic can significantly increase the rate of obtaining chemical equilibrium.

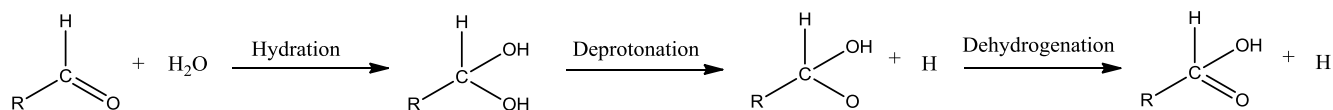


**Figure 1.5.** The general scheme for aldehyde oxidation to an acid.

The dehydrogenation of the geminal diol to an acid is similar to that of alcohol dehydrogenation to an aldehyde. The first step is the deprotonation of one of the alcohols followed by the dehydrogenation of an intermediate carboxylate anion to form a carboxylic acid. The geminal diol could also adsorb to a metal surface to form a metal alkoxide [36]. Figure 1.5 illustrates that a hydrogen atom is released both during the deprotonation and dehydrogenation steps. On a catalytic surface, two metal-hydride bonds will be formed. The carboxylate on the surface can then desorb into solution.

## Focus of this work

While the field of polyol oxidation over Pt has been investigated, the literature still lacks a fundamental understanding of the kinetic mechanism of alcohol oxidation in the aqueous phase over support Pt or the reaction pathway of catalyst deactivation. To better understand these aspects for aqueous alcohol oxidation at acidic conditions, the dissertation set out to investigate the following questions:

1. Can the initial rate of alcohol oxidation be systematically measured at low pH?
2. Does alcohol structure affect the activity of oxidation or ultimate product selectivity?
3. What is the kinetic mechanism of aqueous alcohol oxidation over Pt at acidic conditions?

4. Is there any influence of support type or Pt particle size on the rate of alcohol oxidation or the deactivation behavior?
5. What is the cause of deactivation of Pt during aqueous alcohol oxidation?
6. Do bimetallic nanoparticles involving Pt result in increased activity or selectivity for aqueous alcohol oxidation?

In this dissertation, Chapter 2 addresses the activity and selectivity oxidation trends for various mono-alcohols, diols, and multi-functional alcohols at acidic conditions over Pt, Pd, and Au. Chapter 3 discusses the kinetics of alcohol oxidation over Pt and proposes a mechanistic model that describes the kinetic data during aqueous alcohol oxidation at a low pH. The deactivation of supported Pt catalysts was investigated by catalyst characterization and quantification of byproduct during alcohol oxidation in Chapter 4 and by in-situ ATR-IR spectroscopy of surface species on Pt in Chapter 5. Chapter 6 looks at the synthesis of bimetallic nanoparticles and determines their effectiveness in the catalytic oxidation reaction. To conclude, Chapter 7 will offer remarks on the work described here as well as suggestions for future possible projects.

## References

- [1] S. Shafiee, E. Topal, When will fossil fuel resources be diminished?. *Energ. Policy* 37 (2009) 181-189.
- [2] M. S. Dresselhaus, I. L. Thomas, Alternative energy technologies. *Nature* 414 (2001) 332.
- [3] M. M. Bomgardner, Making rubber from renewables. *Chemical & Engineering News* 89 (2011) 34-35.
- [4] T. L. Donaldson and O. L. Culberson, An industry model of commodity chemicals from renewable resources. *Energy* 9 (1984) 693-707.
- [5] J. J. Bozell and G. R. Petersen, Technology development for the production of biobased products from biorefinery carbohydrates—the US Department of Energy’s “Top 10” revisited. *Green Chem.* 12 (2010) 539-554.

- [6] J. N. Chheda, G. W. Huber, J. A. Dumesic, Liquid-phase catalytic processing of biomass-derived oxygenated hydrocarbons to fuels and chemicals. *Angew. Chem. Int. Ed.* 46 (2007) 7164-7183.
- [7] S. Carrettin, P. McMorn, P. Johnston, K. Griffin, C. J. Kiely, G. J. Hutchings, Oxidation of glycerol using supported Pt, Pd and Au catalysts. *Phys. Chem. Chem. Phys.* 5 (2003) 1329-1336.
- [8] A. P. Markusse, B. F. M. Kuster, J. C. Schouten, Platinum catalysed aqueous methyl  $\alpha$ -D-glucopyranoside oxidation in a multiphase redox-cycle reactor *Catal. Today* 66 (2001) 191-197.
- [9] B. N. Zope, D. D. Hibbitts, M. Neurock, R. J. Davis, Reactivity of the gold/water interface during selective oxidation catalysis. *Science* 330 (2010) 74-78.
- [10] Z. Huang, F. Li, B. Chen, F. Xue, Y. Yuan, G. Chen, G. Yuan, Efficient and recyclable catalysts for selective oxidation of polyols in H<sub>2</sub>O with molecular oxygen. *Green Chem.* 13 (2011) 3414-3422
- [11] Y. Shen, S. Zhang, H. Li, Y. Ren, H. Liu, Efficient synthesis of lactic acid by aerobic oxidation of glycerol on Au–Pt/TiO<sub>2</sub> catalysts. *Chem.* 16 (2010) 7368-7371
- [12] E. G. Rodrigues, S. A. C. Carabineiro, X. Chen, J. J. Delgado, J. L. Figueiredo, M. F. R. Pereira, J. J. M. Órfão, Selective oxidation of glycerol catalyzed by activated carbon supported noble metals. *Catal. Lett.* 141 (2010) 420-431.
- [13] N. Dimitratos, C. Messi, F. Porta, L. Prati, A. Villa, Investigation on the behaviour of Pt(0)/carbon and Pt(0),Au(0)/carbon catalysts employed in the oxidation of glycerol with molecular oxygen in water. *J. Mol. Catal. A-Chem.* 256 (2006) 21-28.
- [14] D. Liang, J. Gao, H. Sun, P. Chen, Z. Hou, X. Zheng, Selective oxidation of glycerol with oxygen in a base-free aqueous solution over MWNTs supported Pt catalysts. *Appl. Catal. B-Env.* 106 (2011) 423-432.
- [15] J. Gao, D. Liang, P. Chen, Z. Hou and X. Zheng, Oxidation of glycerol with oxygen in a base-free aqueous solution over Pt/AC and Pt/MWNTs catalysts. *Catal. Lett.* 130 (2009) 185-191.
- [16] A. Brandner, K. Lehnert, A. Bienholz, M. Lucas, P. Claus, Production of biomass-derived chemicals and energy: Chemocatalytic conversions of glycerol. *Top. Catal.* 52 (2009) 278-287.
- [17] D. Liang, J. Gao, J. Wang, P. Chen, Z. Hou, X. Zheng, Bimetallic Pt—Cu catalysts for glycerol oxidation with oxygen in a base-free aqueous solution. *Catal. Comm.* 10 (2009) 1586-1590.

- [18] W. Hu, D. Knight, B. Lowry, A. Varma, Selective oxidation of glycerol to dihydroxyacetone over Pt– Bi/C catalyst: Optimization of catalyst and reaction conditions. *Ind Eng Chem Res* 49 (2010) 10876-10882.
- [19] A. Villa, G. M. Veith, L. Prati, Selective oxidation of glycerol under acidic conditions Using gold catalysts. *Angew. Chem. Int. Ed.* 49 (2010) 4499-4502.
- [20] S. Biella, L. Prati, M. Rossi, Selective oxidation of D-glucose on gold catalyst. *J. Catal.* 206 (2002) 242-247.
- [21] S. Biella, G. L. Castiglioni, C. Fumagalli, L. Prati, M. Rossi, Application of gold catalysts to selective liquid phase oxidation. *Catal. Today* 206 (2002) 43-49.
- [22] I. V. Delidovich, O. P. Taran, L. G. Matvienko, A. N. Simonov, I. L. Simakova, A. N. Bobrovskaya, V. N. Parmon, Selective oxidation of glucose over carbon-supported Pd and Pt catalysts. *Catal. Lett.* 140 (2010) 14-21.
- [23] A. Abbadi, H. van Bekkum, Selective chemo-catalytic oxidation of lactose and/of lactobionic acid towards 1-carboxylactulose (2-keto-lactobionic acid). *J. Mol. Catal. A-Gen.* 97 (1995) 111-118.
- [24] L. Prati, M. Rossi, Chemoselective catalytic oxidation of polyols with dioxygen on gold supported catalysts. *Stud. Surf. Sci. Catal.* 110 (1997) 509-516.
- [25] L. Prati, M. Rossi, Gold on carbon as a new catalyst for selective liquid phase oxidation of diols. *J. Catal.* 176 (1998) 552-560.
- [26] C. Bianchi, F. Porta, L. Prati, M. Rossi, Selective liquid phase oxidation using gold catalysts. *Top. Catal.* 13 (2000) 231-236.
- [27] J. Huang, W. Dai, H. Li, K. Fan, Au/TiO<sub>2</sub> as high efficient catalyst for the selective oxidative cyclization of 1, 4-butanediol to  $\gamma$ -butyrolactone. *J. Catal.* 252 (2007) 69-76.
- [28] X. Wang, G. Zhao, H. Zou, Y. Cao, Y. Zhang, R. Zhang, F. Zhang, M. Xian, The base-free and selective oxidative transformation of 1, 3-propanediol into methyl esters by different Au/CeO<sub>2</sub> catalysts. *Green Chem.* 13 (2011) 2690-2695.
- [29] T. Hayashi, T. Inagaki, N. Itayama, H. Baba, Selective oxidation of alcohol over supported gold catalysts: methyl glycolate formation from ethylene glycol and methanol. *Catal. Today* 117 (2006) 210-213.
- [30] E. Taarning, A. T. Madsen, J. M. Marchetti, K. Egeblad, C. H. Christensen, Oxidation of glycerol and propanediols in methanol over heterogeneous gold catalysts. *Green Chem.* 10 (2008) 408-414.

- [31] G. L. Brett, Q. He, C. Hammond, P. J. Miedziak, N. Dimitratos, M. Sankar, A. A. Herzing, M. Conte, J. A. Lopez-Sanchez, C. J. Kiely, D. W. Knight, S. H. Taylor, G. J. Hutchings, Selective oxidation of glycerol by highly active bimetallic catalysts at ambient temperature under base-free conditions. *Angew. Chem. Int. Ed.* 50 (2011) 1-4.
- [32] A. Villa, C. E. Chan-Thaw, G. M. Veith, K. L. More, D. Ferri, L. Prati, Au on nanosized NiO: A cooperative effect between Au and nanosized NiO in the base-free alcohol oxidation. 10 (2011) 1612-1618.
- [33] K. Yamaguchi, N. Mizuno, Supported ruthenium catalyst for the heterogeneous oxidation of alcohols with molecular oxygen. *Angew. Chem. Int. Ed.* 41 (2002) 4538-4541.
- [34] X. Yang, X. Wang, J. Qui, Aerobic oxidation of alcohols over carbon nanotube-supported Ru catalysts assembled at the interfaces of emulsion droplets. *Appl. Catal. A-Gen.* 382 (2010) 131-137.
- [35] M. Mugnai, G. Cardini, V. Schettino, C. J. Nielsen, Ab initio molecular dynamics study of aqueous formaldehyde and methanediol. *J. Mol. Phys.* 105 (2007) 2203-2210.
- [36] F. A. Carey, *Organic Chemistry*, New York, 5<sup>th</sup> Ed. 2003, Vol. 1, pp. 712-717.

## Chapter 2: Aqueous Alcohol Oxidation over Supported Pt, Pd, and Au Catalysts

*A portion of this chapter was previously published as M. S. Ide, R. J. Davis, "Perspectives on the kinetics of diol oxidation over supported platinum catalysts in aqueous solution." Journal of Catalysis (2013), <http://dx.doi.org/10.1016/j.jcat.2013.05.017>.*

### Introduction

Interest in the production of commodity chemicals from biomass feedstocks continues to grow as the biological and chemical transformations of carbohydrates becomes more economical. The oxidation of polyols derived from biorenewable feedstocks has been a particularly active area of research and has been highlighted by the US Department of Energy as an attractive method to produce valuable chemicals [1]. Therefore, the oxidation of polyols in an environmentally friendly manner, using water as a solvent and dioxygen as the oxidant, could be an integral part of the future bio-refinery. Although a wide range of catalysts, substrates, and reaction conditions have been explored, there remains a need for the development of alcohol oxidation rules that dictate the activity and selectivity of different substrates.

One motivation to study alcohol and aldehyde oxidation reactions is to produce diacids, which are important monomer compounds. For example, adipic acid is a 6-carbon diacid used in the production of nylon-6,6 that can be derived from renewable resources, such as fructose (Figure 2.1). Dehydration of fructose to HMF can be accomplished with 72% yield and selective hydrogenolysis of HMF can produce 1,6-hexanediol in 86% yield [2, 3]. The subsequent oxidation of 1,6-hexanediol forms the desired adipic acid. Currently, adipic acid is produced from a cyclohexanol mixture (KA oil) via nitric acid oxidation, which is a process that contributes considerably to nitrous oxide emissions [4,5]. A significant amount of industrial



activity has been generated for the production of adipic acid with fermentation, such as by Rennovia, Verdezyne, BioAmber, Genomatica, and DSM, or chemo-catalytically by Rennovia. Many other valuable biomass-derived diacids can be produced from the oxidation of multi-functional sugars as well, such as xylitol to xylaric acid, glucose to glucaric acid, glycerol to tartronic acid, 5-hydroxymethyl furfural (HMF) to 2,5-furandicarboxylic acid.

Recent work in the literature indicates the selectivity to diacid products during both glycerol and HMF oxidation is very low (< 20%) over supported Au at 2:1 or 4:1 molar ratios of sodium hydroxide to substrate concentration. However, the use of excessive amounts of base (20:1 molar ratios) allowed high selectivities to diacid products (> 70%) from HMF and glycerol [6, 7]. The use of high concentrations of base is likely to be unrealistic for an industrial process because of the cost of neutralizing the product stream to recover the free acid. Also, a recent study attributed the lack of diacid selectivity during glycerol oxidation over Au/TiO<sub>2</sub> to deactivation by strongly adsorbed byproducts [8]. Interestingly, oxidation of HMF over Pt/C did not require excess base to achieve high selectivity to the diacid, while under similar conditions diacid selectivity was still quite low during glycerol oxidation [6]. Likewise, the oxidation of 1,2-ethanediol and 1,3-propanediol to their corresponding ω-hydroxy acid products was highly selective over Au/C, but no production of the diacid was observed, even when ω-hydroxy acid was used as the substrate [9, 10]. A low selectivity was also observed during 1,2-ethanediol oxidation over Pt/C and Pd/C at basic conditions [11].

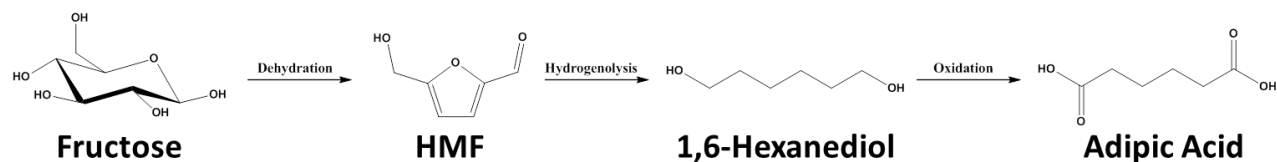


**Figure 2.1.** Reaction pathway for the biorenewable production of adipic acid.

Clearly, there are many unresolved issues in the area of metal-catalyzed oxidation that need to be examined. In this work, the rates of alcohol oxidation reactions in aqueous solutions using dioxygen over supported Pt catalysts were investigated at low pH to avoid the need for eventual product neutralization. The influence of acid type (mineral vs. organic) on the rate of reaction was also determined. In addition, the effects of carbon support and Pt particle size on the rate were explored. The oxidation of various  $\alpha,\omega$ -diols was evaluated over carbon-supported Pt catalysts and compared to the oxidation of analogous mono-alcohols. Finally, the ultimate selectivity of various  $\alpha,\omega$ -diols was determined in order to gauge whether the production of diacids was feasible.

## Experimental Methods

### Catalyst preparation

The 2.69 wt% Pt/C was obtained from Aldrich Chemical Co. The 2.69% Pt/C catalyst was reduced in  $100 \text{ cm}^3 \text{ min}^{-1}$  of flowing  $\text{H}_2$  for 4 h at 473 K, cooled, exposed to air, and stored at ambient temperature. A portion of the 2.69% Pt/C catalyst was reduced similarly for 4 h at 673 K. The activated charcoal (Norit, SX ultra) supported Pt (3 wt%) catalyst was prepared by incipient wetness impregnation of chloroplatinic acid (Sigma-Aldrich). The 3% Pt/NoritC was dried in air for 12 h at 393 K, reduced in  $100 \text{ cm}^3 \text{ min}^{-1}$  of flowing  $\text{H}_2$  for 4 h at 673 K, cooled, exposed to air, and stored at ambient temperature. A Vulcan (Cabot, VXC72R) supported Pt (1 wt%) catalyst was prepared in a similar manner, except the 1% Pt/VulcanC was reduced for 4 h at 573 K.

The 3 wt% Pd/C catalysts was obtained from Aldrich Chemical Co. The Pd catalyst was reduced in  $100 \text{ cm}^3 \text{ min}^{-1}$  of flowing  $\text{H}_2$  for 4 h at 473 K, cooled, exposed to air, and stored at

ambient temperature. The 1.6 wt% Au/TiO<sub>2</sub> catalyst was obtained from the World Gold Council (Sample 137A), stored at 277 K, and used as received.

### Catalyst characterization

The metal dispersion of the Pt and Pd catalysts was determined by H<sub>2</sub> chemisorption using a Micromeritics ASAP 2020 automated adsorption analyzer. The supported Pt catalysts were heated to 473 K at 4 K min<sup>-1</sup> under flowing H<sub>2</sub> (GT&S 99.999%) and reduced for 2 h. The samples were then evacuated and held for 2 h at 473 K before being cooled to 308 K for analysis in the pressure range of 10-450 Torr. The Pd/C catalyst was heated to 473 K at a rate of 4 K min<sup>-1</sup> under flowing H<sub>2</sub>. The sample was evacuated and held for 2 h at 473 K before being cooled down to 373 K for analysis. The analysis was carried out at 373 K in the pressure range of 10-450 Torr to avoid formation of the β-phase Pd hydride. The amount of metal on the surface was evaluated by the total amount of H<sub>2</sub> adsorbed, extrapolated to zero pressure, assuming a stoichiometry (H/M<sub>surf</sub>, M = Pt or Pd) equal to unity.

Elemental analysis (using ICP – AES analysis performed by Galbraith Laboratories, 2323 Sycamore Drive, Knoxville, TN 37921) determined a Pt loading of 2.69 wt% for Pt/C (Aldrich).

The X-ray diffraction (XRD) patterns were recorded on a Scintag automated diffractometer using Cu Kα radiation (40 kV, 30 mA) and continuous scanning of 2θ from 20° to 80° with a step size of 0.05° at a rate of 0.3° min<sup>-1</sup>. The crystalline size of the metal particles was calculated by the Scherrer equation [ $d = K \lambda (\beta_{1/2} \cos (2\theta))^{-1}$ ] using the Pt(111) peak at 2θ = 39.7°.

To prepare the 2.69% Pt/C sample for transmission electron microscopy (TEM), ~1 mg of sample was suspended in 2 cm<sup>3</sup> of ethanol by agitating the mixture for 30 minutes in a sonication bath. A copper grid with a holey carbon film was briefly dipped in the solution and

the ethanol was evaporated. The imaging of the catalyst was performed on a FEI Titan operating at 180 kV and equipped with a Gatan 794 Multi-scan Camera (EFTEM).

### **Alcohol oxidation**

The semi-batch aqueous alcohol oxidation reactions were performed in a 50 cm<sup>3</sup> Parr Instrument Company 4592 batch reactor with a 30 cm<sup>3</sup> glass liner. The appropriate amounts of substrate, acid (to control pH), and catalyst were added to approximately 10 cm<sup>3</sup> of distilled, deionized water in the glass liner. The glass liner was inserted into the reactor, sealed, purged with He, and heated to 343 K. The reaction was initiated by pressurizing the reactor with 10 bar absolute O<sub>2</sub> (GT&S, 99.993%). The pressure was maintained at a constant value by continually feeding O<sub>2</sub>. No conversion was observed after 240 min when N<sub>2</sub> was substituted for O<sub>2</sub>. Samples were periodically removed and the catalyst was filtered using 0.2 μm PTFE filters before analyzing in a Waters e2695 high pressure liquid chromatograph (HPLC). The HPLC was equipped with refractive index and UV/Vis detectors. Product separation in the HPLC was carried out with a Aminex HPX-87H column (Bio-Rad) operating at 318 K with 5 mM H<sub>2</sub>SO<sub>4</sub> in water flowing at 5 cm<sup>3</sup> min<sup>-1</sup>. Carbon balances were typically greater than 90%. The retention times and calibration curves were determined by injecting known concentrations of standards. The pH of the samples was determined by a Orien 3-Star Plus pH Portable Meter with a Thermo Orion 9810BN Micro-pH Electrode after the sample had cooled to room temperature.

The initial turnover frequency (TOF) [mol alcohol converted (mol M<sub>surface</sub>)<sup>-1</sup> s<sup>-1</sup>] for alcohol oxidation was calculated from the initial conversion of the alcohol, usually within the first 15 minutes of the reaction. A sample was also taken at 30 minutes to confirm that significant deactivation had not occurred in the initial rate determination. The maximum O<sub>2</sub> transport rate from the gas phase to the aqueous phase in the pressurized reaction system was determined by

the sulfite oxidation method [12]. The amount of catalyst added to the reactor was chosen so that the alcohol oxidation rate would not be limited by O<sub>2</sub> mass transfer from the gas to the liquid when determining the TOF. No conversion was found after 240 min in the absence of catalyst. Selectivity to a specific product is defined as moles of that product formed divided by moles of all products produced.

## Results and Discussion

### Catalyst characterization

The metal loadings and dispersions of the supported Pt catalysts are reported in Table 2.1. The 2.69% Pt/C catalyst reduced at 473 K was utilized to determine alcohol oxidation kinetics and was therefore extensively characterized. The fraction of platinum metal exposed, also called dispersion ( $d$ ), was determined to be 0.57 by hydrogen chemisorption ( $H/M$ ) with an estimated particle size ( $1/d$ ) of 1.8 nm. The size of the platinum nanoparticles was also determined by analyzing 400 particles from TEM images, which gave an average diameter of  $1.72 \text{ nm} \pm 1.20 \text{ nm}$ . Samples micrographs of the fresh Pt/C catalyst are shown in Figure 2.2 and Figure 2.3. The crystallite size of the platinum particles by XRD analysis was calculated to be 2.1 nm with a  $\beta_{1/2} = 0.085$  radians at  $2\theta = 39.7^\circ$ . All characterization techniques indicated that the 2.69% Pt/C catalyst had an average platinum particle size of about 2 nm.

The 2.69% Pt/C reduced at 673 K, 3% Pt/NoritC, and 1% Pt/VulcanC catalysts were characterized by chemisorption of H<sub>2</sub>. The reduction of the 2.69% Pt/C catalyst at 673 K sintered the catalyst slightly compared to one treated in H<sub>2</sub> at 473 K. The 3% Pt/NoritC catalyst had a greater dispersion than the 1% Pt/VulcanC catalyst, despite the lower platinum loading and lower reduction temperature of the Vulcan-supported catalyst. The 3% Pd/C had a similar dispersion to

the 2.69% Pt/C that was reduced at 673 K. The 1.6% Au/TiO<sub>2</sub> catalyst was characterized by the World Gold Council and the dispersion was estimated as the inverse of the gold particle size.

**Table 2.1.** Catalyst characterization results.

Catalyst	Metal (wt%)	H <sub>2</sub> Reduction Temperature (K)	Dispersion (H/Metal)	Metal Particle Diameter (nm)		
				H <sub>2</sub> <sup>d</sup>	TEM	XRD
Pt/C	2.69 <sup>a</sup>	473	0.57	1.8	1.7	2.1
Pt/C	2.69 <sup>a</sup>	673	0.35	2.8	-	-
Pt/NoritC	3 <sup>b</sup>	673	0.73	1.4	-	-
Pt/VulcanC	1 <sup>b</sup>	573	0.17	5.9	-	-
Pd/C	3 <sup>b</sup>	473	0.37	2.7	-	-
Au/TiO <sub>2</sub>	1.6 <sup>c</sup>	-	0.38 <sup>d</sup>	-	2.6 <sup>e</sup>	-

<sup>a</sup> Determined by elemental analysis.

<sup>b</sup> Nominal weight loading.

<sup>c</sup> Elemental analysis performed by World Gold Council.

<sup>d</sup> Estimated as the inverse of the dispersion.

<sup>e</sup> Particle size analyzed by TEM performed by World Gold Council.

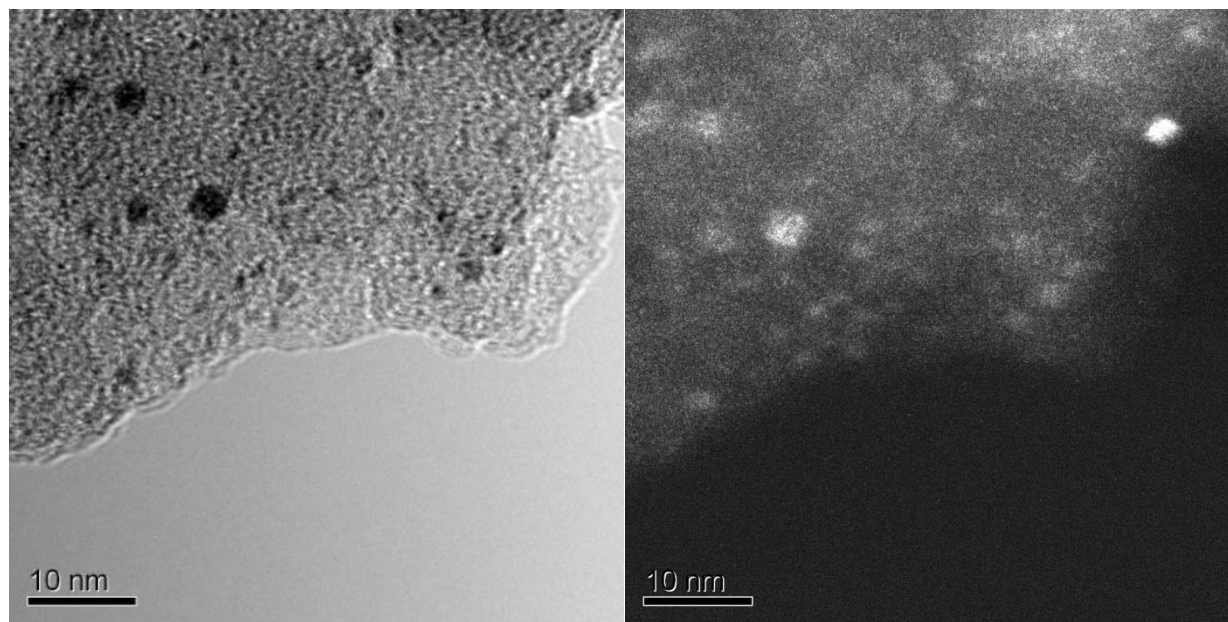


**Figure 2.2.** Bright field and corresponding dark field TEM image of 2.69% Pt/C catalyst reduced at 473 K.

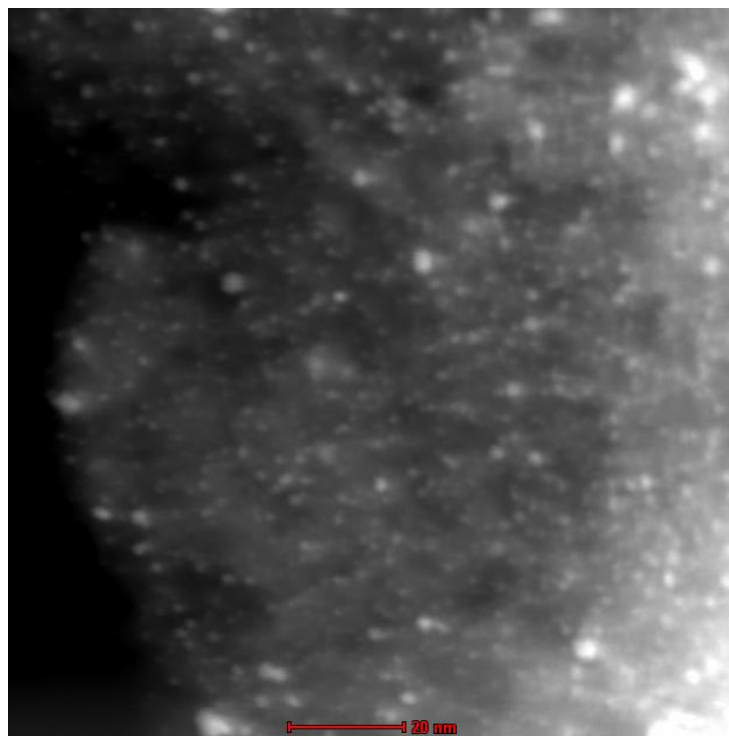


**Figure 2.3.** High angle annular dark-field TEM image of 2.69% Pt/C catalyst.

### **Alcohol oxidation at low pH**

The oxidation of 1,6-hexanediol (HDO) in an aqueous solution with 10 bar dioxygen at 343 K was investigated in the absence and presence of an acid additive. The pH of solution was monitored before the reaction was commenced and after fifteen minutes of reaction, as indicated in Table 2.2. After 15 minutes of HDO oxidation over 2.69% Pt/C with no additive, the pH had decreased from 6.45 to 3.45, which can be attributed to the formation of 6-hydroxyhexanoic acid, a product of HDO oxidation. The acid group of 6-hydroxyhexanoic acid is monoprotic with a pKa of 4.75. The turnover frequency (TOF) for HDO oxidation over Pt/C without an additive was  $0.27 \text{ s}^{-1}$ . The second entry in

Table 2.2 gives the result when the catalyst loading in the reactor was halved. Since the TOF was unaffected and the pH change was similar to the first entry, we conclude that the rate of

oxidation was not limited by O<sub>2</sub> gas-liquid mass transfer and that the catalyst loading did not significantly affect the solution pH.

**Table 2.2.** Results from 1,6-hexanediol oxidation over 2.69% Pt/C in the presence of organic and mineral acids.

Additive	pH		TOF (s <sup>-1</sup> )	Conv. (%)	Selectivity (%) <sup>a</sup>	
	t <sub>0 min</sub>	t <sub>15 min</sub>			ALD	HA
No Additive	6.45	3.45	0.27	29	86	14
No Additive <sup>b</sup>	6.57	3.61	0.28	15	94	6
0.35 M Acetic Acid	2.53	2.52	0.19	20	94	6
0.35 M Acetic Acid <sup>b</sup>	2.48	2.44	0.18	8.9	89	11
0.35 M Propionic Acid	2.55	2.55	0.18	19	95	5
0.004 M Phosphoric Acid	2.56	2.52	0.27	29	86	14
0.0015 M Sulfuric Acid	2.53	2.51	0.29	33	87	13

Reaction conditions: 0.1 M 1,6-hexanediol, 1,6-hexanediol:Pt = 500:1 (mol:mol), T = 343 K, pO<sub>2</sub> = 10 bar, 2.69% Pt/C. ALD = aldehyde-alcohol and HA = ω-hydroxy acid

<sup>a</sup> Selectivity to ALD (6-hydroxyhexanal) and HA (6-hydroxyhexanoic acid) determined at the corresponding conversion.

<sup>b</sup> 1,6-hexanediol:Pt = 1000:1 (mol:mol)

Since the pH varied throughout the reaction, we added excess acid in an effort to maintain a relatively constant pH. Although the use of an organic acid might more closely resemble an industrial process where a portion of the product stream would be recycled, we wanted to check if the acid type influenced the rate. Both phosphoric acid, a weak triprotic acid, and sulfuric acid, a strong diprotic acid, were used to maintain a relatively constant pH of 2.5. Interestingly, the mineral acids and pH control had no effect on the TOF or selectivity of HDO oxidation over Pt/C over the range investigated. At acidic conditions, the pH did not appear to play a significant role in HDO oxidation over Pt/C. It should be noted that strongly anionic species can leach Pt from carbon over extended periods of time [13].

When the pH was held relatively constant at about 2.5 by an organic acid additive, a decrease in the TOF of HDO oxidation was observed. In comparison to HDO oxidation with the added phosphoric acid, the addition of 0.35 M acetic acid decreased the initial TOF by



approximately 30%. The use of propionic acid had a similar effect on the TOF of HDO oxidation as acetic acid. When the catalyst loading was halved but with the same concentration of acetic acid, the TOF and pH observed did not change significantly. The addition of acetic acid has been shown to decrease the rate of HMF and glycerol oxidation over Pt/C below neutral pH [8, 14].

The effect of acetic acid concentration (and pH) on the TOF of HDO oxidation is illustrated in Figure 2.4. Initially, the TOF of HDO oxidation decreased moderately with increasing acetic acid concentration up to 0.2 M. Further increasing the acetic acid concentration to 0.35 M and 0.7 M only slightly decreased the rate of HDO oxidation. It should be noted that the addition of 0.1 M acetic acid decreased the initial pH of solution significantly from 6.5 to approximately 2.8, while higher concentrations of acetic acid had little effect on the initial pH. The lack of correlation between pH and TOF of HDO oxidation for organic acid additives is consistent with the results from the mineral acid experiments. However, unlike mineral acids, acetic acid clearly inhibited HDO oxidation over Pt. The decrease in TOF with increasing concentration of acetic acid likely means that the initial TOF measured without an additive or with a mineral acid depend on conversion level because HDO oxidation produces 6-hydroxyhexanoic acid, an organic acid.

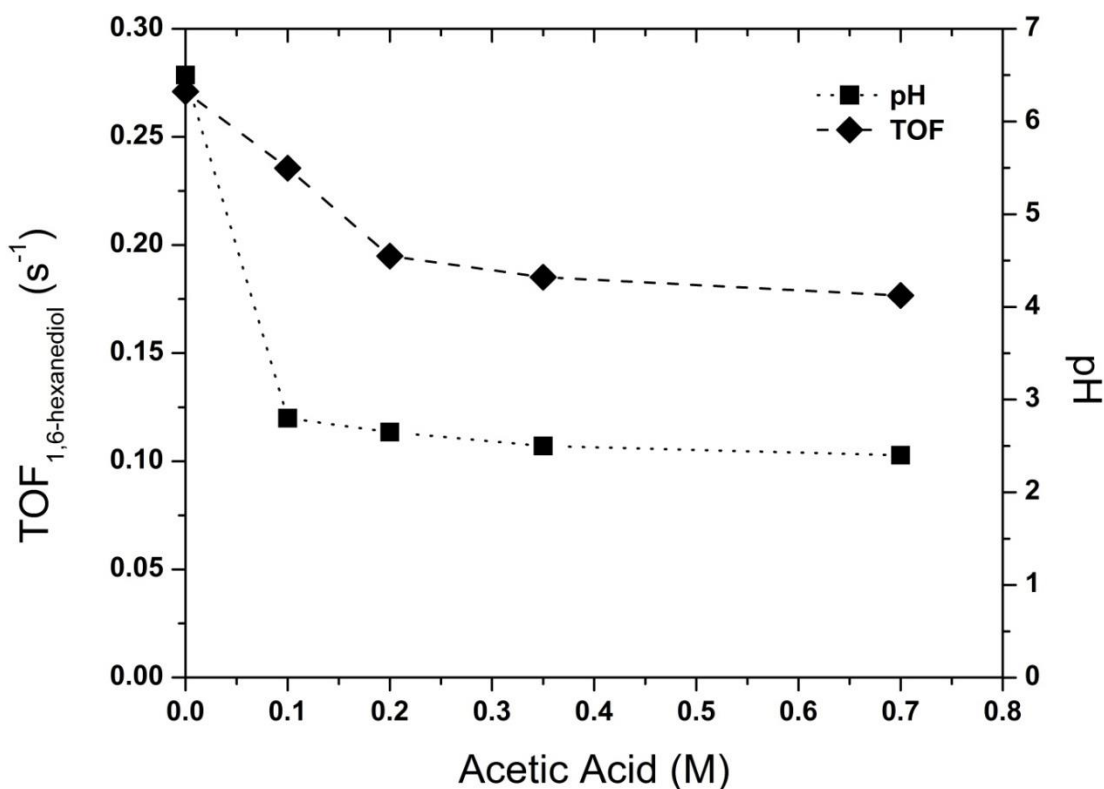


**Figure 2.4.** Influence of acetic acid on the initial turnover frequency (TOF) of 1,6-hexanediol oxidation and initial pH of solution over 2.69% Pt/C with 0.1 M 1,6-hexanediol at 343 K and 10 bar O<sub>2</sub>.

The inhibition of HDO oxidation by organic acids was probably the result of competitive adsorption of the organic acid on the platinum surface. Heinen et al. showed with in situ ATR-FTIRS that acetic acid adsorption on a platinum thin film was dissociative during electro-oxidation [15]. In summary, while the addition of organic acid inhibited the initial oxidation rate of HDO by a modest amount, the pH did not appear to directly affect the TOF. Although the mode of inhibition by organic acid is unknown, its influence seems to be fairly constant at concentrations in excess of 0.2 M in the presence of 0.1 M HDO.

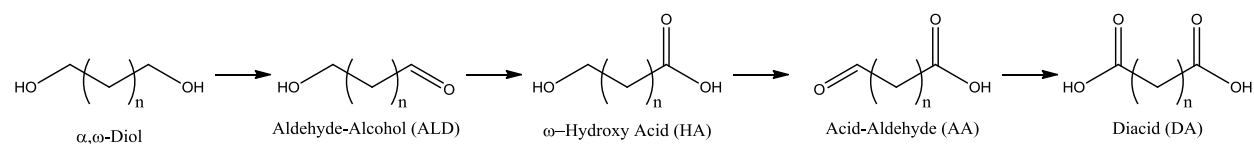


**Figure 2.5.** The general reaction path for the sequential oxidation of an  $\alpha,\omega$ -diol. The oxidation of the diol first produces an aldehyde-alcohol (ALD) and then an  $\omega$ -hydroxy acid (HA). Further oxidation of the  $\omega$ -hydroxy acid (HA) generates an acid-aldehyde (AA) and then the final oxidation product, a diacid (DA).

The observed rate of alcohol oxidation at acidic conditions can be influenced by catalyst deactivation, although the origin of the phenomenon is not readily apparent [16]. In this study, we report initial rates of alcohol oxidation in an effort to reduce the influence of deactivation. Figure 2.5 shows that oxidation of  $\alpha,\omega$ -diols is a sequential reaction from the diol to an aldehyde-alcohol (ALD) and then to a  $\omega$ -hydroxy acid (HA). The  $\omega$ -hydroxy acid can then be oxidized further to an acid-aldehyde (AA) and finally the diacid (DA) product. The reaction profile for the sequential oxidation of 1,6-hexanediol given in Figure 2.6 illustrates rapid conversion over the first 100 minutes followed by relatively slow conversion. Therefore, we typically report the TOF after 15 minutes of reaction, prior to significant deactivation of the catalyst. Removal of the catalyst from solution after 20% conversion (not shown in Figure 2.6) halted the reaction of HDO as well as the subsequent conversion of 6-hydroxyhexanal and 6-hydroxyhexanoic acid.

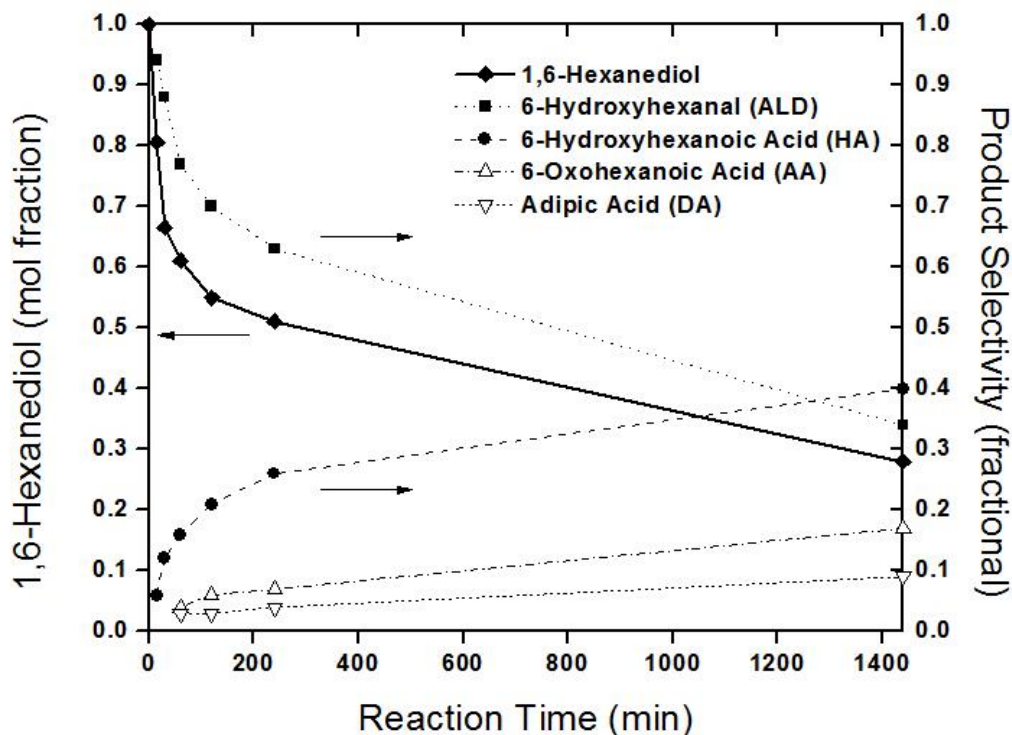


**Figure 2.6.** Reaction profile for 1,6-hexanediol oxidation with 10 bar dioxygen at 343 K over 2.69% Pt/C. The solid line is the conversion of 1,6-hexanediol. The dotted lines are the product selectivities of 6-hydroxyhexanal (ALD), 6-hydroxyhexanoic acid (HA), 6-oxoheptanoic acid (AA), and adipic acid (DA).

### Diol oxidation at acidic and basic conditions over Pt, Pd, and Au

The TOF and selectivities were compared for HDO oxidation over Pt/C and Au/TiO<sub>2</sub> at both acidic and basic conditions in Table 2.3. The oxidation of HDO at 343 K in acidic conditions over Au/TiO<sub>2</sub> determined that the catalyst was inactive. The initial deprotonation of an alcohol on the Au(111) surface has been shown to by DFT calculations have a very high activation barrier in the absence of base [17]. At basic conditions, the TOF of HDO oxidation was significantly faster over Au/TiO<sub>2</sub> than Pt/C. While the adsorption of hydroxide on the platinum surface has been shown to decrease the activation barrier of alcohol deprotonation over Au(111) and Pt(111), the rate of HDO oxidation decreased over Pt/C with the addition of base. The decrease in HDO oxidation rate with the addition of base compared to acidic conditions over

Pt/C is contradictory to results in the literature for glycerol oxidation. [17] However, the HDO experiments with base over Pt/C had many oxidation products that were not identifiable and a product carbon balance of about 30%. The color of the samples was a pale yellow and the color was reproduced when base was added to a sample from HDO oxidation at acidic conditions. The pale yellow color sample was also reported for 1-methoxy-propanol oxidation over Pt/C in the presence of base along with the corresponding rapid deactivation of the catalyst [18]. We believe it is the decomposition or side reactions, such as aldol condensation, of the aldehyde product in solution that produced the yellow color and deactivated Pt/C. Similar aldol condensation products were believed to poison Au catalysts for glycerol oxidation [8]. Interestingly, the Pd/C catalyst exhibited low activity compared to the Pt/C catalyst for HDO oxidation at acidic conditions. Similar results were found for glycerol oxidation at uncontrolled pH [17, 19-21].

**Table 2.3.** Turnover frequencies and product selectivities of  $\alpha,\omega$ -diol oxidation with and without base over Pt/C, Pd/C, and Au/TiO<sub>2</sub>.

Substrate	Catalyst	Sub.:Met. (mol:mol)	NaOH:Sub. (mol:mol)	TOF s <sup>-1</sup>	Conv. %	Selectivity (%)			
						ALD	HA	AA	DA
HDO	2.69% Pt/C <sup>a</sup>	500	-	0.19	20	94	6	0	0
HDO	3% Pd/C <sup>a</sup>	500	-	0.01	4	100	0	0	0
HDO	1.6% Au/TiO <sub>2</sub> <sup>a</sup>	500	-	-	1<	-	-	-	-
HDO	2.69% Pt/C	500	2	0.06	6	0	100	0	0
HDO	2.69% Pt/C	500	20	0.07	7	0	100	0	0
HDO	1.6% Au/TiO <sub>2</sub>	2000	20	1.1	14	0	100	0	0
PDO	1.6% Au/TiO <sub>2</sub>	2000	20	0.54	7	0	100	0	0
HDO	1.6% Au/TiO <sub>2</sub>	100	20	-	100	0	0	0	100
HDO	2.69% Pt/C <sup>b</sup>	100	0	-	100	0	0	0	100 <sup>b</sup>

Reaction conditions: 0.1 M substrate, T = 343 K, pO<sub>2</sub> = 10 atm. ALD = aldehyde-alcohol, HA =  $\omega$ -hydroxy acid, AA = acid-aldehyde, DA = diacid, HDO = 1,6-hexanediol, PDO = 1,3-propanediol

<sup>a</sup> Reaction run with 0.35 M acetic acid at a pH of 2.5

<sup>b</sup> Carbon balance gives actual yield of 86% diacid.

At basic conditions, both Pt/C and Au/TiO<sub>2</sub> were capable of selectively oxidizing HDO to the diacid product, adipic acid. The oxidation of HDO to 100% conversion over Au/TiO<sub>2</sub> had an

almost quantitative yield of adipic acid (99%) at a low molar ratio of HDO to Au. When an identical experiment was performed at acidic conditions over Pt/C, an 86% yield of adipic acid was achieved for HDO oxidation. Both Pt/C and Au/TiO<sub>2</sub> were able to produce high yields of adipic acid, despite the fact that Au/TiO<sub>2</sub> has a significantly higher TOF than Pt/C. While highly basic conditions greatly increased the rate of HDO oxidation over Au/TiO<sub>2</sub>, these conditions also produced a salt that must be ion exchanged before the product acid can be used as a monomer. At acidic conditions, a costly neutralization is not needed as the product is a free acid. The TOF for the oxidation of 1,6-hexanediol was twice as high as 1,3-propanediol (PDO) over Au/TiO<sub>2</sub>. Biella et al. similarly reported that 1,3-propanediol had a higher rate of oxidation than 1,2-ethanediol over Au/C at basic conditions [10]

#### **Effect of carbon support and Pt particle size**

The influences of Pt particle size (dispersion) and carbon support were tested in the oxidation of 1,6-hexanediol at 343 K and 10 bar dioxygen pressure. The average particle size of 2.69% Pt/C was increased by increasing the temperature of reduction from 473 K to 673 K. Although the dispersion of the catalyst reduced at 473 K was 0.57 and the dispersion of the sample reduced at 673 K was 0.35 (Table 2.1) the TOFs for 1,6-hexanediol oxidation were 0.19 and 0.20 s<sup>-1</sup>, respectively. Likewise, 3% Pt/NoritC with a dispersion of 0.73 and 1% Pt/VulcanC with a dispersion of 0.17 exhibited TOFs for 1,6-hexanediol oxidation reaction of 0.19 and 0.17 s<sup>-1</sup>, respectively. Thus, the three different carbon-supported platinum catalysts with different Pt weight loadings and Pt particle sizes ranging from about 2 to 6 nm had essentially the same TOF for HDO oxidation in the presence of acetic acid. These results verify the carbon support did not affect the rate, suggest the alcohol oxidation reaction is structure insensitive, and indicate the measured rates were likely free of any artifacts from mass transfer limitations.

### Effect of alcohol structure on the oxidation rate over Pt

The oxidation of two carbon (C2) through six carbon (C6)  $\alpha,\omega$ -diols with 10 bar dioxygen at 343 K were investigated over 2.69% Pt/C at acidic conditions. Table 2.4 shows that the initial rates of 1,4-butanediol (BDO), 1,5-pentanediol (PEDO), and 1,6-hexanediol (HDO) were significantly faster than those for 1,2-ethanediol (EG) and 1,3-propanediol (PDO). Clearly, the initial TOF of  $\alpha,\omega$ -diol oxidation increased with increasing carbon chain length, however, the difference in TOF between HDO and PEDO was within experimental error. At the early reaction time when the initial TOF was measured, the product selectivity was approximately 80% or greater to the aldehyde-alcohol for all substrates. Table 2.4 shows the product selectivity of  $\alpha,\omega$ -diol oxidation at a slightly higher conversion of 14 -20%. The product selectivity associated with EG oxidation was 100% to the  $\omega$ -hydroxy acid whereas the product selectivity associated with HDO oxidation was 94% to the aldehyde-alcohol (see Figure 2.5 for the reaction path). Evidently, short-chain aldehyde-alcohols are more quickly converted to acid-alcohols compared to long chain aldehyde-alcohols. In contrast, BDO did not form  $\gamma$ -hydroxybutyric acid from the oxidation of the aldehyde, but instead produced the lactone,  $\gamma$ -butyrolactone. The lactone products of PEDO and HDO were not observed.

**Table 2.4.** Results from the oxidation of C2 through C6  $\alpha,\omega$ -diols over 2.69% Pt/C.

Substrate	TOF s <sup>-1</sup>	Conv. %	Selectivity			
			ALD	HA	AA	DA
1,2-ethanediol (EG)	0.032 <sup>a</sup>	14	0	100	0	0
1,3-propanediol (PDO)	0.047 <sup>a</sup>	20	35	54	0	11
1,4-butanediol (BDO)	0.15	16	91	9 <sup>b</sup>	0	0
1,5-pentanediol (PEDO)	0.18	18	86	14	0	0
1,6-hexanediol (HDO)	0.19	20	94	6	0	0
3-hydroxypropionic acid	-	1 <sup>c</sup>	-	-	-	100
6-hydroxyhexanoic acid	0.038 <sup>a</sup>	21	-	-	55	45

Reaction conditions: 0.1 M substrate, substrate:Pt = 500:1 (mol:mol), T = 343 K, pO<sub>2</sub> = 10 bar, 0.35 M acetic acid, pH = 2.5, 2.69% Pt/C. ALD = aldehyde-alcohol, HA =  $\omega$ -hydroxy acid, AA = acid-aldehyde, DA = diacid.

<sup>a</sup> The initial TOF was determined at conversions ranging from 5-8%.

<sup>b</sup> HA selectivity for 1,4-butanediol oxidation was to  $\gamma$ -butyrolactone (GBL), not  $\gamma$ -hydroxybutyric acid (GHB). GBL and GHB have an equilibrium ratio of 68% to 32%, but inter-conversion is slow [22]. Only GBL was observed by HPLC in this study.

<sup>c</sup> Conversion after 4 h of reaction.

In an effort to further explore the reaction path (Figure 2.5) over a Pt catalyst, we compared in Table 2.4 the rates of oxidizing the second alcohol group to that of the first alcohol group. For 3-carbon substrates, we found the oxidation of 1,3-propanediol to be much more rapid than the oxidation of 3-hydroxypropionic acid. In fact, we observed only 1% conversion of 3-hydroxypropionic acid after 4 h. For 6 carbon substrates, the oxidation of 1,6-hexanediol was about 4-5 times faster than the oxidation of 6-hydroxyhexanoic acid. Evidently the rate of oxidizing  $\alpha,\omega$ -diols and  $\omega$ -hydroxy acids increased with increasing chain length, over the range of molecules investigated.



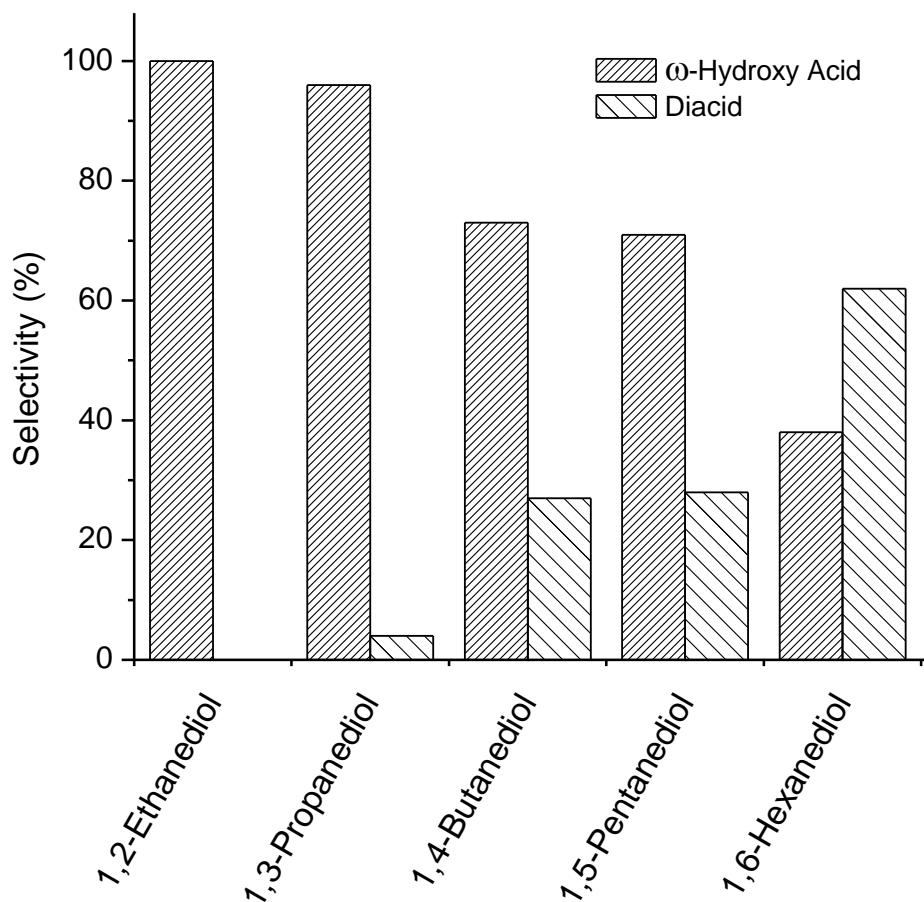


**Figure 2.7.** Product selectivities from the oxidation of various  $\alpha,\omega$ -diols at approximately 90% conversion over 2.69% Pt/C at 343 K, 10 bar  $O_2$ , 0.1 M substrate, and 100:1 substrate:Pt (mol:mol), 0.35 M acetic acid. All carbon balances were greater than 85%.

The product selectivity at 90% conversion of  $\alpha,\omega$ -diols was determined at a substrate to Pt molar ratio of 100 and is summarized in Figure 2.7. In an attempt to achieve the higher conversion a lower ratio of substrate to catalyst (100:1) was utilized, which might have increased the  $O_2$  flux into a mass transfer limited regime. Therefore, only product selectivities will be discussed under these high conversion conditions. The oxidation of 1,2-ethanediol and 1,3-propanediol produced mostly the  $\omega$ -hydroxy acid product, even at high conversion. Increasing the chain length to 4, 5, and 6 carbons resulted in increasing amounts of diacid being produced at 90% conversion. When the oxidation of 1,6-hexanediol was allowed to continue for 24 h (100%

conversion of the diol), the final yield of diacid was 86%. It appears that the C2 and C3  $\alpha,\omega$ -diols were not effectively converted to diacids under conditions that readily convert the C4, C5, and C6  $\alpha,\omega$ -diols to diacids.

The selectivity trends for  $\alpha,\omega$ -diol oxidation over Pt/C shown in Figure 2.7 were consistent with the results reported in Table 2.4 indicating the rate of 3-hydroxypropionic acid was much slower than that of 6-hydroxyhexanoic acid. Even after complete conversion of 1,3-propanediol, the selectivity to the diacid was still below 10%. Evidently, the proximity of the acid group to the alcohol group not only affected the rate of oxidation, but also influenced the final yield of diacid at complete conversion. The oxidation of  $\omega$ -hydroxy acids with homogeneous chromic acid involved a transition state believed to be of a cyclic nature, so that short carbon chain substrates had difficulty with the severe bond angles formed [23, 24]. While the exact mechanism of  $\omega$ -hydroxy acid oxidation has not been determined on supported metals, one might suspect the proximity of the acid group also affects the configuration of the transition state and influences the rate of oxidation.

As discussed above, the length of the carbon chain linking terminal alcohol groups for  $\alpha,\omega$ -diol oxidation appears to be important for both the rate of oxidation of the first alcohol as well as the subsequent oxidation of the second alcohol. To investigate the role of the carbon chain length and proximity of the second alcohol group on oxidation rate, mono-alcohols and various polyols were oxidized over 2.69% Pt/C at identical conditions and the rates are summarized in Table 2.5. The rate of mono-alcohol oxidation was always higher than the corresponding  $\alpha,\omega$ -diol with the same number of carbons. The increase in TOF was especially pronounced for ethanol compared to 1,2-ethanediol (factor of 4.7) and propanol compared to 1,3-propanediol (factor of 3.8), but the same trend was observed for butanol compared to 1,4-

butanediol (factor of 1.5). Thus, the removal of one of the terminal alcohol groups significantly increased the TOF of oxidation over 2.69% Pt/C. It should be mentioned that the rate of methanol oxidation was substantially lower than the other mono-alcohols.

**Table 2.5.** Turnover frequencies for the oxidation of various alcohols over 2.69% Pt/C.

Substrate	TOF (s <sup>-1</sup> )	Relative TOF to Corresponding Carbon Chain $\alpha,\omega$ -Diol <sup>a</sup>
Methanol (C1)	0.010	-
Ethanol (C2)	0.15	4.7
Propanol (C3)	0.18	3.8
Butanol (C4)	0.22	1.5
1,2-Propanediol (C3)	0.039	0.83
1,2-Butanediol (C4)	0.056	0.37
1,2-Hexanediol (C6)	0.14	0.74
1,3-Butanediol (C4)	0.069	0.46
Glycerol (C3)	0.056	1.2
Sorbitol (C6)	0.012	0.063
Benzyl Alcohol (C7)	0.32	-

Reaction conditions: 0.1 M substrate, substrate:Pt = 500:1 (mol:mol), T = 343 K, pO<sub>2</sub> = 10 bar, 0.35 M acetic acid, pH = 2.5, 2.69% Pt/C.

<sup>a</sup> The relative TOF to the  $\alpha,\omega$ -diol with the same number of carbon atoms was determined by: TOF<sub>substrate</sub> / TOF <sub>$\alpha,\omega$ -diol</sub>.

The rate of oxidation of a primary alcohol was also investigated as a function of the proximity of an additional alcohol group in the molecule. The main product of these reactions involved the oxidation of the terminal group only. For the oxidation of four carbon substrates, the order of initial TOF was: butanol > 1,4-butanediol > 1,3-butanediol > 1,2-butanediol. Clearly, the proximity of a secondary alcohol group significantly influenced the rate of oxidation of the primary alcohol group. Likewise, 1,2-hexanediol had a lower TOF than 1,6-hexanediol and 1,2-propanediol had a lower TOF than 1,3-propanediol.

As a comparison, we also examined the oxidation of the polyols glycerol (C3) and sorbitol (C6). Whereas glycerol oxidized at about the same rate as 1,3-propanediol, sorbitol oxidized much slower than 1,6-hexanediol. A slightly faster rate of oxidation for glycerol

compared to 1,3-propanediol at initially neutral conditions has been reported over a Pt-Au/C catalyst at 373 K [19]. During our reaction of sorbitol, the 2.69% Pt/C catalyst appeared to deactivate rapidly within the first thirty minutes of reaction. The deactivation of Pt catalysts during the oxidation of sugars has been reported frequently in the literature at acidic conditions [25]. Given the rapid deactivation observed during sorbitol oxidation, we cannot confidently evaluate an initial rate.

In summary, the proximity of an electron withdrawing group, such as OH or COOH, appeared to slow the oxidation of a primary alcohol. These results suggest that the presence of an electron donating group would enhance the rate of alcohol oxidation. We therefore measured the rate of benzyl alcohol oxidation over 2.69% Pt/C and observed a TOF of  $0.32 \text{ s}^{-1}$ , which was the highest rate of all the substrates tested. The proximity of benzyl and allyl groups to a primary alcohol group has been suggested to increase the rate of the alcohol group oxidation, albeit at basic conditions [26].

## Conclusions

The intrinsic rates of alcohol oxidation were evaluated over carbon-supported Pt catalysts at acidic conditions. The addition of an organic acid additive allowed reproducible TOFs and selectivities to be determined for a wide range of alcohol substrates. To minimize the impact of catalyst deactivation, rates were determined at low conversion and short reaction times. No influences of carbon support or Pt particle size (from 2 - 6 nm) were observed on the rate of 1,6-hexanediol oxidation. Experiments with a variety of  $\alpha,\omega$ -diols, as well as other multifunctional substrates showed how the proximity of electron withdrawing groups negatively impact the terminal alcohol oxidation rates. Further work revealed that as the carbon length of  $\alpha,\omega$ -diols

increased so did the diacid selectivity. A high yield of adipic acid from the oxidation of 1,6-hexanediol could be achieved with Pt/C at acidic conditions or Au/TiO<sub>2</sub> at basic conditions.

## Acknowledgements

I thank Bhushan Zope for his helpful advice in the construction of the semi-batch reactor experimental setup. This material is based upon work supported by the National Science Foundation under Award Nos. EEC-0813570 and OISE 0730277. Helpful discussions with David Hibbitts and Professor Matthew Neurock are also acknowledged.

## References

- [1] T. Werpy and G. R. Petersen, Top value added chemicals from biomass, No. DOE/GO-102004-1992, Department of Energy, Office of Scientific and Technical Information, Washington, DC, 2004.
- [2] Y. Roman-Leshkov, J.N. Chheda, J.A. Dumesic, Phase modifiers promote efficient production of hydroxymethylfurfural from fructose. *Science* 312 (2006) 1933.
- [3] T. Buntara, S. Noel, P.H. Phua, I. Melián-Cabrera, J.G. de Vries, H.J. Heeres, Caprolactam from renewable resources: Catalytic conversion of 5-hydroxymethylfurfural into caprolactone. *Angew. Chem. Int. Ed.* 50 (2011) 7083.
- [4] K. Sato, M. Aoki, R. Noyori, A "green" route to adipic acid: Direct oxidation of cyclohexenes with 30 percent hydrogen peroxide. *Science* 281 (1998) 1646.
- [5] B.G. Hermann, K. Blok, M.K. Patel, Producing bio-based bulk chemicals using industrial biotechnology saves energy and combats climate change. *Environ. Sci. Technol.* 41 (2007) 7915.
- [6] B.N. Zope, S.E. Davis, R.J. Davis, On the mechanism of selective oxidation of 5-hydroxymethylfurfural to 2, 5-furandicarboxylic acid over supported Pt and Au catalysts. *Top. Catal.* 55 (2012) 24.
- [7] S.E. Davis, L.R. Houk, E.C. Tamargo, A.K. Datye, R.J. Davis, Oxidation of 5-hydroxymethylfurfural over supported Pt, Pd and Au catalysts. *Catal. Today* 160 (2011) 55.
- [8] B.N. Zope, R.J. Davis, Inhibition of gold and platinum catalysts by reactive intermediates produced in the selective oxidation of alcohols in liquid water. *Green Chem.* 13 (2011) 3484.
- [9] L. Prati, M. Rossi, Gold on carbon as a new catalyst for selective liquid phase oxidation of diols. *J. Catal.* 176 (1998) 552.

- [10] S. Biella, G.L. Castiglioni, C. Fumagalli, L. Prati, M. Rossi, Application of gold catalysts to selective liquid phase oxidation. *Catal. Today* 72 (2002) 43.
- [11] L. Prati, M. Rossi, Chemoselective catalytic oxidation of polyols with dioxygen on gold supported catalysts. *Stud. Surf. Sci. Catal.* 110 (1997) 509.
- [12] B. Maier, C. Dietrich, J. Büchs, Correct application of the sulphite oxidation methodology of measuring the volumetric mass transfer coefficient  $k_L a$  under non-pressurized and pressurized conditions. *Food Bioprod. Process.* 79 (2001) 107.
- [13] Y. Shao, G. Yin, Y. Gao, Understanding and approaches for the durability issues of Pt-based catalysts for PEM fuel cell. *J. Power Sources* 171 (2007) 558.
- [14] M.A. Lilga, R.T. Hallen, M. Gray, Production of oxidized derivatives of 5-hydroxymethylfurfural (HMF). *Top. Catal.* 53 (2010) 1264.
- [15] M. Heinen, Z. Jusys, R.J. Behm, Ethanol, acetaldehyde and acetic acid adsorption/electrooxidation on a Pt thin film electrode under continuous electrolyte flow: an in situ ATR-FTIRS flow cell study. *The Journal of Physical Chemistry C* 114 (2010) 9850.
- [16] T. Mallat, A. Baiker, Oxidation of alcohols with molecular oxygen on platinum metal catalysts in aqueous solutions. *Catal. Today* 19 (1994) 247.
- [17] B.N. Zope, D.D. Hibbitts, M. Neurock, R.J. Davis, Reactivity of the gold/water interface during selective oxidation catalysis. *Science* 330 (2010) 74.
- [18] T. Mallat, A. Baiker, L. Botz, Liquid-phase oxidation of 1-methoxy-2-propanol with air III: Chemical deactivation and oxygen poisoning of platinum catalysts. *Appl. Catal. A-Gen.* 86 (1992) 147.
- [19] A. Villa, G.M. Veith, L. Prati, Selective oxidation of glycerol under acidic conditions using gold catalysts. *Angew. Chem. Int. Ed.* 49 (2010) 4499.
- [20] L. Prati, P. Spontoni, A. Gaiassi, From renewable to fine chemicals through selective oxidation: the case of glycerol. *Top. Catal.* 52 (2009) 288.
- [21] S. Hirasawa, Y. Nakagawa, K. Tomishige, Selective oxidation of glycerol to dihydroxyacetone over a Pd–Ag catalyst. *Catal. Sci. Tech.* 2 (2012) 1150.
- [22] L.A. Ciolino, M.Z. Mesmer, R.D. Satzger, A.C. Machal, H.A. McCauley, A.S. Mohrhaus, The chemical interconversion of GHB and GBL: forensic issues and implications. *J. Forensic Sci.* 46 (2001) 1315.

- [23] K.G. Srinivasan, J. Rocek, Three-electron oxidations. 13. Intramolecular cooxidation of 2, 7-dihydroxyheptanoic acid: Structure of the transition state in the chromium (VI) oxidation of alcohols. *J. Am. Chem. Soc.* 100 (1978) 2789.
- [24] F. Hasan, J. Rocek, Three-electron oxidations: IX. Chromic acid oxidation of glycolic acid. *J. Am. Chem. Soc.* 97 (1975) 1444.
- [25] S.E. Davis, M.S. Ide, R.J. Davis, Selective oxidation of alcohols and aldehydes over supported metal nanoparticles. *Green Chem.* 15 (2013) 17.
- [26] A.F. Lee, J.J. Gee, H.J. Theyers, Aspects of allylic alcohol oxidation—a bimetallic heterogeneous selective oxidation catalyst. *Green Chem.* 2 (2000) 279.

## Chapter 3: Kinetics and Mechanism of Aqueous Alcohol

### Oxidation over Supported Pt at Acidic Conditions

*A portion of this chapter was previously published as M. S. Ide, R. J. Davis, "Perspectives on the kinetics of diol oxidation over supported platinum catalysts in aqueous solution." Journal of Catalysis (2013), <http://dx.doi.org/10.1016/j.jcat.2013.05.017>.*

#### Introduction

Over the past decade or so, experimental and theoretical studies on the catalytic oxidation of alcohols in aqueous media have revealed important aspects of the reaction path. The recent flurry of research activity on Au catalysts for alcohol oxidation is instructive for understanding the reactivity of Pt catalysts. For example, the role of added base on oxidation catalysis by gold has been the focus of many studies. Carretin et al. first demonstrated the high activity of supported Au particles for glycerol oxidation in basic solutions, which contrasts the inactivity of Au at acidic conditions [1]. Later work by Ketchie et al. found that raising the pH promoted the Au-catalyzed oxidation rate of glycerol by over an order of magnitude compared to that in neutral solution [2]. More specifically, the turnover frequency (TOF) for glycerol oxidation over supported Au catalysts increased almost linearly with increasing concentration of base, regardless of reactor configuration [3].

In a study of ethanol oxidation, density functional theory (DFT) calculations for the ethanol deprotonation step to form an adsorbed ethoxide on Pt(111), Pd(111), and Au(111) in water confirmed that adsorbed hydroxide lowers the activation barrier by an order of magnitude relative to the bare surface [3, 4]. The adsorbed hydroxide acts as a Brønsted base to assist in the deprotonation of ethanol, similar to the alcohol dissociation reaction in basic solution. The activation energy for the dissociation of adsorbed ethanol to ethoxide and hydrogen on bare



Au(111) is approximately twice as high as that on bare Pt(111) and Pd(111) and this higher barrier helps explain why gold is relatively inactive at non-basic conditions for alcohol oxidation. The presence of hydroxide on the surface of Au can also participate in the activation of the C-H bond of the adsorbed alkoxide to form an aldehyde [3]. Huang et al. also showed that supported Au catalysts can be active for 1,4-butanediol oxidation in non-aqueous solvent as long as strongly basic sites are present on the support [5].

The conversion of glycerol at low temperature over supported Au, Pt, and Pd at basic conditions does not proceed without an oxidant, such as dioxygen. Interestingly, multiple studies have reported the order of reaction with respect to dioxygen to be essentially zero for glycerol and 5-hydroxymethyl furfural (HMF) oxidation in semi-batch and flow reactor studies [3, 6-8]. The role of dioxygen in the mechanism has been discussed previously in the literature [9-12]. Isotopic-labeling experiments involving the oxidation of glycerol, ethanol, and HMF in basic aqueous solution over supported Pt and Au showed that when  $^{18}\text{O}_2$  was used as the oxidant no labeled oxygen was incorporated into the acid product [3, 13]. However, when  $\text{H}_2^{18}\text{O}$  was used as the solvent one or more labeled oxygen atoms were incorporated into the acid product. Analogous labeling experiments involving the aqueous phase oxidation of glycerol and HMF over supported Pt in the absence of added base confirmed that water was the source of the oxygen atoms incorporated into the acid product [3, 13]. Thus, the mechanism for aldehyde oxidation to the acid was proposed to proceed through reversible hydration to form a geminal diol followed by dehydrogenation of the diol to form the acid.

Although dioxygen did not provide oxygen atoms that incorporate into the acid product during alcohol oxidation, it was still required for the reaction to proceed. During glycerol oxidation over supported Pt, Pd, and Au, the presence of hydrogen peroxide was detected in the

product solution [2, 14]. The presence of peroxide indicates dioxygen is partially reduced during the reaction. In this way, dioxygen serves as a scavenger of electrons deposited into the metal catalyst during the alcohol oxidation cycle. Supporting evidence from DFT calculations showed that reduction of dioxygen to hydroxide is energetically feasible in these systems [3]. Careful measurement of the solution pH during alcohol oxidation suggests that some of the hydroxide consumed in the reaction is regenerated by dioxygen reduction [6]. The combination of experimental and theoretical results indicates the primary role of dioxygen in the oxidation reaction is to scavenge electrons from the metal catalysts, whereas the water and hydroxide are critical to the transformation of the alcohol to the acid. In fact, electrochemical experiments involving glycerol oxidation in high pH electrolyte over a gold electrode revealed the same distribution of products as those reported over Au catalysts with dioxygen [15]. In the case of the electrochemical experiments, electrons generated at the gold electrode are removed via an external circuit so that dioxygen was not required for oxidation to proceed.

In this work, the influence of dioxygen pressure and substrate concentration on rate was determined at two different startup conditions so that a mechanistic model could be proposed for alcohol oxidation at acidic conditions over supported Pt. In addition, a kinetic isotope effect for ethanol oxidation was probed to determine the kinetically-relevant step of alcohol oxidation. The surface coverage before oxidation begins was assumed to be either an adsorbed alkoxide or hydroxide depending on the startup conditions based on the kinetic experimental data.

## Experimental Methods

### Catalyst preparation

The 2.69 wt% Pt/C was obtained from Aldrich Chemical Co. The 2.69% Pt/C catalyst was reduced in  $100 \text{ cm}^3 \text{ min}^{-1}$  of flowing  $\text{H}_2$  for 4 h at 473 K, cooled, exposed to air, and stored at ambient temperature.

### Catalyst characterization

The metal dispersion of the Pt catalyst was determined by  $\text{H}_2$  chemisorption using a Micromeritics ASAP 2020 automated adsorption analyzer. The supported Pt catalysts were heated to 473 K at  $4 \text{ K min}^{-1}$  under flowing  $\text{H}_2$  (GT&S 99.999%) and reduced for 2 h. The samples were then evacuated and held for 2 h at 473 K before being cooled to 308 K for analysis in the pressure range of 10-450 Torr. The amount of metal on the surface was evaluated by the total amount of  $\text{H}_2$  adsorbed, extrapolated to zero pressure, assuming a stoichiometry ( $\text{H}/\text{Pt}_{\text{surf}}$ ) equal to unity and determined to be 0.57. Elemental analysis (using ICP – AES analysis performed by Galbraith Laboratories, 2323 Sycamore Drive, Knoxville, TN 37921) determined a Pt loading of 2.69 wt% for Pt/C (Aldrich).

### Alcohol oxidation

The semi-batch aqueous alcohol oxidation reactions were performed in a  $50 \text{ cm}^3$  Parr Instrument Company 4592 batch reactor with a  $30 \text{ cm}^3$  glass liner. The appropriate amounts of substrate, acid (to control pH), and catalyst were added to approximately  $10 \text{ cm}^3$  of distilled, deionized water in the glass liner. The glass liner was inserted into the reactor, sealed, purged with He, and heated to 343 K. The reaction was initiated by pressurizing the reactor with 10 bar absolute  $\text{O}_2$  (GT&S, 99.993%). The pressure was maintained at a constant value by continually feeding  $\text{O}_2$ . No conversion was observed after 240 min when  $\text{N}_2$  was substituted for  $\text{O}_2$ . Samples

were periodically removed and the catalyst was filtered using 0.2  $\mu\text{m}$  PTFE filters before analysis with a Waters e2695 high pressure liquid chromatograph (HPLC). The HPLC was equipped with refractive index and UV/Vis detectors. Product separation in the HPLC was carried out with a Aminex HPX-87H column (Bio-Rad) operating at 318 K with 5 mM  $\text{H}_2\text{SO}_4$  in water flowing at 5  $\text{cm}^3 \text{min}^{-1}$ . Carbon balances were always greater than 90% except when specifically mentioned in the text. The retention times and calibration curves were determined by injecting known concentrations of standards.

The initial turnover frequency (TOF) [ $\text{mol alcohol converted} (\text{mol Pt}_{\text{surface}})^{-1} \text{s}^{-1}$ ] for alcohol oxidation was calculated from the initial conversion of the alcohol, usually within the first 15 minutes of the reaction. A sample was also taken at 30 minutes to confirm that significant deactivation had not occurred in the initial rate determination. The maximum  $\text{O}_2$  transport rate from the gas phase to the aqueous phase in the pressurized reaction system was determined by the sulfite oxidation method [16]. The amount of catalyst added to the reactor was chosen so that the alcohol oxidation rate would not be limited by  $\text{O}_2$  mass transfer from the gas to the liquid when determining the TOF. No conversion was found after 240 min in the absence of catalyst.

The concentration of hydrogen peroxide formed during the reaction was quantified using a colorimetric method [17]. After removing the catalyst from 1  $\text{cm}^3$  of sample, the hydrogen peroxide was stabilized by the addition of 1  $\text{cm}^3$  of 0.5 M  $\text{H}_2\text{SO}_4$ . Then, 0.1  $\text{cm}^3$  of 15 wt%  $\text{TiO}(\text{SO}_4)$  in dilute  $\text{H}_2\text{SO}_4$  (Aldrich) was added to the sample and the absorbance was measured at 405 nm on a Varian Cary 3E UV-Vis spectrometer. The calibration curve was established by diluting 30 wt%  $\text{H}_2\text{O}_2$  (Fisher) with distilled deionized water. The detection limit was determined to be 0.1 mM.

## Results and Discussion

### Kinetics of alcohol oxidation to an aldehyde over Pt at acidic conditions

The effect of dioxygen pressure on the initial oxidation of 1,6-hexanediol (HDO) to 6-hydroxyhexanal (aldehyde-alcohol) was investigated from 5 to 20 bar at 303, 323, and 343 K at acidic conditions as shown in

Figure 3.1. Although, the dioxygen pressure was increased by a factor of four at 343 K, the rate of HDO oxidation did not change by more than 10%. In addition, the oxidation of ethanol (EtOH) was determined to be almost zero order with respect to dioxygen pressure. In all cases, the oxidation rate was kept below the known gas-liquid mass transfer limit of our system determined by the sulfite oxidation method [17]. The oxidation of HDO was nearly zero order with respect to dioxygen pressure at all three temperatures investigated, which is similar to reported results for the oxidation of glycerol and 5-hydroxymethyl furfural (HMF) at basic conditions over both Au/TiO<sub>2</sub> and Pt/C ranging from 7 to 20 bar dioxygen pressure [3, 6-8].

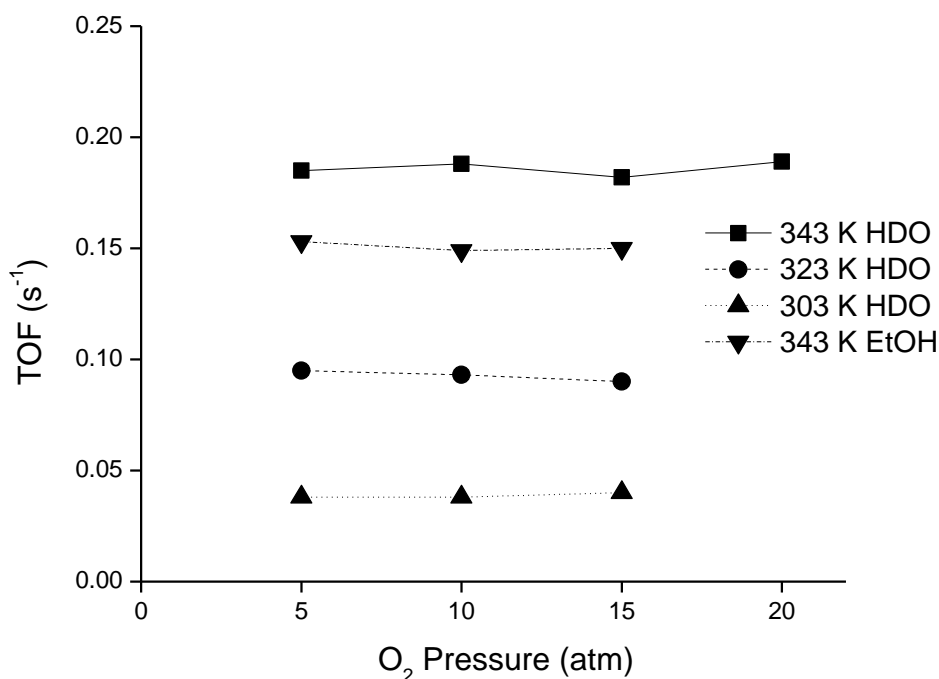


**Figure 3.1.** Influence of dioxygen pressure on the turnover frequency of 1,6-hexanediol (HDO) and ethanol (EtOH) oxidation after inert startup over 2.69% Pt/C from 303 to 343 K at 0.1 M 1,6-hexanediol, 1,6-hexanediol:Pt = 500:1 (mol:mol), 0.35 M acetic acid, pH = 2.5.

The effect of substrate concentration on the oxidation rate was also investigated for 1,6-hexanediol (HDO), 1,3-propanediol (PDO), and ethanol (EtOH) conversion over the range of 0.05 to 0.20 M, as summarized in Figure 3.2. Similar to the results with dioxygen, the oxidation of HDO was found to be nearly zero order with respect to diol concentration at 303, 323, and 343 K. Although the oxidation of PDO was slower than that of HDO, the rate was zero order in both cases. Vleeming et al. studied the oxidation of methyl  $\alpha$ -D-glucopyranoside over Pt at 323 K and a pH of 8 and reported reaction orders of nearly zero for both dioxygen (20 to 100 kPa) and substrate (0.1 to 0.4M) [18]. Vinke et al. also reported the oxidation of 5-hydroxymethyl furfural (HMF) to be nearly zero order with respect to substrate concentration at basic conditions from 0.05 to 0.2 M [19]. Likewise, Villa et al. found the concentration of benzyl alcohol from 0.15 to

0.6 M had a negligible effect on the rate of oxidation over a Au<sub>60</sub>-Pd<sub>40</sub>/activated carbon catalyst in the presence of low concentrations of base [20].

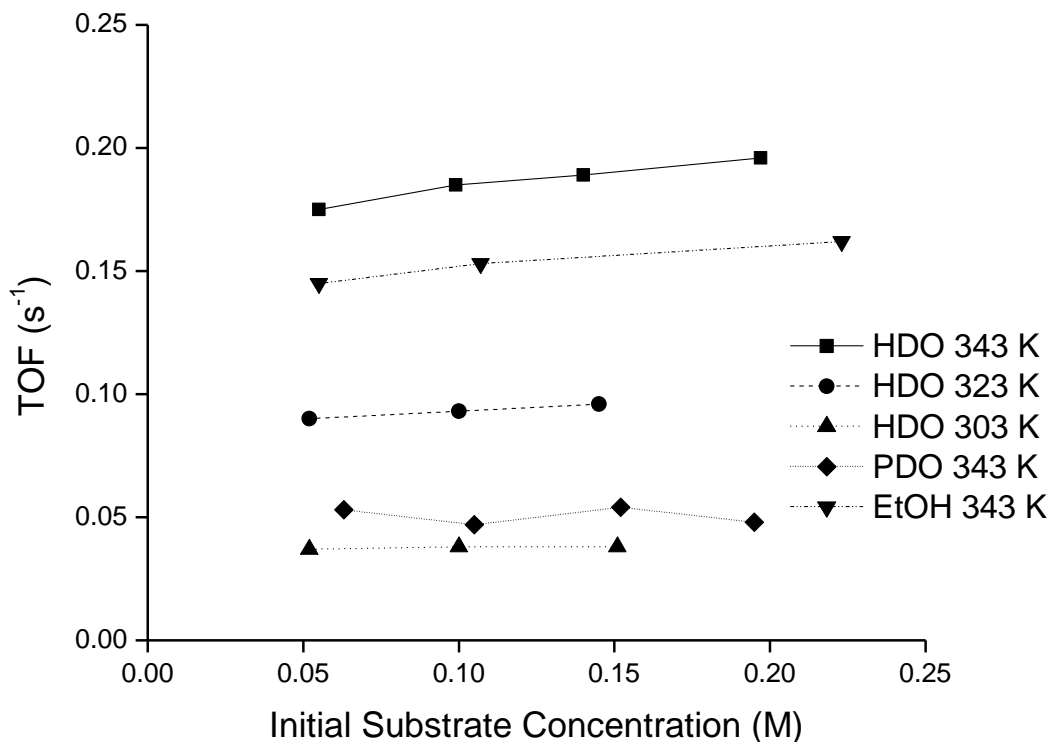


**Figure 3.2.** Influence of substrate concentration on the turnover frequency for 1,6-hexanediol (HDO), 1,3-propanediol (PDO), and ethanol (EtOH) oxidation after inert startup over 2.69% Pt/C from 303 to 343 K at  $pO_2 = 10$  bar, 0.35 M acetic acid, pH = 2.5.

To further explore the kinetics of alcohol oxidation to an aldehyde, the apparent activation energy of 1,6-hexanediol, 1,3-propanediol, and 6-hydroxyhexanoic acid (an intermediate in the sequential oxidation of 1,6-hexanediol) was determined over the temperature range from 303 to 343 K. The Arrhenius-type plots associated with 1,6-hexanediol, 1,3-propanediol, and 6-hydroxyhexanoic acid oxidation are shown in Figure 3.3 together with their corresponding apparent activation energies. The apparent activation energy of 1,6-hexanediol ( $35 \text{ kJ mol}^{-1}$ ) and 1,3-propanediol ( $34 \text{ kJ mol}^{-1}$ ) oxidation were essentially identical. The slightly

higher apparent activation energy for 6-hydroxyhexanoic acid oxidation was consistent with its lower rate of conversion, but was nevertheless in the same range as the other substrates. For comparison, the apparent activation energy of HMF oxidation was reported to be  $37 \text{ kJ mol}^{-1}$  over Pt/C at basic conditions, whereas the apparent activation of 2-propanol oxidation over Pt/C without base was  $38 \text{ kJ mol}^{-1}$  [19, 21].

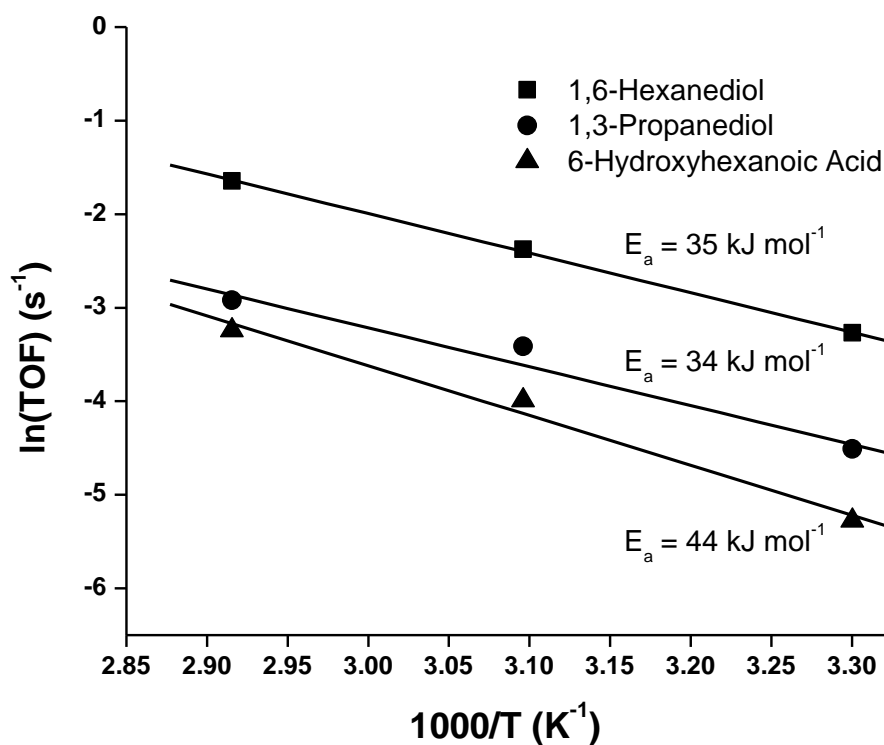


**Figure 3.3.** Arrhenius-type plot from oxidation of 1,6-hexanediol, 1,3-propanediol, and 6-hydroxyhexanoic acid after inert startup over 2.69% Pt/C at 0.1 M substrate, substrate:Pt = 500:1 (mol:mol),  $p\text{O}_2 = 10 \text{ bar}$ , 0.35 M acetic acid,  $\text{pH} = 2.5$ .

### Influence of reactor startup conditions

For all experiments reported thus far, the reaction medium containing alcohol substrate, acetic acid, and reaction medium at 343 K for 30 minutes, dioxygen was added to initiate the reaction. These typical startup conditions are referred to as an inert startup. In contrast, an



oxidative startup is defined by purposefully exposing the catalyst mixed in the water solvent to 10 bar dioxygen at 343 K for one hour before adding the substrate and acetic acid to initiate the reaction. Figure 3.4 compares the effect of substrate concentration on the initial TOF of 1,6-hexanediol (HDO) oxidation at 343 K and acidic conditions after either an inert startup or an oxidative startup. For the 1,6-hexanediol concentration range from 0.05 to 0.40 M, the rate after the inert startup was nearly zero order with respect to concentration (as discussed above), whereas the rate increased with increasing substrate concentration after the oxidative startup. The highest TOF of HDO oxidation after the oxidative startup never exceeded the lowest TOF after the inert startup over this concentration range of substrate. The dependence of the rate on dioxygen pressure was also tested under the oxidation startup procedure and was shown in Figure 3.5 to be nearly zero order for 0.1 M HDO at 343 K.

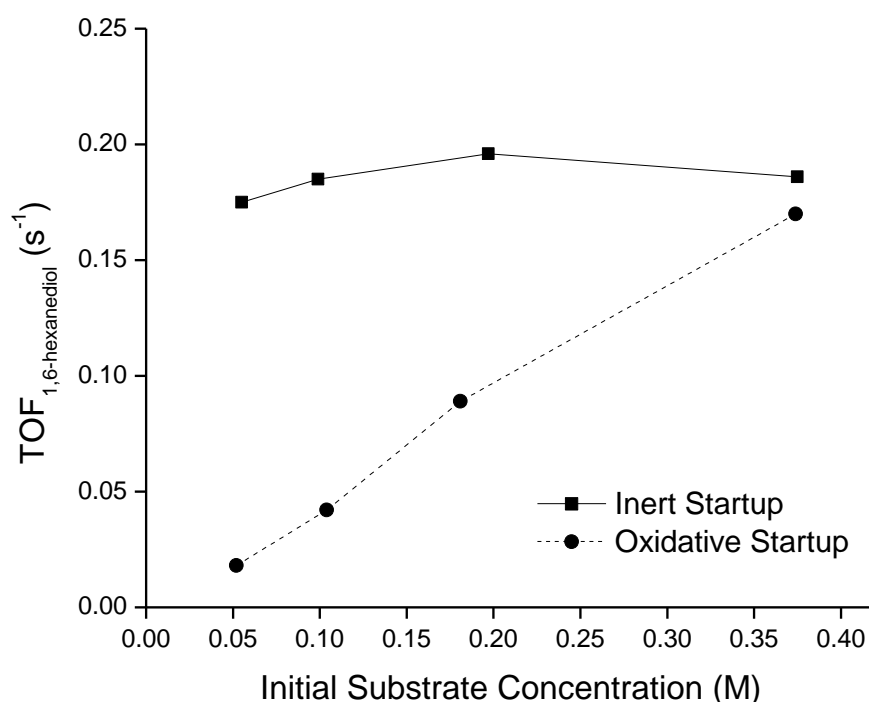


**Figure 3.4.** Influence of substrate concentration on turnover frequency for 1,6-hexanediol oxidation over 2.69% Pt/C after inert or oxidative startup conditions at  $pO_2 = 10$  bar,  $T = 343$  K,  $pH = 2.5$ .

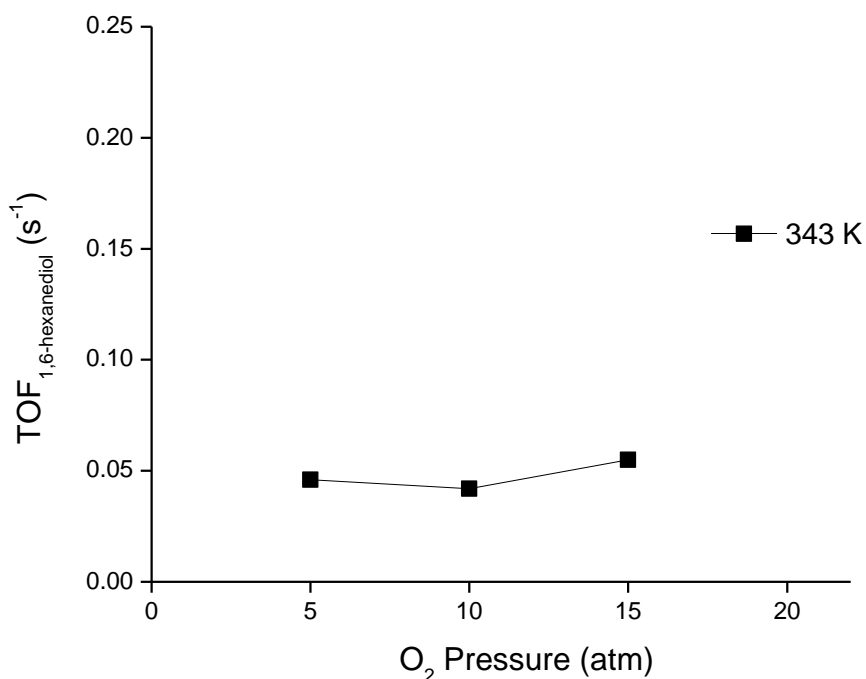


**Figure 3.5.** Influence of dioxygen pressure on the turnover frequency of 1,6-hexanediol (HDO) and ethanol (EtOH) oxidation after oxidative startup over 2.69% Pt/C for 343 K at 0.1 M 1,6-hexanediol, 1,6-hexanediol:Pt = 500:1 (mol:mol), 0.35 M acetic acid, pH = 2.5.

Figure 3.6 summarizes how the initial rate of HDO oxidation increased with increasing concentration of substrate at 303, 323, and 343 K after the oxidative startup conditions. The reaction orders for 1,6-hexanediol concentration and dioxygen pressure over Pt/C at 303, 323, and 343 K were calculated from these experiments and the results are summarized in Table 3.1. Although the reaction order with respect to dioxygen was almost zero regardless of the startup condition, the reaction order with respect to 1,6-hexanediol was about zero after the inert startup but nearly one after the oxidative startup.

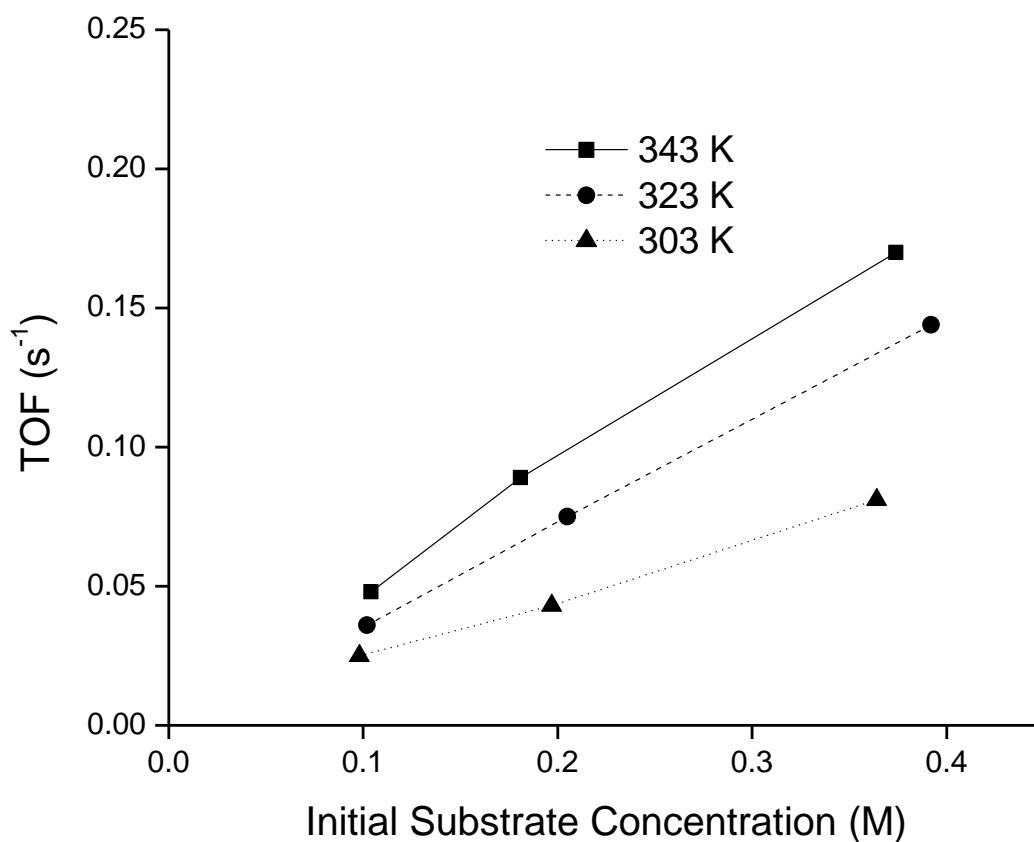


**Figure 3.6.** Influence of substrate concentration on the turnover frequency for 1,6-hexanediol oxidation after oxidative startup over 2.69% Pt/C from 303 K to 343 K at  $pO_2 = 10$  bar,  $pH = 2.5$ .

**Table 3.1.** Reaction orders for 1,6-hexanediol oxidation over 2.69% Pt/C at acidic conditions after inert or oxidative startup conditions.

$T_{RXN}$ (K)	Reaction Order (Inert Startup)		Reaction Order (Oxidative Startup)	
	HDO	$O_2$	HDO	$O_2$
303	0.03	0.04	1.0	-
323	0.06	-0.05	1.0	-
343	0.04	0.01	1.1	0.13

### Proposed kinetic model and kinetic isotope effect

The oxidation of 1,6-hexanediol (HDO) over 2.69% Pt/C at acidic conditions after an inert startup had reaction orders that were nearly zero order with respect to HDO concentration

and dioxygen pressure. The zero order behavior for both reagents is clearly an unusual case and suggests that there are two types of non-competing sites on the platinum surface. This is reminiscent of the dehydrogenation of hydrocarbons over transition metal surfaces where the relatively small H atoms prefer to sit in high-coordination three-fold and four-fold sites, such as those found on low index planes of Pt, and are relatively inaccessible to other species [22]. In our case, we will allow only H atoms to access these special sites denoted as S in our kinetic model, whereas all other species will adsorb on the other metal sites denoted as \*.

A plausible reaction sequence for alcohol oxidation to the aldehyde is provided in Table 3.2. The first step involves the initial deprotonation of the alcohol to ultimately form an adsorbed alkoxide. Recent theoretical work on the deprotonation of ethanol to produce an adsorbed ethoxide on Pt(111) determined the activation energy to be  $116 \text{ kJ mol}^{-1}$ , which was lowered to  $18 \text{ kJ mol}^{-1}$  when the proton transfer was assisted by adsorbed hydroxide [3]. Since the enthalpy of reaction for the hydroxide-assisted deprotonation of ethanol was only  $-5 \text{ kJ mol}^{-1}$ , we considered step 1 to be reversible and equilibrated.

**Table 3.2.** Proposed two site mechanism for alcohol oxidation over supported Pt at acidic conditions.

Step Number	Reaction	Parameter
(1)	$\text{RCH}_2\text{OH} + \text{OH}^* = \text{RCH}_2\text{O}^* + \text{H}_2\text{O}$	$K_1$
(2)	$\text{RCH}_2\text{O}^* + \text{S} \rightarrow \text{RCHO}^* + \text{H-S}$	$k_2$
(3)	$\text{OH}^* + \text{H-S} \rightarrow \text{H}_2\text{O}^* + \text{S}$	$k_3$
(4)	$\text{O}_2 + 2\text{H}_2\text{O} + 4^* = 4\text{OH}^*$	$K_4$

The second step in Table 3.2 is the transfer of an H atom from the adsorbed alkoxide to the metal surface (S) resulting in the production of an adsorbed aldehyde. Theoretical calculations have shown that the C-H activation of adsorbed ethoxide has an activation energy of  $15 \text{ kJ mol}^{-1}$  on bare Pt(111), which increased to  $24 \text{ kJ mol}^{-1}$  when assisted by an adsorbed

hydroxide [3]. Other researchers have considered this C-H activation step to be irreversible and perhaps rate determining [11, 12, 18, 23-25].

**Table 3.3.** Kinetic isotope effect of deuterated ethanol and deuterated oxide over 2.69% Pt/C at acidic conditions after inert startup conditions.

Substrates	TOF (s <sup>-1</sup> )	k <sub>H</sub> /k <sub>D</sub>
CH <sub>3</sub> CH <sub>2</sub> OH + H <sub>2</sub> O	0.15	-
CH <sub>3</sub> CD <sub>2</sub> OH + H <sub>2</sub> O	0.081	1.9
CD <sub>3</sub> CH <sub>2</sub> OH + H <sub>2</sub> O	0.15	1.0
CH <sub>3</sub> CH <sub>2</sub> OH + D <sub>2</sub> O	0.15	1.0
CH <sub>3</sub> DH <sub>2</sub> OH + D <sub>2</sub> O	0.086	1.8

Reaction conditions: 0.1 M substrate, substrate:Pt = 500:1 (mol:mol), T = 343 K, pO<sub>2</sub> = 10 bar, 0.35 M acetic acid, pH = 2.5, 2.69% Pt/C.

In this work, the kinetic isotope effect for ethanol oxidation was evaluated and the results are summarized in Table 3.3. A value of  $k_H/k_D = 1.9$  was observed with ethanol-1,1-D<sub>2</sub> (CH<sub>3</sub>CD<sub>2</sub>OH) as a substrate whereas  $k_H/k_D = 1.0$  was found with ethanol-2,2,2-D<sub>3</sub> (CD<sub>3</sub>CH<sub>2</sub>OH), confirming the kinetic relevance of C-H cleavage. As a control experiment, ethanol oxidation in deuterated oxide (D<sub>2</sub>O) was also performed to explore the importance of OD activation in CH<sub>3</sub>CH<sub>2</sub>OD. The use of D<sub>2</sub>O in place of H<sub>2</sub>O had no effect on the initial TOF of ethanol oxidation. As expected, when both ethanol-1,1-D<sub>2</sub> (CH<sub>3</sub>CD<sub>2</sub>OH) and D<sub>2</sub>O were used in the reactor, a  $k_H/k_D = 1.8$  was observed. In related work, the electro-oxidation of CH<sub>3</sub>OH over a Pt(111) electrode was approximately three times faster than for CD<sub>3</sub>OH at 0.2 V and 0.4 V [26]. Likewise, the oxidation of deuterated benzyl alcohol (C<sub>6</sub>H<sub>5</sub>CD<sub>2</sub>OH) with dioxygen over Au/TiO<sub>2</sub> had a  $k_H/k_D = 1.8$ , albeit in organic solvent [27]. Thus, the observed kinetic isotope effect for ethanol oxidation over Pt at low pH suggests an important kinetic role of the C-H activation step in alcohol oxidation.

The third step in Table 3.2 is the reaction of a surface H atom with adsorbed hydroxide to produce water. The activation energy for the reaction of adsorbed hydrogen with adsorbed hydroxide on Pt(111) was calculated to be  $30 \text{ kJ mol}^{-1}$  but the enthalpy of reaction was highly exothermic [3]. Thus, step three is considered to be irreversible under our conditions.

The final step of the proposed reaction mechanism closes the cycle by regenerating surface hydroxide with the reaction of water and dioxygen. Reactions performed under acidic conditions likely require the adsorbed hydroxide to be produced from water on the Pt surface. Analysis of supported Pt by Weber et al. using X-ray absorption spectroscopy during the electrochemical dioxygen reduction reaction in aqueous solution determined that the surface stoichiometry never exceeded  $\text{PtO}_{0.5}$  even at very high applied potentials [28]. Further work by van den Tillaart et al. showed that flowing dioxygen in the gas phase over Pt/C significantly increased the oxidation state of Pt, revealing coordination numbers of Pt-Pt and Pt-O typical of  $\text{PtO}_2$  [29]. In contrast, the oxidation state of the Pt catalyst in the presence of dioxygen and liquid water was consistent with reduced metal, having a Pt-Pt coordination number of 7.4 and a Pt-O coordination number of only 1.1. The authors concluded that contact of aqueous dioxygen with supported Pt forms an adsorbed surface hydroxide species. More recently, surface science experiments have determined that a hydroxyl can easily be produced by the adsorption of both dioxygen and water on Pt(111) [30-32]. Although dioxygen is needed to complete the catalytic cycle, our experimental results suggest it does not play a kinetic role in the mechanism. In addition, theoretical calculations for the reaction of molecularly adsorbed dioxygen and water on Pt(111) to form a peroxide intermediate (OOH) and an adsorbed hydroxide gave an activation energy of  $18 \text{ kJ mol}^{-1}$  with an enthalpy of reaction of only  $16 \text{ kJ mol}^{-1}$  [3]. We detected a concentration of hydrogen peroxide of approximately 0.15 mM in solution after 4 hours of 1,6-

hexanediol oxidation at 343 K and 10 bar O<sub>2</sub> over Pt/C at acidic conditions. Since peroxide is detected in small amounts, we consider it to be a side product of incomplete dioxygen reduction.

### Rate equation after inert startup conditions

The experimentally-observed zero order behavior in alcohol concentration suggests that the metal catalyst is saturated with an alcohol-derived species, assumed here to be RCH<sub>2</sub>O\* (adsorbed alkoxide). The rate of alcohol oxidation can be written as  $r = \text{rate of step 2} = k_2 [\text{RCH}_2\text{O}^*] [\text{S}]$ , realizing that RCH<sub>2</sub>O\* and S must be adjacent. With the assumptions of saturation coverage of [RCH<sub>2</sub>O\*] and very low hydrogen coverage, the site balances become  $[\text{*}]_0 = [\text{RCH}_2\text{O}^*]$  and  $[\text{S}]_0 = [\text{S}]$  so that the rate of reaction is now independent of substrate and dioxygen and the TOF is proportional to  $k_2$ . A complete derivation of the rate expression is provided in Appendix B.

The implication of the analysis above is that the activation of the C-H bond of an alcohol is the only kinetically-relevant step in the sequence. This might explain why the apparent activation energies for 1,6-hexanediol, 1,3-propanediol, and 6-hydroxyhexanoic acid oxidation in this work and for 2-propanol in the literature were similar. While the activation energy predicted by DFT for the C-H activation of ethoxide on Pt(111) was 15 kJ mol<sup>-1</sup>, the apparent activation energy determined experimentally for 1,6-hexanediol was 35 kJ mol<sup>-1</sup>. However, Calaza et al. demonstrated experimentally and theoretically that high coverage of an adsorbate on the surface can increase the activation energy for reactions involving C-H bond cleavage [33]. Specifically, the activation barrier for the β-hydride elimination of acetoxyethyl on Pd(111) increased from 43 kJ mol<sup>-1</sup> at low coverage to 61 kJ mol<sup>-1</sup> at high coverage. In our case, [RCH<sub>2</sub>O\*] was assumed to be adsorbed at high coverage on the platinum surface and, thus, the measured apparent activation energy is expected to be higher than the activation barrier predicted by DFT at low coverage.

### Rate equation after oxidative startup conditions

The oxidation of 1,6-hexanediol over 2.69% Pt/C at oxidative startup conditions was nearly first order in substrate. Since the oxidative startup involved both O<sub>2</sub> and H<sub>2</sub>O together with Pt initially, we assume the surface is saturated with adsorbed hydroxide, i.e.  $[*]_o = [\text{OH}^*]$ . The suggestion that OH is present on the platinum surface during alcohol oxidation was discussed by Jelemensky et al., who investigated aqueous ethanol oxidation at a pH of 8 in a CSTR under reductive (high ethanol concentration) or oxidative (low ethanol concentration) conditions [25]. Their model proposed that dioxygen and water could react irreversibly to form adsorbed OH and that two OH species could undergo a slow reaction to form adsorbed atomic oxygen and water. Thus, at conditions similar to our oxidative startup, they suggest the surface would be almost fully covered by atomic oxygen, while at conditions similar to our inert startup, the surface would be covered mostly by ethanol. The model did not account for the adsorption of OH directly from the basic solution. In our model, which was developed from results measured under acidic conditions, we assume the surface is covered by an alcohol species after an inert startup and that adsorbed OH is the dominant surface species after an oxidative startup.

The rate of alcohol oxidation can be written as  $r = \text{rate of step 3} = k_3 [\text{OH}^*] [\text{H-S}]$  where  $[\text{H-S}]$  is determined from the steady state approximation (rate step 2 = rate step 3) and the equilibrium relationship established by step 1. Thus, the final rate equation is  $r = k' [\text{RCH}_2\text{OH}] [*]_o [S]_o$ , where  $k'$  is a collection of equilibrium and rate constants. The derived rate expression is first order in alcohol, which is consistent with our observations after oxidative startup conditions. The influence of start-up procedure on the observed reaction kinetics suggests that at least two different kinetic steady state conditions can be achieved, which is constant with the multiple steady states reported in the continuous oxidation of ethanol by Jelemensky et al. [25].



## Conclusions

The kinetics of 1,6-hexanediol oxidation over 2.69% Pt/C were shown to be nearly zero order with respect to dioxygen pressure regardless of startup conditions and nearly zero or first order with respect to substrate concentration depending on whether the startup was inert or oxidative, respectively. A two-site mechanism that describes the alcohol oxidation kinetics was proposed. For a reaction that was started under inert conditions (reduced Pt), the kinetically-relevant step was proposed to be the C-H activation of adsorbed alkoxide and a kinetic isotope effect was observed when  $\text{CH}_3\text{CD}_2\text{OH}$  was used as the substrate. The rate of reaction following an oxidative startup (which presumably has Pt covered with adsorbed hydroxyl) was always lower than that of our inert startup conditions.

## Acknowledgements

I thank Sara Davis for her helpful advice and suggestions when collecting my kinetic data. This material is based upon work supported by the National Science Foundation under Award Nos. EEC-0813570 and OISE 0730277. Helpful discussions with David Hibbitts and Professor Matthew Neurock are also acknowledged.

## References

- [1] S. Carrettin, P. McMorn, P. Johnston, K. Griffin, G.J. Hutchings, Selective oxidation of glycerol to glyceric acid using a gold catalyst in aqueous sodium hydroxide. *Chem. Comm.* 7 (2002) 696.
- [2] W.C. Ketchie, M. Murayama, R.J. Davis, Influence of gold particle size on the aqueous-phase oxidation of carbon monoxide and glycerol. *Top. Catal.* 44 (2007) 307.
- [3] B.N. Zope, D.D. Hibbitts, M. Neurock, R.J. Davis, Reactivity of the gold/water interface during selective oxidation catalysis. *Science* 330 (2010) 74.
- [4] D.D. Hibbitts, M. Neurock, Influence of oxygen and pH on the selective oxidation of ethanol on Pd catalysts. *J. Catal.* 299 (2013) 261.

- [5] J. Huang, Y. Wang, J. Zheng, W. Dai, K. Fan, Influence of support surface basicity and gold particle size on catalytic activity of Au/ $\gamma$ -AlOOH and Au/ $\gamma$ -Al<sub>2</sub>O<sub>3</sub> catalyst in aerobic oxidation of  $\alpha,\omega$ -diols to lactones. *Applied Catalysis B: Environmental* 103 (2011) 343.
- [6] B.N. Zope, S.E. Davis, R.J. Davis, Influence of reaction conditions on diacid formation during Au-catalyzed oxidation of glycerol and hydroxymethylfurfural. *Top. Catal.* 55 (2012) 24.
- [7] S.E. Davis, L.R. Houk, E.C. Tamargo, A.K. Datye, R.J. Davis, Oxidation of 5-hydroxymethylfurfural over supported Pt, Pd and Au catalysts. *Catal. Today* 160 (2011) 55.
- [8] W. Ketchie, Y. Fang, M. Wong, M. Murayama, R. Davis, Influence of gold particle size on the aqueous-phase oxidation of carbon monoxide and glycerol. *J. Catal.* 250 (2007) 94.
- [9] V. Gangwal, J. Vanderschaaf, B. Kuster, J. Schouten, Influence of pH on noble metal catalysed alcohol oxidation: reaction kinetics and modeling. *J. Catal.* 229 (2005) 389.
- [10] C. Keresszegi, T. Burgi, T. Mallat, A. Baiker, On the role of oxygen in the liquid-phase aerobic oxidation of alcohols on palladium. *J. Catal.* 211 (2002) 244.
- [11] J.A.A. van den Tillaart, B.F.M. Kuster, G.B. Marin, Platinum particle size effect on the oxidative dehydrogenation of aqueous ethanol. *Catal. Lett.* 36 (1996) 31.
- [12] L. Jelemensky, B.F.M. Kuster, G.B. Marin, Relaxation processes during the selective oxidation of aqueous ethanol with oxygen on a platinum catalyst. *Ind. Eng. Chem. Res.* 36 (1997) 3065.
- [13] S.E. Davis, B.N. Zope, R.J. Davis, On the mechanism of selective oxidation of 5-hydroxymethylfurfural to 2, 5-furandicarboxylic acid over supported Pt and Au catalysts. *Green Chem.* 14 (2012) 143.
- [14] V. R. Gangwal, J. van der Schaaf, B. F. M. Kuster, J. C. Schouten, Noble-metal-catalysed aqueous alcohol oxidation: reaction start-up and catalyst deactivation and reactivation *J. Catal.* 232 (2005) 432.
- [15] Y. Kwon, S.C. Lai, P. Rodriguez, M.T. Koper, Electrocatalytic oxidation of alcohols on gold in alkaline media: base or gold catalysis? *J. Am. Chem. Soc.* 133 (2011) 6914.
- [16] B. Maier, C. Dietrich, J. Büchs, Correct application of the sulphite oxidation methodology of measuring the volumetric mass transfer coefficient  $k_La$  under non-pressurized and pressurized conditions. *Food Bioprod. Process.* 79 (2001) 107.
- [17] C.N. Satterfield, A.H. Bonnell, Interferences in titanium sulfate method for hydrogen peroxide. *Anal. Chem.* 27 (1955) 1174.

- [18] J.H. Vleeming, B.F.M. Kuster, G.B. Marin, Selective oxidation of methyl  $\alpha$ -D-glucopyranoside with oxygen over supported platinum: Kinetic modeling in the presence of deactivation by overoxidation of the catalyst. *Ind. Eng. Chem. Res.* 36 (1997) 3541.
- [19] P. Vinke, H.E. van Dam, H. van Bekkum, Platinum catalyzed oxidation of 5-hydroxymethylfurfural. *Stud. Surf. Sci. Catal.* 55 (1990) 147.
- [20] A. Villa, N. Janjic, P. Spontoni, D. Wang, D.S. Su, L. Prati, Au–Pd/AC as catalysts for alcohol oxidation: Effect of reaction parameters on catalytic activity and selectivity. *Appl. Catal. A* 364 (2009) 221.
- [21] J.W. Nicoletti, G.M. Whitesides, Liquid-phase oxidation of 2-propanol to acetone by dioxygen using supported platinum catalysts. *J. Phys. Chem.* 93 (1989) 759.
- [22] M.A. Vannice, *Kinetics of Catalytic Reactions*, Springer Science, New York, NY, 2005.
- [23] J.H.J. Kluytmans, A.P. Markusse, B.F.M. Kuster, G.B. Marin, J.C. Schouten, Engineering aspects of the aqueous noble metal catalysed alcohol oxidation. *Catal. Today* 57 (2000) 143.
- [24] J.A.A. van den Tillaart, B.F.M. Kuster, G.B. Marin, Oxidative dehydrogenation of aqueous ethanol on a carbon supported platinum catalyst. *Appl. Catal. A* 120 (1994) 127.
- [25] L. Jelemensky, B.F.M. Kuster, G.B. Marin, Kinetic modelling of multiple steady-states for the oxidation of aqueous ethanol with oxygen on a carbon supported platinum catalyst. *Chem. Eng. Sci.* 51 (1996) 1767.
- [26] K. Franaszczuk, E. Herrero, P. Zelenay, A. Wieckowski, J. Wang, R.I. Masel, A comparison of electrochemical and gas-phase decomposition of methanol on platinum surfaces. *J. Phys. Chem.* 96 (1992) 8509.
- [27] P. Fristrup, L.B. Johansen, C.H. Christensen, Mechanistic investigation of the gold-catalyzed aerobic oxidation of alcohols. *Catal. Lett.* 120 (2007) 184.
- [28] R.S. Weber, M. Peuckert, R.A. DallaBetta, M. Boudart, Oxygen reduction on small supported platinum particles II: Characterization by X-ray absorption spectroscopy. *J. Electrochem. Soc.* 135 (1988) 2535.
- [29] J.A.A. van den Tillaart, B.F.M. Kuster, G.B. Marin, in: S.T. Oyama and J.W. Hightower (Eds.), *Catalytic Selective Oxidation*, American Chemical Society, 1993, p. 298.
- [30] C. Clay, S. Haq, A. Hodgson, Growth of intact water ice on Ru(0001) between 140 and 160 K: Experiment and density-functional theory calculations. *Phys. Rev. Lett.* 92 (2004) 68.
- [31] W. Lew, M.C. Crowe, E. Karp, C.T. Campbell, Energy of molecularly adsorbed water on clean Pt (111) and Pt (111) with coadsorbed oxygen by calorimetry. *The J. Phys. Chem. C* 115 (2011) 9164.

[32] S. Völkening, K. Bedürftig, K. Jacobi, J. Wintterlin, G. Ertl, Dual-path mechanism for catalytic oxidation of hydrogen on platinum surfaces. *Phys. Rev. Lett.* 83 (1999) 2672.

[33] F. Calaza, D. Stacchiola, M. Neurock, W.T. Tysoe, Coverage effects on the palladium-catalyzed synthesis of vinyl acetate: Comparison between theory and experiment. *J. Am. Chem. Soc.* 132 (2010) 2202.

## Chapter 4: Deactivation of Supported Pt Catalysts during

### Alcohol Oxidation

*The work in this chapter was the basis for portions of the publication, M. S. Ide, D. D. Falcone, R. J. Davis, "On the Deactivation of Supported Pt Catalysts for Selective Oxidation of Alcohols," in preparation.*

#### Introduction

The production of high-value chemicals from biomass is a promising strategy to economically convert bio-renewable carbohydrates. The selective oxidation of alcohols derived from biomass feedstocks is a particularly attractive route when the oxidation can be performed in an environmentally friendly manner [1]. The selective oxidation of alcohols to acids in water over heterogeneous catalysts with molecular oxygen as the oxidant is a green chemistry alternative to traditional petrochemical oxidation reactions with toxic, inorganic oxidants [2]. Two prominent examples of green oxidation reactions are the conversion of glycerol to glyceric acid, a valuable additive for cosmetics, and the transformation of 5-hydroxymethylfurfural to 2,5-furandicarboxylic acid, a monomer for bio-renewable plastics [3,4].

One of the major challenges of alcohol oxidation catalysis by supported metals is deactivation. The deactivation of Pt catalysts during alcohol oxidation [5] and electro-oxidation [6] has been suggested to be a major barrier to commercialization. Although common modes of catalyst deactivation, such as metal particle sintering or metal leaching might contribute to observed behavior, a common explanation for platinum deactivation during alcohol oxidation is the formation of an inactive oxide surface layer produced by the over-oxidation of the Pt catalyst [7-12]. Indeed, irreversible deactivation of Pt is speculated by some to be caused by oxygen atoms that penetrate the Pt lattice and form sub-oxides that are not easily reduced by the alcohol

substrate [13-16]. In contrast, there is some evidence that Pt is fairly resistant to oxidation by dioxygen in the presence of water [17]. Another explanation of Pt deactivation during alcohol oxidation is the strong adsorption of byproducts produced during the reaction [18]. For example, base-catalyzed aldol condensation reactions of products formed in alkaline solutions yield species capable of strongly adsorbing to the Pt surface [19-21]. Furthermore, during the electro-oxidation of 1,2-ethanediol and methyl- $\alpha$ -D-glucopyranoside over Pt in basic electrolyte solution, CO was observed by infrared (IR) spectroscopy to be adsorbed to the Pt surface [22]. Similar evidence for the formation of adsorbed CO during electro-oxidation has been reported for 1,3-propanediol,[23] benzyl alcohol,[24] and glycerol [25]. In addition to CO, IR spectroscopy also revealed evidence of strongly adsorbed hydrocarbon species ( $C_xH_y$ ) formed during the electro-oxidation of glycerol on the Pt surface. The poisoning of Pt electrodes by CO during electro-oxidation of alcohols has been recognized for more than two decades [26].

Recent studies of glycerol oxidation in aqueous solution over Pt/C have reported the formation of  $CO_2$  at acidic conditions and moderate temperature (373 K) [27-28]. The oxidation of CO from the C-C bond breaking of glycerol by Pt was suggested as the origin of  $CO_2$ . In-situ ATR-IR spectroscopy identified CO as an adsorbed species during the anaerobic dehydrogenation of benzyl alcohol in cyclohexane on Pd/ $Al_2O_3$  [29-30]. The adsorbed CO was produced via benzaldehyde decarbonylation and blocked further benzyl alcohol dehydrogenation. Adsorbed CO was also identified by ATR-IR spectroscopy during the liquid phase anaerobic dehydrogenation of benzyl alcohol over Pt/ $Al_2O_3$  in toluene at 323 K [31] The role of surface adsorbates on Pt during aqueous alcohol oxidation and what affect, if any, they have in the deactivation of supported Pt is particularly intriguing.

The goal of this work is to explore the various modes of deactivation of supported platinum catalysts used for alcohol oxidation reactions to elucidate the appropriate strategies for improving catalyst stability. The dissolution of Pt metal, sintering of Pt nanoparticles, over-oxidation of the Pt surface, and poisoning by strongly adsorbed products formed in solution or on the Pt surface were all investigated. Although we investigated the oxidation of both mono-alcohol and diol substrates, most of our work focused on the oxidation of 1,6-hexanediol because of its potential importance in the production of bio-renewable adipic acid [32].

## **Experimental Methods**

### **Catalyst preparation**

The 2.69 wt% Pt/C and the 4.86% Pt/Al<sub>2</sub>O<sub>3</sub> were obtained from Aldrich Chemical Co. The Pt/C catalyst was reduced in 100 cm<sup>3</sup> min<sup>-1</sup> of flowing H<sub>2</sub> for 4 h at 473 K, cooled, exposed to air, and stored at ambient temperature. The SiO<sub>2</sub> (Davidson) supported Pt (2 wt%) and TiO<sub>2</sub> (Degussa P25) supported Pt (3 wt%) were prepared by incipient wetness impregnation of chloroplatinic acid (Sigma-Aldrich). The 2% Pt/SiO<sub>2</sub> and 3% Pt/TiO<sub>2</sub> catalysts were dried in air for 12 h at 393 K followed by calcination in 100 cm<sup>3</sup> min<sup>-1</sup> of flowing air for 4 h at 673 K. The catalysts were then reduced in 100 cm<sup>3</sup> min<sup>-1</sup> of flowing H<sub>2</sub> for 4 h at 673 K, cooled, exposed to air, and stored at ambient temperature. A boron nitride supported Pt (5 wt%) catalyst was prepared in a similar manner to the oxide supported catalysts, except the 5% Pt/BN was not calcined and was reduced for 4 h at only 473 K.

### **Catalyst characterization**

The metal dispersion of the Pt catalysts was determined by H<sub>2</sub> chemisorption using a Micromeritics ASAP 2020 automated adsorption analyzer. The supported Pt catalysts were heated to 473 K at 4 K min<sup>-1</sup> under flowing H<sub>2</sub> (GT&S 99.999%) and reduced for 2 h. The

samples were then evacuated and held for 2 h at 473 K before being cooled to 308 K for analysis in the pressure range of 10-450 Torr. The amount of metal on the surface was evaluated by the total amount of H<sub>2</sub> adsorbed, extrapolated to zero pressure, assuming a stoichiometry (H/Pt<sub>surf.</sub>) equal to unity.

The elemental analysis (using ICP – AES performed by Galbraith Laboratories, 2323 Sycamore Drive, Knoxville, TN 37921) determined a Pt loading of 2.69 wt% for the Pt/C catalyst and 4.86 wt% for the Pt/Al<sub>2</sub>O<sub>3</sub> catalyst. The leaching of Pt into solution was measured by elemental analysis of the filtrate after 24 h of 1,6-hexanediol oxidation for Pt/C and Pt/Al<sub>2</sub>O<sub>3</sub>.

To prepare the fresh and used 2.69% Pt/C sample for transmission electron microscopy (TEM), ~1 mg of sample was suspended in 2 cm<sup>3</sup> of ethanol by agitating the mixture for 30 minutes in a sonication bath. A copper grid with a holey carbon film was briefly dipped in the solution and the ethanol was then evaporated. The imaging of the catalyst was performed on a FEI Titan operating at 180 kV and equipped with a Gatan 794 Multi-scan Camera (EFTEM). The used Pt/C sample for TEM was obtained after 24 h of 1,6-hexanediol oxidation at 343 K.

### **Alcohol oxidation**

The semi-batch aqueous alcohol oxidation reactions were performed in a 50 cm<sup>3</sup> Parr Instrument Company 4592 batch reactor with a 30 cm<sup>3</sup> glass liner. The appropriate amounts of substrate, acetic acid (to lower the pH), and catalyst were added to approximately 10 cm<sup>3</sup> of distilled, deionized water in the glass liner. The importance of organic acid for evaluation of alcohol oxidation kinetics over Pt has been discussed in Chapter 2 [32]. The glass liner was inserted into the reactor, sealed, purged with He, and heated to 343 K. The reaction was initiated by pressurizing the reactor with 10 bar absolute O<sub>2</sub> (GT&S, 99.993%). The pressure was



maintained at a constant value by continually feeding O<sub>2</sub>. No conversion was observed after 240 min when N<sub>2</sub> was substituted for O<sub>2</sub>.

Samples were periodically removed and the catalyst was filtered using 0.2 μm PTFE filters before analysis with a Waters e2695 high pressure liquid chromatograph (HPLC). The HPLC was equipped with refractive index and UV/Vis detectors. Product separation in the HPLC was carried out with a Aminex HPX-87H column (Bio-Rad) operating at 318 K with 5 mM H<sub>2</sub>SO<sub>4</sub> in water flowing at 5 cm<sup>3</sup> min<sup>-1</sup>. The retention times and calibration curves were determined by injecting known concentrations of standards. The initial turnover frequency (TOF) [mol alcohol converted (mol Pt<sub>surface</sub>)<sup>-1</sup> s<sup>-1</sup>] for alcohol oxidation was calculated from the initial conversion of the alcohol, usually within the first 15 minutes of the reaction. Selectivity to a specific product is defined as moles of that product formed divided by moles of all products produced. For the recycle experiments, the catalyst was recovered from solution by centrifugation at 4000 RPM for 30 min. The catalyst was then washed with DI water and subsequently recovered ten times to remove loose surface contaminants before re-use in oxidation experiments.

The evaluation of headspace gas was performed after batchwise aqueous alcohol at 343 K and 3 bar of dioxygen. After 20 h, the gas in the headspace volume was analyzed by a gas chromatograph (HP 5890 Series II) equipped with a thermal conductivity detector (TCD) for detection and quantification of CO<sub>2</sub>, O<sub>2</sub>, and CH<sub>4</sub> with known response factors [33]. Gas separation was carried out with a ShinCarbon ST 80/100 packed column. The pressure of the headspace did not change significantly during the reaction. When a blank experiment with just the Pt/C catalyst was performed (no substrate), a small amount of CO<sub>2</sub> was observed. This background amount of CO<sub>2</sub> was subtracted from all other experiments that used Pt/C as the

catalyst. The oxidation of ethylene glycol (EG) without a catalyst produced negligible amounts of CO<sub>2</sub>.

## Results and Discussion

### Catalyst characterization

The Pt weight loading and metal dispersion of the carbon, boron nitride and oxide supported Pt catalysts are provided in Table 4.1. The 2.69% Pt/C catalyst has been extensively characterized in Chapter 2 [32]. The fraction of platinum exposed, also referred to as dispersion (d), was determined by hydrogen chemisorption for all of the catalysts. The Pt/C, Pt/SiO<sub>2</sub>, and Pt/TiO<sub>2</sub> catalysts had similar platinum dispersions (0.57 - 0.65) and thus similar estimated particle sizes (1/d) of about 2 nm. The Pt/Al<sub>2</sub>O<sub>3</sub> sample had a lower dispersion compared to the other oxide supported catalysts. The Pt/BN catalyst had a very low dispersion (0.1), despite the lower reduction temperature of 473 K compared to 673 K for the oxide supported catalysts. The low surface area (24 m<sup>2</sup> g<sup>-1</sup>) of boron nitride and absence of surface functional groups to anchor platinum may have contributed to the low dispersion [34]. Figure 4.1(a) shows a TEM image of the fresh Pt/C sample revealing an average diameter of 1.7 nm ± 1.2 nm, which is consistent with chemisorption.

**Table 4.1.** Summary of catalyst characterization results.

Catalyst	Pt (wt%)	Dispersion (H/Pt)	Pt particle size (nm)	
			H <sub>2</sub> <sup>c</sup>	TEM
Pt/C	2.69	0.57	1.8	1.7 ± 1.2
Pt/C (Used)	2.65 <sup>a</sup>	-	-	1.9 ± 1.5
Pt/BN	5 <sup>b</sup>	0.10	10	
Pt/SiO <sub>2</sub>	2 <sup>b</sup>	0.65	1.6	
Pt/TiO <sub>2</sub>	3 <sup>b</sup>	0.63	1.6	
Pt/Al <sub>2</sub> O <sub>3</sub>	4.86	0.24	4.2	

<sup>a</sup> Calculated by subtracting leached Pt.

<sup>b</sup> Nominal weight loading.

<sup>c</sup> Estimated as the inverse of the dispersion.

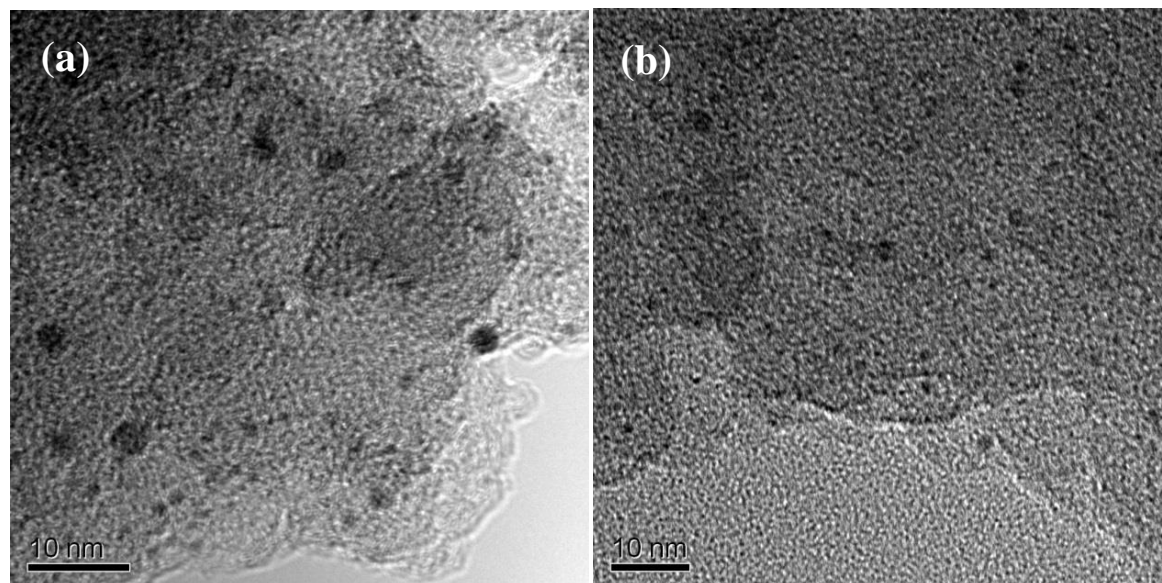


**Figure 4.1.** Comparison of (a) fresh and (b) deactivated 2.69% Pt/C catalyst with bright field TEM images.

### Deactivation of Pt during alcohol oxidation

Figure 4.2 depicts reaction profiles of various alcohols oxidized over Pt/C in liquid water at 343 K. In particular, the influence of acetic acid on the profile of 1,6-hexanediol oxidation is directly compared. The rate of conversion of 1,6-hexanediol decreased significantly after about 1h regardless of the presence of acetic acid. The inhibition of the initial rate of 1,6-hexanediol oxidation over Pt/C by organic acids was explored in other work [32]. While the initial rate of 1,6-hexanediol oxidation was a little greater ( $0.27 \text{ s}^{-1}$ ) without acetic acid compared to when acetic acid was present ( $0.19 \text{ s}^{-1}$ ), the reaction profile was similar and the conversion of 1,6-hexanediol after 4 h was approximately the same. Thus, regardless of whether organic acid was present at the start of the reaction or produced in-situ by the oxidation of 1,6-hexanediol to 6-hydroxyhexanoic acid, the Pt/C catalyst deactivated in a similar manner. An increase in the concentration of acetic acid from 0.35 M to 0.7 M at the start of the reaction neither changed the

initial rate of 1,6-hexanediol oxidation nor the reaction profile of oxidation (not shown). It should be noted that under the conditions of this study, the order of reaction with respect to 1,6-hexanediol is zero, suggesting the decrease in rate with time as illustrated in Figure 4.2 is the result of catalyst deactivation [32].

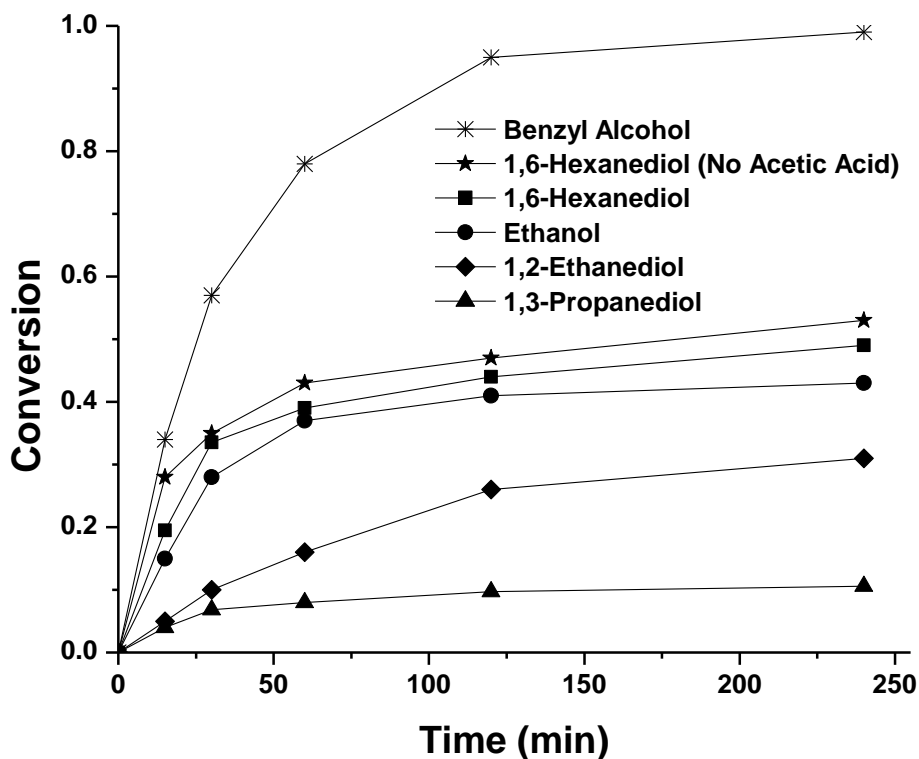


**Figure 4.2.** Reaction profile of benzyl alcohol, 1,6-hexanediol, ethanol, 1,2-ethanediol, and 1,3-propanediol oxidation over 2.69% Pt/C with 0.1 M substrate, substrate:Pt = 500:1 (mol:mol), and 0.35 M acetic acid at 10 bar O<sub>2</sub> and 343 K.

The oxidation of ethanol, 1,2-ethanediol, and 1,3-propanediol over Pt/C in the presence of acetic acid also gave reaction profiles consistent with significant catalyst deactivation with the first hour of oxidation (Figure 4.2). Ethanol and 1,6-hexanediol had initial rates of oxidation that were approximately four times faster than that of 1,2-ethanediol and 1,3-propanediol [32], yet the Pt/C catalyst appeared to deactivate on a similar time scale. Interestingly, the oxidation of 1,2-

ethanediol showed just a minor decrease in oxidation activity up to 2 h, but the rate slowed considerably after that. The reaction profile of benzyl alcohol oxidation over Pt/C did not reveal significant deactivation compared to all of the other substrates investigated at these conditions, but severe Pt deactivation during benzyl alcohol oxidation has been reported [35].

Figure 4.3 displays the reaction profiles for 1,6-hexanediol over Pt/C, Pt/BN, Pt/Al<sub>2</sub>O<sub>3</sub>, Pt/TiO<sub>2</sub>, and Pt/SiO<sub>2</sub>. Regardless of the support for the Pt nanoparticles, a decrease in the initial rate of oxidation was observed after about 1 h. The low TOF observed over Pt/SiO<sub>2</sub> and Pt/TiO<sub>2</sub> compared to all of the other samples (Table 4.2) was unexpected and we do not yet have an explanation for this phenomenon. Nevertheless, the deactivation of Pt during 1,6-hexanediol oxidation was consistent across the entire range of support and Pt particle sizes used in this study.

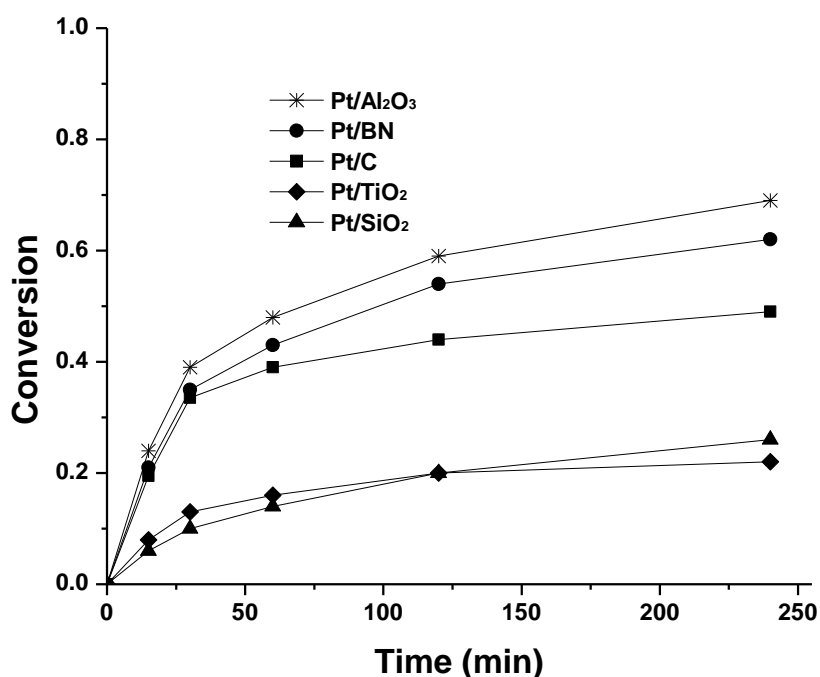


**Figure 4.3.** Reaction profile of 1,6-hexanediol oxidation over Pt/Al<sub>2</sub>O<sub>3</sub>, Pt/BN, Pt/C, Pt/TiO<sub>2</sub>, and Pt/SiO<sub>2</sub> with 0.1 M 1,6-hexanediol, 1,6-hexanediol:Pt = 500:1 (mol:mol), and 0.35 M acetic acid at 10 bar O<sub>2</sub> and 343 K.

**Table 4.2.** Results from the oxidation of 1,6-hexanediol.

Catalyst	TOF (s <sup>-1</sup> )	Conv. (%)	Liquid Sel. (%)	
			ALD	HA
2.69% Pt/C	0.19	20	94	6
5% Pt/BN	0.20	22	96	4
2% Pt/SiO <sub>2</sub>	0.04	7	100	0
3% Pt/TiO <sub>2</sub>	0.06	8	100	0
4.86% Pt/Al <sub>2</sub> O <sub>3</sub>	0.24	14	100	0

Reaction conditions: 0.1 M 1,6-hexanediol, 1,6-hexanediol:Pt = 500:1 (mol:mol), T = 343 K, pO<sub>2</sub> = 10 bar, 0.35 M acetic acid, pH = 2.5, ALD = 6-hydroxyhexanal and HA = 6-hydroxyhexanoic acid.

### Investigation of leaching and sintering

The irreversible deactivation of a supported Pt catalyst during alcohol oxidation by physical modification of the surface through leaching or sintering could significantly decrease catalyst activity. The leaching of platinum into aqueous solution at low pH is mentioned frequently in the electro-oxidation literature [36]. To determine the extent of platinum leaching from the 2.69% Pt/C catalyst, elemental analysis of the filtrate was performed after 24 h of 1,6-hexanediol oxidation. Table 4.3 shows that 1.5% of the total amount of Pt loaded in the reactor leached into solution. When an identical experiment was performed with 4.86% Pt/Al<sub>2</sub>O<sub>3</sub>, approximately 0.82% of the total available Pt and 2.9% of the total Al leached into solution. The dissolution of the alumina support by corrosion or leaching at acidic conditions may contribute to the presence of Pt in solution.

**Table 4.3.** Elemental analysis of filtrate after 24 h of 1,6-hexanediol oxidation.

Catalyst	Adipic Acid Yield (%)	Pt leached <sup>a</sup> (%)	Adipic Acid:Leached Pt (mol:mol)
2.69% Pt/C	85%	1.5	6,400
4.86% Pt/Al <sub>2</sub> O <sub>3</sub> <sup>b</sup>	91%	0.82	8,900

Reaction conditions: 0.1 M 1,6-hexanediol, 1,6-hexanediol:Pt = 100:1 (mol:mol), T = 343 K, pO<sub>2</sub> = 10 bar, 24 h.

<sup>a</sup> Pt leached (%) = [(mol Pt leached)/(total mol Pt in reactor) \* 100]

<sup>b</sup> Al leached is 2.9% of total Al in the reactor.

The presence of carboxylic acids in solution have been associated with the promotion of Pt leaching from the catalytic surface [37]. During the oxidation of 1,6-hexanediol, the pH of solution decreased from 6.5 to 2.5 as 100% conversion of 1,6-hexanediol produced an 85% yield of adipic acid. The ratio of adipic acid to leached Pt was approximately 6,400, thus, the adipic acid with a  $pK_{a1} = 4.43$  did not appear to cause considerable leaching of Pt. In the literature, a small amount of Pt was reported to leach into solution even at basic conditions. Prati et al. determined that a 5% Pt/C catalyst leached approximately 2% of the total platinum metal available after four 2 h recycle experiments involving glycerol oxidation at 323 K and a pH of 13 [38]. After the oxidation of 5-hydroxymethylfurfural at 373 K and a pH of 8, approximately 2-3% of the available platinum had leached from a 5.1% Pt/C catalyst after 12 h [39]. The oxidation of methyl  $\alpha$ -D-glucopyranoside over Pt/C had a 4% loss of platinum after five 8 h recycle experiments at 323 K and a pH of 9 [40]. The leaching of small amounts of Pt into the aqueous solution after 24 h of alcohol oxidation is not ideal for industrial application; however, the low level of Pt leaching does not appear to significantly contribute to the significant deactivation of the catalyst observed after just 4 h.

The sintering of metal nanoparticles can occur by metal atom migration across the support or by metal dissolution followed by re-deposition onto other metal nanoparticles (Ostwald ripening). Either process would increase the average particle size of the catalyst. The severe sintering of graphite-supported Pt at 363 K in aqueous solution in a hydrogen atmosphere has been reported in the literature [40]. Thus, the Pt particle size of the Pt/C catalyst was evaluated by TEM before and after the oxidation of 1,6-hexanediol for 24 h at 343 K and acidic aqueous conditions. Figure 4.1 shows that the Pt particle size slightly increased from 1.7 nm for the fresh catalyst to 1.9 nm for the used catalyst (Table 4.1). The decrease in Pt metal dispersion

from approximately 59% to 53% is small compared to the severe decrease in alcohol oxidation rate after 24 h.

Despite numerous reports of Pt deactivation during aqueous alcohol oxidation, sintering has been infrequently investigated in the literature. After the oxidation of methyl  $\alpha$ -D-glucopyranoside over Pt/C at 323 K for 2.8 h at basic conditions (pH = 9), a small increase in particle size from 1.45 nm to 1.64 nm was observed by TEM, whereas the dispersion measured by the chemisorption of CO decreased from 0.56 for the fresh Pt/C to 0.27 for the used Pt/C [40]. The chemisorption protocol included a reduction with dihydrogen at 373 K. The catalyst deactivation in that work was hypothesized to be the influence of a strongly adsorbed oxidation side product.

### **Effect of startup conditions**

To explore the possibility of Pt over-oxidation as a cause of Pt deactivation, Pt/C was exposed to several different startup conditions before the oxidation of 1,6-hexanediol. Table 4.4 shows the TOF's determined for 1,6-hexanediol oxidation at 343 k and 10 bar O<sub>2</sub> at acidic conditions. In a typical experiment, the Pt/C catalyst was heated to 343 k in the presence of 1,6-hexanediol in an inert (He) atmosphere for 0.5 h. During this inert treatment, Pt is reduced by the alcohol from a slightly oxidized state (from exposure to air) to metallic, which is considered the active site for alcohol dehydrogenation [7]. The inert startup conditions had an initial TOF for 1,6-hexanediol oxidation of 0.19 s<sup>-1</sup>. When the Pt/C catalyst was exposed to flowing O<sub>2</sub> in water for 2 h at 343 K (oxidative treatment) and 1,6-hexanediol was added to initiate the reaction, the TOF decreased by 79% to 0.04 s<sup>-1</sup>. However, exposure of the oxidized Pt/C catalyst to 1,6-hexanediol in an inert atmosphere for just 0.5 h (inert treatment) recovered a significant portion of the catalytic activity (0.15 s<sup>-1</sup>) and a 1 h inert treatment after purposefully exposing the Pt to



O<sub>2</sub> recovered almost all of the catalytic activity for 1,6-hexanediol oxidation (0.17 s<sup>-1</sup>). While the exposure of the Pt catalyst to O<sub>2</sub> in water decreased the initial oxidation activity, the over-oxidation was easily reversed by reduction of the catalytic surface with an alcohol. These results are analogous to experiments in the literature that demonstrate a Pt catalyst can be partially regenerated in a flow reactor by flowing N<sub>2</sub> instead of air in the presence of methyl- $\alpha$ -D-glucopyranoside for a short period of time [15]. In addition, evidence from X-ray absorption spectroscopy suggests that the presence of water inhibits platinum oxide formation so the Pt surface is covered instead with atomic oxygen or hydroxide species [41-42].

**Table 4.4.** Influence of Pt/C treatment before and after Pt/C recycle for 1,6-hexanediol oxidation.

Experiment	TOF (s <sup>-1</sup> )	% Decrease in oxidation rate
Inert (0.5 h)	0.19	-
Oxidative (2 h)	0.04	79
Oxidative (2 h) then Inert (0.5 h)	0.15	21
Oxidative (2 h) then Inert (1 h)	0.17	11
Recycle then Inert (1 h)	0.04	79
Recycle then He at 473 K (2 h) then Inert (0.5 h)	0.12	31
Recycle then H <sub>2</sub> at 473 K (2 h) then Inert (0.5 h)	0.17	11

Reaction conditions: 0.1 M 1,6-hexanediol, 1,6-hexanediol:Pt = 500:1 (mol:mol), T = 343 K, pO<sub>2</sub> = 10 bar, 0.35 M acetic acid. Inert treatment: N<sub>2</sub> with aqueous 1,6-hexanediol. Oxidative treatment: flow O<sub>2</sub> in water. Recycle: catalyst recovered after 4 h of 1,6-hexanediol oxidation and washed with DI water. H<sub>2</sub> and He treatment under flowing gas.

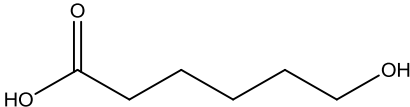
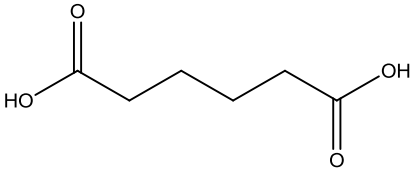
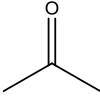
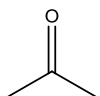
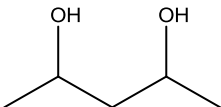
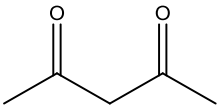
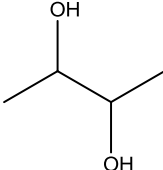
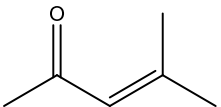
Given the fact that over-oxidation of the Pt was easily reversed by an inert treatment in alcohol, a deactivated Pt/C sample was recovered by centrifugation after 4 h of 1,6-hexanediol oxidation at 343 K and subsequently washed ten times with distilled, deionized water. The recovered catalyst was then subjected to an inert treatment for 1 h. The initial 1,6-hexanediol oxidation activity of the washed and recycled catalyst (0.04 s<sup>-1</sup>) was measured to be 79% less than that of the fresh catalyst. Thus, a significant portion of original Pt/C activity was not recovered by the alcohol substrate and could not be attributed to over-oxidation of the Pt surface

(Table 4.4). When the recovered and washed Pt/C catalyst was treated with either flowing He or H<sub>2</sub> at 473 K without water, a significant increase in 1,6-hexanediol oxidation activity was observed. While the He treatment was mildly effective at recovering the catalytic activity of Pt with a TOF of 0.12 s<sup>-1</sup>, the H<sub>2</sub> treatment regenerated most, but not all, of the initial oxidation activity with a TOF of 0.17 s<sup>-1</sup> (Table 4.4). The regeneration of Pt/C by a high temperature H<sub>2</sub> treatment after methyl- $\alpha$ -D-glucopyranoside oxidation was also shown to be effective [40]. Although the reduction of Pt by alcohol substrate in water was not effective at regenerating catalytic activity, a high temperature H<sub>2</sub> treatment was, which suggests a reducible species strongly adsorbed on Pt may be one cause of deactivation.

### **Influence of chemical additives**

The inhibition of supported Pt catalysts by strongly adsorbed byproducts of alcohol oxidation is suspected to partially account for the reaction profile. Since the number of catalytic sites is typically very low compared to the amount of substrate molecules, only trace quantities of strong adsorbates could deactivate the catalyst. Some researchers suggest that carboxylic acids, the primary product of alcohol oxidation under aqueous conditions, can strongly adsorb on Pt, so the inhibition of 1,6-hexanediol oxidation by carboxylic acids and the effect of concentration was recently investigated in Chapter 2 [32]. A moderate decrease in the initial oxidation rate of 1,6-hexanediol (30%) was observed upon the addition of 0.35 M acetic acid. All experiments shown in Table 4.5 were performed in the presence of acetic acid (except when noted). Addition of adipic acid did not affect the rate of 1,6-hexanediol oxidation, suggesting the diacid product is not the inhibitory agent responsible for deactivation. The addition of 6-hydroxyhexanoic acid decreased the initial TOF of 1,6-hexanediol oxidation by 42%, but this result was most likely the result of competitive oxidation.

**Table 4.5.** Influence of additives on the rate of 1,6-hexanediol oxidation over Pt/C.

Additive	Structure	TOF (s <sup>-1</sup> )	% Decrease in oxidation rate
None		0.19	-
NaOH		0.06	68
6-Hydroxyhexanoic Acid		0.11	42
Adipic Acid		0.19	0
Acetone		0.19	0
Acetone w/ NaOH <sup>a</sup>		0.01	95
2,4-Pentanediol		0.19	0
2,4-Pentanedione		0.03	84
2,3-Butanediol		0.19	0
Mesityl Oxide		0.06	68

Reaction conditions: 0.1 M 1,6-hexanediol, 1,6-hexanediol:Pt = 500:1 (mol:mol), T = 343 K, pO<sub>2</sub> = 10 bar, 0.35 M acetic acid, pH = 2.5, 0.1 M additive.

<sup>a</sup> 0.1 M NaOH

Mallet et al. suggested that Pt/C deactivated because of strong adsorption of aldol dimerization products of the substrate 1-methoxy-2-propanol at basic conditions with NaOH [19]. Bonello et al. proposed that aldol condensation of methyl pyruvate poisoned the Pt surface even in the absence of oxygen [20-21]. Similarly, Zope et al. determined that at basic conditions, compounds with secondary alcohol groups could be oxidized to ketones that would form products that strongly adsorb on the surfaces of Au and Pt catalysts [4]. Table 4.5 presents the effect of adding secondary alcohols and ketones on the initial rate of 1,6-hexanediol oxidation over Pt. The addition of acetone had no effect on the alcohol oxidation rate, which is consistent with the reported lack of influence on the oxidation of 2-propanol over Pt/SiO<sub>2</sub> at neutral conditions [43]. As shown in Table 4.5, addition of the secondary alcohols 2,4-pentanediol and 2,3-butanediol did not affect the rate of oxidation. In contrast, the addition of 2,4-pentanedione resulted in an 84% decrease in oxidation activity. The addition of mesityl oxide, also decreased the initial rate of 1,6-hexanediol oxidation by 68%. When acetone and NaOH were added to solution, the initial alcohol oxidation activity decreased 95%. The aldol condensation of acetone can produce mesityl oxide in the presence of base, thus, the large decrease in rate was unexpected when compared to the addition of just mesityl oxide. However, the addition of 0.1 M NaOH alone decreased the TOF of 1,6-hexanediol oxidation by 68%. The solution also turned pale yellow. We believe the decomposition or aldol condensation of 1,6-hexanediol and its oxidation products at basic conditions produced species capable of poisoning the Pt surface. The production of these deactivating species, though, was not promoted at acidic conditions. Apparently, under the acidic conditions of this study, secondary alcohols and mono-ketones (acetone) do not strongly adsorb on the Pt surface during alcohol oxidation. The low pH prevents the rapid formation of aldol condensation products that can block metal sites. Addition of aldol

products or diketones, however, substantially lowers the rate of alcohol oxidation, presumably by strong adsorption on Pt.

### **Detection of byproducts in the gas phase**

Table 4.6 shows the amount of CO<sub>2</sub> produced in the headspace of the reactor after alcohol oxidation for 20 h at 343 K and 3 bar O<sub>2</sub>. As mentioned in the introduction, CO has been observed in both the electro-catalytic and heterogeneous catalytic oxidation of alcohols over Pt. The production of CO<sub>2</sub> during glycerol oxidation has been observed over Pt at acidic aqueous conditions [27-28]. Evaluation of headspace was performed to gain insight into the byproducts of selective alcohol oxidation reactions. The production of CO<sub>2</sub> was observed during oxidation of mono-alcohols, diols, and benzyl alcohol. While the quantification of small amounts of CO<sub>2</sub> was difficult, the overall carbon balance based on the moles of carbon in the identified products (Table 4.6) was adequate for qualitative comparisons. When the Pt/C catalyst was exposed to O<sub>2</sub> in water for 20 h, a small amount of CO<sub>2</sub> was observed from the oxidation of the carbon support. This value was subtracted from all of the following experiments that used Pt/C as the catalyst. The oxidation of 1,2-ethanediol in the absence of the catalyst produced a negligible amount of CO<sub>2</sub>. Thus, Pt was required to produce CO<sub>2</sub> in the presence of alcohol and O<sub>2</sub>.

**Table 4.6.** Amount of CO<sub>2</sub> produced after 20 h for substrate oxidation over Pt/C.

Substrate	Conv. (%)	CO <sub>2</sub> Prod. (mol x 10 <sup>4</sup> )	CB Liq. Prod. (%)	CB Gas Prod. (%)	Total CB (%)
None (Pt/C) <sup>a</sup>	-	0.11	-	-	-
1,2-Ethanediol (No Pt/C)	0	0.043	-	-	-
1,2-Ethanediol	94	6.3	74.1	29.9	104.0
1,3-Propanediol	38	1.0	89.4	8.5	97.9
1,3-Propanediol <sup>b</sup>	84	5.0	86.2	18.9	105.1
Ethanol <sup>c</sup>	91	0.41	99.7	2.1	101.8
Ethanol <sup>d</sup>	95	0.33	97.7	1.8	99.5
1,6-Hexanediol	71	0.79	92.5	1.9	94.3
Acetic Acid	0	0.081	-	-	-
HDO + Acetic Acid	78	0.77	90.9	1.6	92.5
Malonic Acid	3	0.92	68.7	52.7	121.4
Adipic Acid	3	0.28	82.5	15.4	97.9
Benzyl Alcohol <sup>e</sup>	98	0.68	97.8	1.0	98.9

Reaction conditions: 0.1 M Substrate, Sub.:Pt = 500:1 (mol:mol), T = 343 K, pO<sub>2</sub> = 3 bar, 20 h. Carbon balance (CB) (%) = [(mol carbon in products)/(mol carbon substrate converted) \* 100]

<sup>a</sup> Background CO<sub>2</sub> production from Pt/C alone subtracted from other experiments.

<sup>b</sup> Substrate to Pt ratio = 250:1 (mol:mol)

<sup>c</sup> Methane production measured to be 0.063 mol x 10<sup>4</sup> or 3900 ppm at 3 bar and 343 K.

<sup>d</sup> After headspace analysis, 3 bar H<sub>2</sub> injected for 1 h. Methane and ethane observed.

<sup>e</sup> Experiment performed with 2% Pt/SiO<sub>2</sub>

The amount of CO<sub>2</sub> produced from 1,2-ethanediol and 1,3-propanediol was significantly higher than from ethanol or 1,6-hexanediol. When the amount of catalyst loaded in the reactor was doubled to achieve similar level of conversion in for 1,3-propanediol oxidation, both 1,3-propanediol and 1,2-ethanediol produced approximately the same amount of CO<sub>2</sub>. Interestingly, the initial rate of oxidation was faster for ethanol and 1,6-hexanediol than 1,2-ethanediol and 1,3-propanediol (Figure 4.2). The addition of acetic acid to solution did not change the amount of CO<sub>2</sub> produced during 1,6-hexanediol oxidation and acetic acid did not undergo a significant amount of oxidative decarboxylation at these reaction conditions. One potential route for the production of CO<sub>2</sub> is the decarboxylation of diacids produced during diol oxidation. For example, malonic acid is known to decarboxylate without a catalyst at higher temperatures [44]. While both malonic acid and adipic acid produced some CO<sub>2</sub> in the presence of O<sub>2</sub> and Pt/C, the

conversion of the diacid was much slower than the conversion of the corresponding diol, and the diacid produced less CO<sub>2</sub> than the diol over the same period of time. Interestingly, the oxidative decarboxylation of malonic acid produced almost a quantitative amount of acetic acid, while no acetic acid was observed in either of the 1,3-propanediol experiments (no initial amount of acetic acid in either experiment). Thus, decarboxylation of the product acid was not considered the primary route of CO<sub>2</sub> production.

The decarbonylation of an aldehyde to CO that subsequently can be oxidized to produce CO<sub>2</sub> is another possible reaction path. Mondelli et al. observed adsorbed CO during ATR-IR spectroscopy of benzyl alcohol oxidation over Pt/Al<sub>2</sub>O<sub>3</sub> in toluene [31]. However, the decarbonylation of the aldehyde of ethanol oxidation, acetaldehyde, should then also produce CH<sub>4</sub> as a co-product. While the headspace analysis of ethanol oxidation indicated a small amount of CH<sub>4</sub> was produced in addition to CO<sub>2</sub>, the molar ratio of CO<sub>2</sub>:CH<sub>4</sub> was approximately 6.5 instead of the expected molar ratio of 1. The high molar ratio of CO<sub>2</sub>:CH<sub>4</sub> after ethanol oxidation suggests that carbonaceous species deposited on the surface of Pt might be slowly oxidized to CO<sub>2</sub> which could alter the expected ratio of CO<sub>2</sub>:CH<sub>4</sub>. If after ethanol oxidation for 20 h the headspace was exhausted and 3 bar H<sub>2</sub> was introduced to the reactor at room temperature for 1 h, both ethane and methane are observed by gas chromatography. However, the substrate was not removed from the reactor before pressurizing with H<sub>2</sub> and, thus, the hydrogenolysis or dehydration of ethanol and its oxidation products is a possibility over Pt. In summary, CO<sub>2</sub> could be produced from both the decarbonylation of an aldehyde and the oxidation of carbon-containing species on the Pt surface.

## Conclusions

The deactivation of supported Pt catalysts during aqueous alcohol oxidation over Pt catalysts was investigated at acidic and neutral conditions. A significant decrease in the oxidation rate with time was observed for both mono-alcohols and diols over Pt/C. No influence of support type or Pt dispersion was determined for the deactivation behavior. Neither the leaching of Pt into solution nor the sintering of Pt nanoparticles was a significant enough to account for the observed Pt deactivation. While over-oxidation of the Pt catalyst by treatment with O<sub>2</sub> prior to the reaction decreased the initial oxidation rate, treatment of the oxidized catalyst with alcohol in an inert atmosphere completely recovered the activity. Although aldol condensation products can poison Pt catalysts, aldol condensation was negligible at acidic conditions of the alcohol oxidation reactions studied here. Headspace analysis revealed that small amounts of CO<sub>2</sub> were produced during alcohol oxidation. The CO<sub>2</sub> produced may be from the decarbonylation of aldehyde intermediate products.

## Acknowledgements

I thank Richard White for helping get the TEM micrographs. This material is based upon work supported by the National Science Foundation under Award Nos. EEC-0813570 and OISE 0730277.

## References

- [1] T. Werpy and G. R. Petersen, Top Value Added Chemicals from Biomass, No. DOE/GO-102004-1992, Department of Energy, Office of Scientific and Technical Information, Washington, DC, 2004.
- [2] R. A. Sheldon, J. Dakka, Heterogeneous catalytic oxidations in the manufacture of fine chemicals. *Catal. Today* 19 (1994) 215-246.



- [3] S. E. Davis, M. S. Ide, R. J. Davis, Selective oxidation of alcohols and aldehydes over supported metal nanoparticles. *Green Chem.* 15 (2013) 17-45.
- [4] B. N. Zope, R. J. Davis, Inhibition of gold and platinum catalysts by reactive intermediates produced in the selective oxidation of alcohols in liquid water. *Green Chem.* 13 (2011) 3484-3491.
- [5] P. Gallezot, Selective oxidation with air on metal catalysts. *Catal. Today* 37 (1997) 405-418.
- [6] M. Betwoska-Brzezinska, T. Uczak, R. Holze, Electrocatalytic oxidation of mono- and polyhydric alcohols on gold and platinum. *J. Appl. Electrochem.* 27 (1997) 999-1011.
- [7] T. Mallat, A. Baiker, Oxidation of alcohols with molecular oxygen on platinum metal catalysts in aqueous solutions. *Catal. Today* 19 (1994) 247-283.
- [8] A. P. Markusse, B. F. M. Kuster, D. C. Koningsberger, G. B. Marin, Platinum deactivation: in situ EXAFS during aqueous alcohol oxidation reaction. *Catal. Lett.* 55 (1998) 141-145.
- [9] C. Brönnimann, Z. Bodnar, P. Hug, T. Mallat, A. Baiker, Direct oxidation of L-sorbose to 2-keto-L-gulonic acid with molecular oxygen on platinum- and palladium-based catalysts. *J. Catal.* 150 (1994) 199-211.
- [10] M. Besson, P. Gallezot, Selective oxidation of alcohols and aldehydes on metal catalysts. *Catal. Today* 57 (2000) 127-141.
- [11] J. Dirkx, H. S. Baan, The oxidation of gluconic acid with platinum on carbon as catalyst. *J. Catal.* 67 (1981) 14-20.
- [12] T. Mallat, A. Baiker, Liquid-phase oxidation of 1-methoxy-2-propanol with air III: chemical deactivation and oxygen poisoning of platinum catalysts. *Appl. Catal. A-Gen.* 86 (1992) 147-163.
- [13] P. J. M. Dijkgraaf, H. A. M. Duisters, B. F. M. Kuster, K. van der Wiele, Deactivation of platinum catalysts by oxygen: 2. Nature of the catalyst deactivation. *J. Catal.* 112 (1988) 337-344.
- [14] V. R. Gangwal, B. G. M. van Wachem, B. F. M. Kuster, J. C. Schouten, Platinum catalysed aqueous alcohol oxidation: model-based investigation of reaction conditions and catalyst design. *Chem. Eng. Sci.* 57 (2002) 5051-5063.
- [15] J. H. Vleeming, B. F. M. Kuster, G. B. Marin, Selective oxidation of methyl  $\alpha$ -D-glucopyranoside with oxygen over supported platinum: Kinetic modeling in the presence of deactivation by overoxidation of the catalyst. *Ind. Eng. Chem. Res.* 36 (1997) 3541-3553.

- [16] L. Jelemensky, B. F. M. Kuster, G. B. Marin, Multiple steady-states for the oxidation of aqueous ethanol with oxygen on a carbon supported platinum catalyst. *Catal. Lett.* 30 (1995) 269-277.
- [17] H. E. van Dam, L. J. Wisse, H. Van Bekkum, Platinum/carbon oxidation catalysts: VIII. Selecting a metal for liquid-phase alcohol oxidations. *Appl. Catal.* 61 (1990) 187-197.
- [18] T. Mallat, A. Baiker, Oxidation of alcohols with molecular oxygen on solid catalysts. *Chem. Rev.* 104 (2004) 3037-3058.
- [19] T. Mallat, A. Baiker, Liquid-phase oxidation of 1-methoxy-2-propanol with air: I. Lead and bismuth promotion and deactivation of palladium catalysts. *Appl. Catal. A-Gen.* 79 (1991) 41-58.
- [20] J. M. Bonello, R. M. Lambert, N. Künzle, A. Baiker, Platinum-catalyzed enantioselective hydrogenation of  $\alpha$ -ketoesters: An unprecedented surface reaction of methyl pyruvate. *J. Am. Chem. Soc.* 122 (2000) 9864-9865.
- [21] J. M. Bonello, F. J. Williams, A. K. Santra, R. M. Lambert, Fundamental aspects of enantioselective heterogeneous catalysis: the surface chemistry of methyl pyruvate on Pt {111}. *J. Phys. Chem. B* 104 (2000) 9696-9703.
- [22] J. F. E. Gootzen, A. H. Wonders, A. P. Cox, W. Visscher, J. A. R. van Veen, On the adsorbates formed during the platinum catalyzed (electro)oxidation of ethanol, 1,2-ethanediol and methyl- $\alpha$ -D-glucopyranoside at high pH. *J. Mol. Catal. A-Chem.* 127 (1997) 113-131.
- [23] M. E. M. Chbihi, D. Takky, F. Hahn, H. Huser, J. M. Léger, C. Lamy, In-situ infrared reflectance spectroscopic study of propanediol electrooxidation at platinum and gold: Part 1. 1,3-Propanediol. *J. Electroanal. Chem.* 463 (1999) 63-71.
- [24] J. L. Rodríguez, R. M. Souto, S. González, E. Pastor, DEMS study on the adsorption and reactivity of benzyl alcohol on palladium and platinum. *Electrochim. Acta* 44 (1998) 1415-1422.
- [25] J. F. E. Gootzen, A. H. Wonders, W. Visscher, J. A. R. van Veen, Adsorption of C3 alcohols, 1-butanol, and ethene on platinized platinum as studied with FTIRS and DEMS. *Langmuir* 13 (1997) 1659-1667.
- [26] H. A. Gasteiger, N. Markovic, P. N. Ross, E. J. Cairns, Electro-oxidation of small organic molecules on well-characterized Pt-Ru alloys. *Electrochim. Acta* 39 (1994) 1825-1832.
- [27] A. Villa, G. M. Veith, L. Prati, Selective oxidation of glycerol under acidic conditions using gold catalysts. *Angew. Chem. Int. Ed.* 49 (2010) 4499-4502.
- [28] D. Liang, J. Gao, J. Wang, P. Chen, Z. Hou, X. Zheng, Selective oxidation of glycerol in a base-free aqueous solution over different sized Pt catalysts. *Catal. Comm.* 10 (2009) 1586-1590.

- [29] C. Keresszegi, D. Ferri, T. Mallat, A. Baiker, Unraveling the surface reactions during liquid-phase oxidation of benzyl alcohol on Pd/Al<sub>2</sub>O<sub>3</sub>: an in situ ATR-IR study. *J. Phys. Chem. B* 109 (2005) 958-967.
- [30] D. Ferri, A. Baiker, *Top. Catal. Advances in infrared spectroscopy of catalytic solid-liquid interfaces: The case of selective alcohol oxidation.* 52 (2009) 1323-1333.
- [31] C. Mondelli, J. Grunwaldt, D. Ferri, A. Baiker, Role of Bi promotion and solvent in platinum-catalyzed alcohol oxidation probed by in situ X-ray absorption and ATR-IR spectroscopy. *Phys. Chem. Chem. Phys.* 12 (2010) 5307-5316.
- [32] M S. Ide, R. J. Davis, Perspectives on the kinetics of diol oxidation over supported platinum catalysts in aqueous solution. *J. Catal.* (2013), <http://dx.doi.org/10.1016/j.jcat.2013.05.017>.
- [33] W. A. Dietz, Response factors for gas chromatographic analyses. *J. Gas Chromatogr.* 5 (1967) 68-71.
- [34] N. Meyer, K. Bekaert, D. Pirson, M. Devillers, S. Hermans, Particle size effects in selective oxidation of lactose with Pd/h-BN catalysts. *Catal. Comm.* 5 (2012) 170-174.
- [35] P. Korovchenko, C. Donze, P. Gallezot, M. Besson, Oxidation of primary alcohols with air on carbon-supported platinum catalysts for the synthesis of aldehydes or acids. *Catal. Today* 121 (2007) 13-21.
- [36] Y. Shao, G. Yin, Y. Gao, Understanding and approaches for the durability issues of Pt-based catalysts for PEM fuel cell. *J. Power Sources* 171 (2007) 558.
- [37] F. R. Venema, J. A. Peters and H. van Bekkum, Platinum-catalyzed oxidation of aldopentoses to aldaric acids. *J. Mol. Catal.* 77 (1992) 75-85.
- [38] L. Prati, M. Rossi, Gold on carbon as a new catalyst for selective liquid phase oxidation of diols. *J. Catal.* 176 (1998) 552-560.
- [39] H. A. Rass, N. Essayem, M. Besson, Selective aqueous phase oxidation of 5-hydroxymethylfurfural to 2,5-furandicarboxylic acid over Pt/C catalysts: influence of the base and effect of bismuth promotion. *Green Chem.* 15 (2013) 2240-2251.
- [40] J. H. Vleeming, B. F. M. Kuster, G. B. Marin, F. Oudet, P. Courtine, Graphite-supported platinum catalysts: Effects of gas and aqueous phase treatments. *J. Catal.* 166 (1997) 148-159.
- [41] R.S. Weber, M. Peuckert, R.A. DallaBetta, M. Boudart, Oxygen reduction on small supported platinum particles II. Characterization by X-ray absorption spectroscopy. *J. Electrochem. Soc.* 135 (1988) 2535-2538.
- [42] J.A.A. van den Tillaart, B.F.M. Kuster, G.B. Marin, in: S.T. Oyama and J.W. Hightower (Eds.), *Catalytic Selective Oxidation*, American Chemical Society, 1993, p. 298.

[43] J. W. Nicoletti, G. M. Whitesides, Liquid-phase oxidation of 2-propanol to acetone by dioxygen using supported platinum catalysts. *J. Phys. Chem.* 93 (1989) 759-767.

[44] G. A. Hall, The kinetics of the decomposition of malonic acid in aqueous solution. *J. Am. Chem. Soc.* 71 (1949) 2691-2693.

## Chapter 5: In-situ ATR-IR Spectroscopy on Pt

*The work in this chapter was the basis for portions of the publication, M. S. Ide, D. D. Falcone, R. J. Davis, "On the Deactivation of Supported Pt Catalysts for Selective Oxidation of Alcohols," in preparation.*

### Introduction

The ATR-IR spectroscopic technique is excellent for probing the vibrational spectra of species adsorbed to a metal surface in the liquid phase [1]. While transmission spectroscopy of catalyst surfaces has been used for years to probe gas-solid interactions, the small path length of IR transmission in the liquid phase makes it nearly impossible to probe species of interest. In addition, the absorption of the liquid solvent, such as water, in the spectral region of concern can be significantly stronger than the IR absorption of the species of interest. The ATR-IR technique takes advantage of total internal reflectance by reflecting light within a solid element that has a high refractive index, such as ZnSe. The wave of light is reflected off the interface of the internal reflectance element (IRE) and a small portion of the IR beam penetrates into the liquid solution as an evanescent wave with a relatively small penetration depth ( $d_p$ ). An overview of internal reflectance of the IR beam and probing depth is shown in Figure 5.1. The penetration depth is a function of the wavelength of incident light. For a ZnSe IRE in water, the penetration depth of the evanescent wave is approximately  $0.7 \mu\text{m}$  at  $2000 \text{ cm}^{-1}$  and  $1.5 \mu\text{m}$  at  $1000 \text{ cm}^{-1}$  [2]. The evanescent wave probes a very small area beyond the surface of the IRE and thus, is able to observe species very close to the IRE surface.

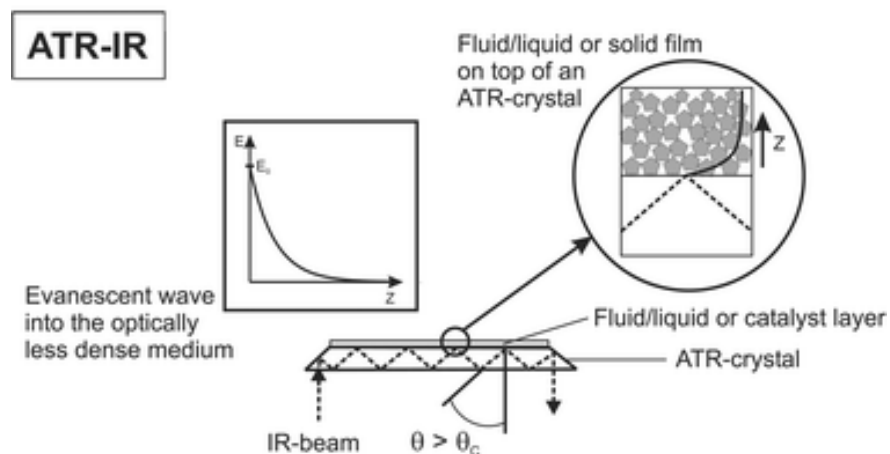


**Figure 5.1.** Attenuated total reflectance IR spectroscopy of a thin catalyst layer on an internal reflectance element crystal. Modified and reprinted from reference [8].

The ability to probe very closely to the IRE surface is invaluable to in-situ ATR-IR spectroscopy of catalysts. The powder catalyst is coated on the surface of the IRE with a thin layer and is probed by the evanescent wave of the IR radiation. If a liquid solution is introduced to the IRE, any chemical reaction on or near the surface of the catalyst could be within the penetration depth from the IRE as shown in Figure 5.2. A comprehensive review of the technique for heterogeneous catalysis in the liquid phase can be found elsewhere [3,4], but it has been successfully used for hydrogenation, oxidation, and reforming reactions over Pt/Al<sub>2</sub>O<sub>3</sub> [5-7]. In addition, the ATR-IR technique has been used for benzyl alcohol oxidation in cyclohexane over Pd/Al<sub>2</sub>O<sub>3</sub>. The anaerobic dehydrogenation of benzyl alcohol identified benzaldehyde and CO as species close to the IRE surface [9]. The oxidation of benzyl alcohol over Pt/Al<sub>2</sub>O<sub>3</sub> in toluene has also been performed in ATR-IR [10]. The role of surface adsorbates on Pt during aqueous alcohol oxidation and what affect, if any, they have in the deactivation of supported Pt is particularly intriguing and is the focus of this work.

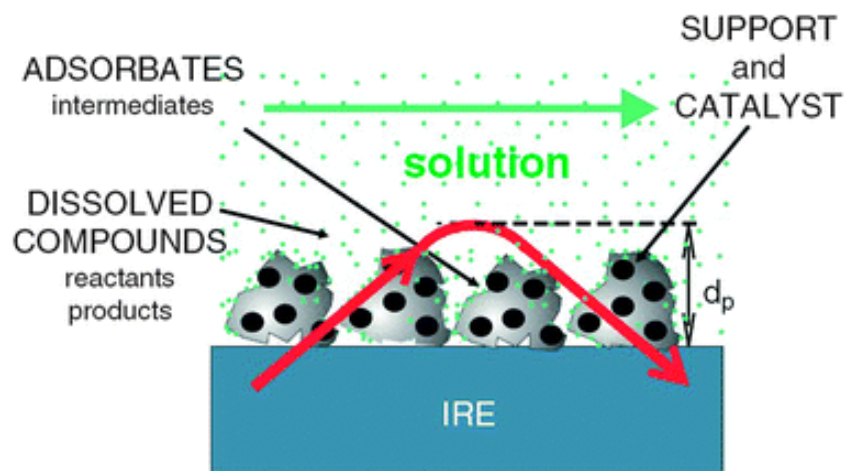


**Figure 5.2.** In-situ ATR-IR spectroscopy of a catalyst film on an IRE. The penetration depth ( $d_p$ ) probes the surface of the IRE. Modified and reprinted from reference [3].

## Experimental Methods

### In-situ ATR-IR spectroscopy

The in-situ ATR (attenuated total reflectance) IR spectra were collected on a Bruker Vertex 70 spectrometer with a liquid nitrogen cooled MCT detector. The spectra were recorded by co-adding 300 scans at  $4\text{ cm}^{-1}$  resolution from approximately  $4000$  to  $700\text{ cm}^{-1}$ . Background spectra were collected with either  $\text{N}_2$ ,  $\text{H}_2$ , or  $\text{O}_2$  saturated distilled, deionized water flowing at  $1\text{ cm}^3\text{ min}^{-1}$  over the coated internal reflectance element (IRE) at 5 bar and 298 K. In a typical procedure, the  $\text{Pt/SiO}_2$  or  $\text{Pt/BN}$  catalyst was deposited onto a cylindrical ZnSE IRE (length of 8.255 cm by width of 0.635 cm) by dipping the IRE in a well dispersed aqueous solution of 1 wt% catalyst followed by drying at 393 K. The procedure was repeated ten times or until a thin layer of catalyst covered the surface of the IRE. The IRE was then secured in a stainless steel continuous flow reactor sample cell mounted on an ATR attachment (Axiom Analytical TNL-130). The  $\text{Pt/SiO}_2$  and  $\text{Pt/BN}$  catalyst layers were tested for stability up to 10 bar.

The N<sub>2</sub>, O<sub>2</sub>, or H<sub>2</sub> saturated water solutions and N<sub>2</sub> or O<sub>2</sub> saturated alcohol solutions were prepared by flowing 50 cm<sup>3</sup> min<sup>-1</sup> of gas through the solution in a stainless steel reservoir for 1 h. The alcohol solution was either 0.1 M benzyl alcohol or ethanol saturated with the desired gas. All solutions were pumped over the catalyst layer on the IRE at 1 cm<sup>3</sup> min<sup>-1</sup> and 5 bar. The experimental procedure generally started with flowing N<sub>2</sub> saturated H<sub>2</sub>O through the ATR cell until a steady signal was achieved in the IR spectrum. After a background scan, the solution was switched to a N<sub>2</sub> or O<sub>2</sub> saturated alcohol solution for approximately 60 min prior to subsequently purging the cell with flowing N<sub>2</sub> saturated H<sub>2</sub>O to remove the alcohol substrate from the cell. In some cases, O<sub>2</sub> or H<sub>2</sub> saturated H<sub>2</sub>O was pumped to the cell.

### **TGA-MS**

Thermal gravimetric analysis (TGA) coupled with mass spectrometry (MS) was collected on a SDT Q600 (TA Instruments) attached to an OmniStar Quadrupole MS GSD 300 O2 (Pfeiffer Vacuum) equipped with a Faraday cup and an SEM detector. A constant heating rate of 10 °C min<sup>-1</sup> from room temperature to 973 K with a He purge flow of 100 ml min<sup>-1</sup> was used for all experiments. The amount of sample loaded in the TGA was approximately 20 mg. The signal intensity of gaseous products during the heating was measured with the MS. The used Pt/BN was recovered from solution by centrifugation after 24 h of ethanol oxidation at 343 K and 10 bar O<sub>2</sub>. The catalyst was then washed with DI water and subsequently recovered ten times to remove loose surface contaminants. Before TGA-MS experiments, both the fresh and used Pt/BN was dried overnight at 393 K.



## Results and Discussion

### Catalyst stability

In an attempt to probe the species adsorbed on the Pt surface, in-situ ATR-IR spectroscopy was performed. While flat internal reflectance elements (IRE) are commonly used to investigate heterogeneous catalysts, a cylindrical ZnSe IRE was utilized in this work because it is capable of withstanding elevated pressures. A drawback of the cylindrical configuration is that the amount of catalyst adhered to the IRE during dip coating is difficult to quantify. A catalyst layer that is too thick tends to decrease signal throughput, while a layer that is too thin has too few adsorption sites for detection. The stability of the catalyst on the IRE surface in liquid water had to be confirmed. The Pt/C did not adhere well to the IRE and easily detached into the liquid phase. The ease of deposition and stability in water of Pt/SiO<sub>2</sub> and Pt/BN made them suitable candidates for use in the ATR-IR experiments. Figure 5.3 shows the stability of the Pt/SiO<sub>2</sub> catalyst that has been dip coated on the ZnSe IRE. The intensity of the 1085 cm<sup>-1</sup> peak of the Si-O-Si asymmetric stretch was monitored after the dip coating and was unchanged after the N<sub>2</sub> gas treatment for 1 h. While pumping H<sub>2</sub>O/N<sub>2</sub> over the catalyst increased the signal peak intensity compared to the gas phase, neither a treatment with still H<sub>2</sub>O for 72 h nor the oxidation of benzyl alcohol for 4 h significantly decreased the peak signal. More importantly, the signal was unchanged before and after the oxidation experiments.

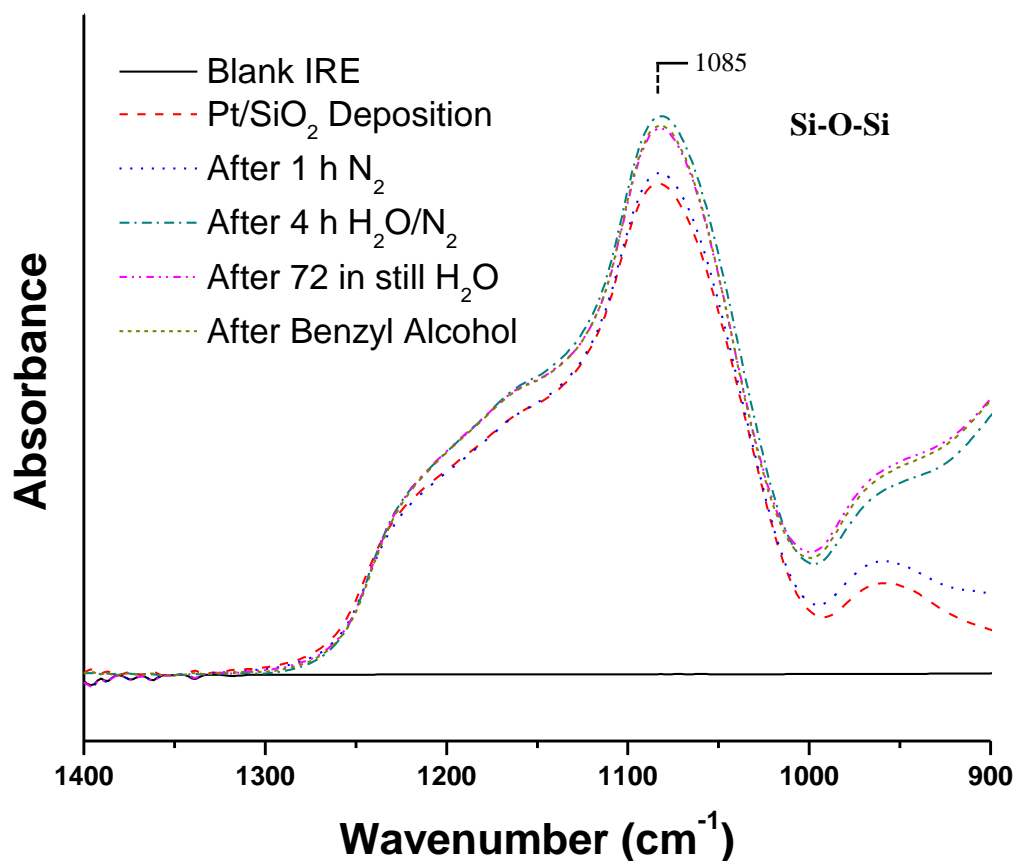


**Figure 5.3.** ATR-IR spectra of silica dip coated onto the IRE and after treatment with N<sub>2</sub> gas, liquid H<sub>2</sub>O/N<sub>2</sub>, still H<sub>2</sub>O, and benzyl alcohol oxidation.

A second difficulty encountered in this study was the use of water as the solution phase. Organic solvents such as cyclohexane or toluene that have been used in other work give sharp and discernible IR absorption peaks. The IR absorption spectrum of water, however, is quite broad and significantly reduces signal throughput, both of which contribute to a low signal to noise ratio. Water has a strong absorption from 3,700 to 3,000 cm<sup>-1</sup> attributed to O-H stretches, weak absorption from 2250 to 2050 cm<sup>-1</sup> attributed to a combination band, and moderate absorption from 1700 to 1550 cm<sup>-1</sup> attributed to O-H bends.

## Benzyl alcohol oxidation

Figure 5.4 shows the ATR spectra collected after having pumped an aqueous solution of 0.1 M benzyl alcohol saturated with N<sub>2</sub> at 1 cm<sup>3</sup> min<sup>-1</sup> at RT (298 K) and 5 bar over the 2% Pt/SiO<sub>2</sub> catalyst deposited on the ZnSe IRE. Table 5.1 results show that the TOF for benzyl alcohol oxidation over Pt/SiO<sub>2</sub> was similar to that of ethanol and 1,6-hexanediol over Pt/C, thus, benzyl alcohol was chosen as the probe molecule. The absorption bands at approximately 1004 cm<sup>-1</sup> (C-O stretch) and 1212 cm<sup>-1</sup> (O-H bend) in Figure 5.4(a) indicate the appearance of benzyl alcohol close to the IRE surface within the probing depth of the evanescent wave. Figure 5.4(b) shows an absorption band centered at approximately 2038 cm<sup>-1</sup> produced during the admission of benzyl alcohol to the cell in Figure 5.4(a), which is assigned to the linear adsorption of CO on Pt in the presence of water. Ebbeson et al. observed a linear CO absorption feature at 2034 cm<sup>-1</sup> on Pt/Al<sub>2</sub>O<sub>3</sub> in the aqueous phase [11]. The CO band increased with time after the introduction of benzyl alcohol to an eventual maximum after approximately 20 min. Figure 5.5 shows the ATR-IR spectra as benzyl alcohol was removed from the cell by flowing water saturated with N<sub>2</sub>. While the signal of benzyl alcohol (Figure 5.5 (a)) disappeared completely with time, the CO feature remained relatively unchanged as shown in Figure 5.5(b), indicating the strong adsorption of CO on Pt.

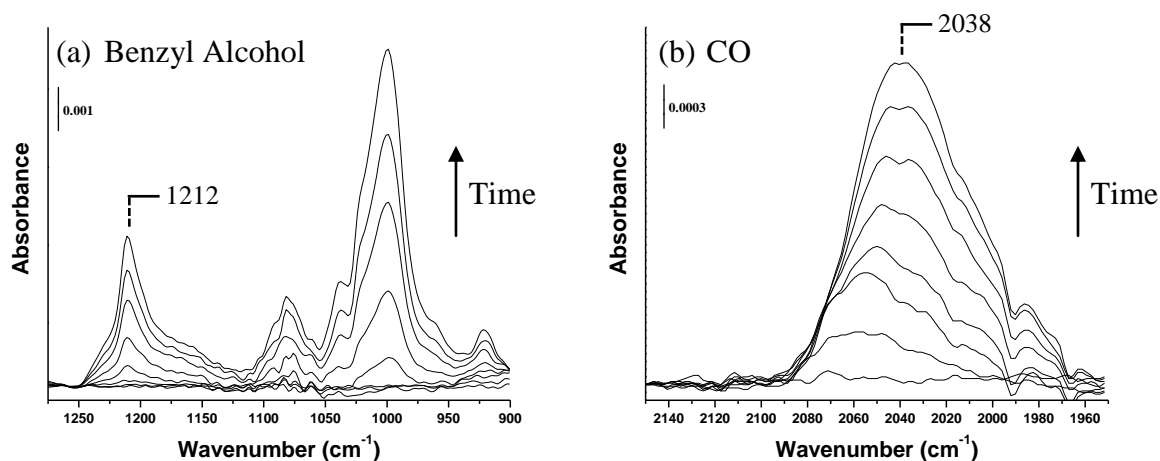


**Figure 5.4.** In-situ ATR-IR spectra of aqueous benzyl alcohol (a) saturated with N<sub>2</sub> flowing over Pt/SiO<sub>2</sub> and the production of CO adsorbed on Pt (b) over 20 min at 5 bar and 298 K. The water background has been removed.

The conditions used to generate the spectra in Figure 5.4 are analogous to those in the inert startup of the semi-batch reactor experiments described earlier. The decomposition of benzyl alcohol or decarbonylation of benzaldehyde produced CO that was strongly adsorbed to the catalyst surface. Reaction of benzyl alcohol in a cyclohexane solvent over Pd/Al<sub>2</sub>O<sub>3</sub> in an inert atmosphere also produced a CO absorption peak from the decarbonylation of benzaldehyde [9] While the C=O feature of benzaldehyde located at approximately 1700 cm<sup>-1</sup> was not observed in this work, it may have been obscured by the very broad absorption peak associated with water in that region. Moreover, benzaldehyde may not remain adsorbed on the Pt surface and instead may diffuse away from the IRE.

**Table 5.1.** Results from the oxidation of ethanol and benzyl alcohol.

Catalyst	Substrate	TOF (s <sup>-1</sup> )
2.69% Pt/C	Ethanol	0.15
5% Pt/BN	Ethanol	0.17
2% Pt/SiO <sub>2</sub>	Ethanol	0.03
2.69% Pt/C	Benzyl Alcohol	0.32
2% Pt/SiO <sub>2</sub>	Benzyl Alcohol	0.13

Reaction conditions: 0.1 M Substrate, Sub.:Pt = 500:1 (mol:mol), T = 343 K, pO<sub>2</sub> = 10 bar, 0.35 M acetic acid, pH = 2.5.

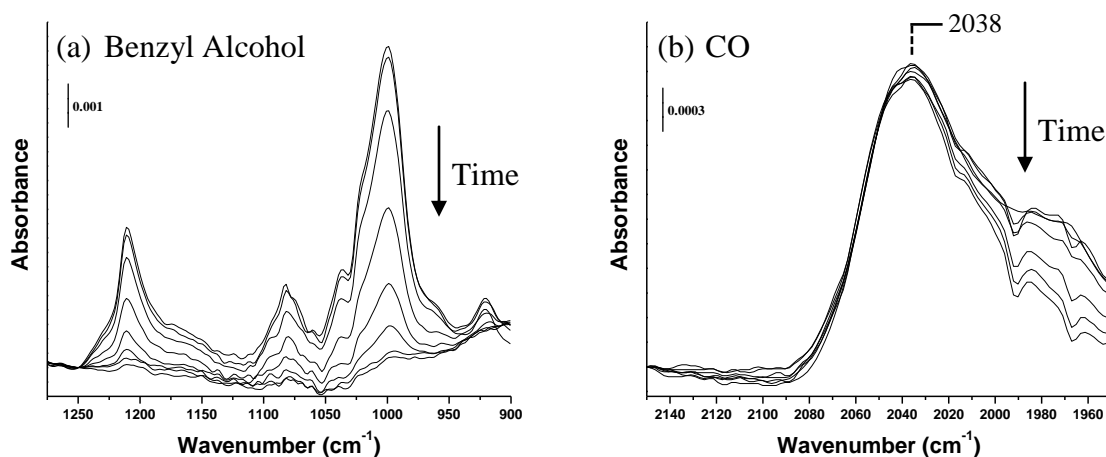


**Figure 5.5.** In-situ ATR-IR spectra of the disappearance of benzyl alcohol (a) with H<sub>2</sub>O saturated N<sub>2</sub> flowing over Pt/SiO<sub>2</sub> and the strong adsorption of CO on Pt (b) over 45 min at 5 bar and 298 K. The water background has been removed.

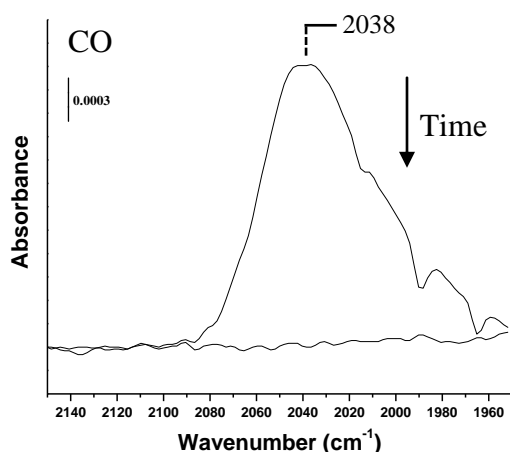


**Figure 5.6.** In-situ ATR-IR spectra of the rapid disappearance of CO after flowing H<sub>2</sub>O saturated O<sub>2</sub> flowing over Pt/SiO<sub>2</sub> at 5 bar and 298 K. The water background has been removed.

Figure 5.6 shows that upon flowing water saturated with O<sub>2</sub> over the catalyst containing CO produced by benzyl alcohol exposure resulted in complete removal of the CO, most likely as CO<sub>2</sub>. The oxidation of CO on a Pt surface is reportedly faster in aqueous solution than in the gas phase over Pt/Al<sub>2</sub>O<sub>3</sub> [11]. Our results suggest that any CO that is produced in the semi-batch reactor either during the inert startup or during alcohol oxidation with O<sub>2</sub> would be easily

oxidized to  $\text{CO}_2$  and therefore removed from the catalyst surface. Figure 5.7 shows ATR spectra of benzyl alcohol saturated with  $\text{O}_2$  flowing over the  $\text{Pt}/\text{SiO}_2$  catalyst. No CO was observed on the Pt surface, confirming that any CO produced was quickly oxidized to  $\text{CO}_2$ . Thus, CO does not appear to be a strong poison of the Pt surface or the cause of Pt deactivation during the conditions of alcohol oxidation. It should be noted that the decomposition of benzyl alcohol or decarbonylation of benzaldehyde would not produce only CO, but also benzene or a carbonaceous species.

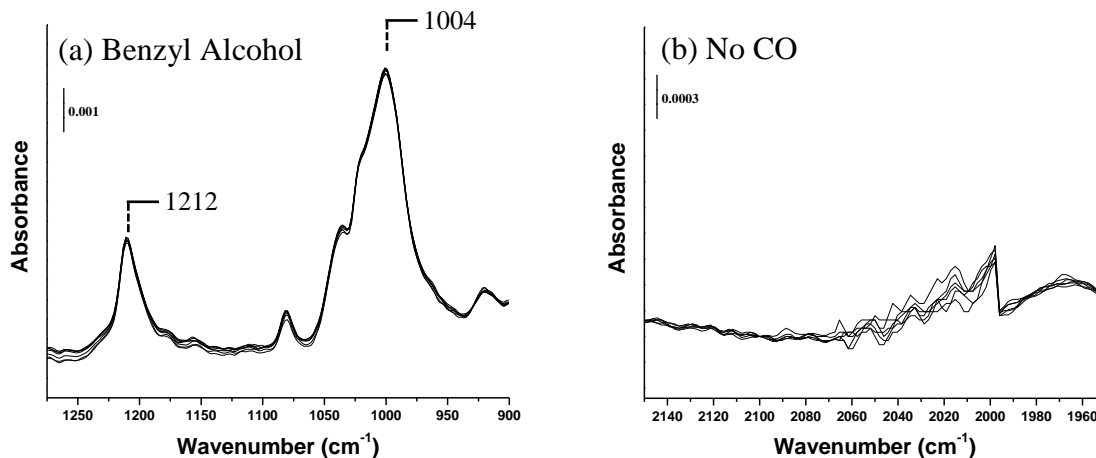


**Figure 5.7.** In-situ ATR-IR spectra of aqueous benzyl alcohol (a) saturated with  $\text{O}_2$  flowing over  $\text{Pt}/\text{SiO}_2$  and the lack of CO (b) over 45 min at 5 bar and 298 K. The water background has been removed.

### Ethanol oxidation

To investigate a supported Pt catalyst with an inert support and oxidation activity (Table 5.1) more similar to that of  $\text{Pt}/\text{C}$ , an identical in-situ ATR-IR study was performed over  $\text{Pt}/\text{BN}$  using ethanol as the substrate. The use of boron nitride as a support eliminates the interaction of hydroxyl groups, such as those found on silica and alumina in liquid water, with the substrate. The inert character of boron nitride makes it a better support to observe adsorbed species on Pt.

Figure 5.8 shows ATR-IR spectra after pumping  $1 \text{ cm}^3 \text{ min}^{-1}$  of  $0.1 \text{ M}$  ethanol solution saturated with  $\text{N}_2$  over the  $5\% \text{ Pt/BN}$  catalyst for approximately  $20 \text{ min}$ . The IR absorption bands at  $2982 \text{ cm}^{-1}$  and  $2904 \text{ cm}^{-1}$  have been assigned to  $\text{sp}^3$  hybridized C-H stretches of ethanol in the proximity of the solid-liquid interface [12]. Figure 5.8(b) shows the IR absorption feature of CO on Pt at approximately  $2040 \text{ cm}^{-1}$  in the presence of water. Figure 5.9(a) shows ATR-IR spectrum as ethanol was removed from the cell by water saturated with  $\text{N}_2$ , whereas Figure 5.9 (b) shows the retention of CO on the Pt surface even after ethanol removal. Figure 10 shows that CO can be rapidly oxidized from the Pt/BN using an air-saturated water stream instead of a pure  $\text{O}_2$  saturated water stream. Clearly, CO on Pt is easily removed by exposure to low levels of dioxygen dissolved in the water phase.

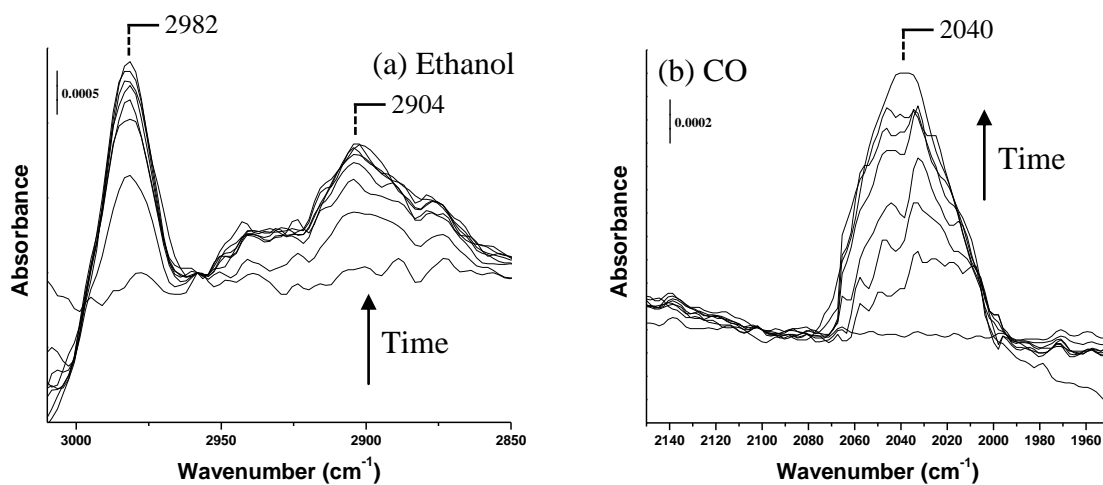


**Figure 5.8.** In-situ ATR-IR spectra of aqueous ethanol (a) saturated with  $\text{N}_2$  flowing over Pt/BN and the production of CO adsorbed on Pt (b) over  $20 \text{ min}$  at  $5 \text{ bar}$  and  $298 \text{ K}$ . The water background has been removed.

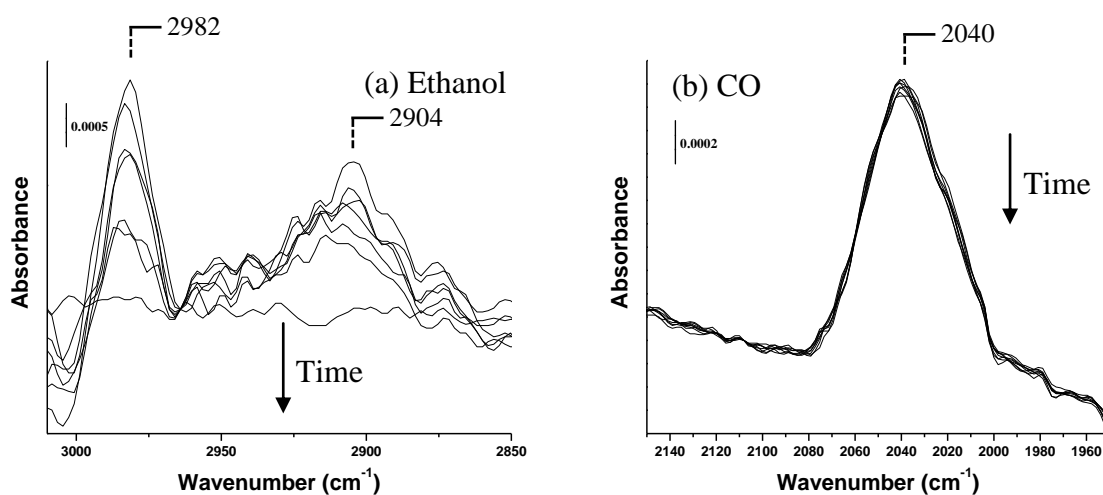


**Figure 5.9.** In-situ ATR-IR spectra of the disappearance of ethanol (a) with H<sub>2</sub>O saturated N<sub>2</sub> flowing over Pt/BN and the strong adsorption of CO on Pt (b) over 45 min at 5 bar and 298 K. The water background has been removed.

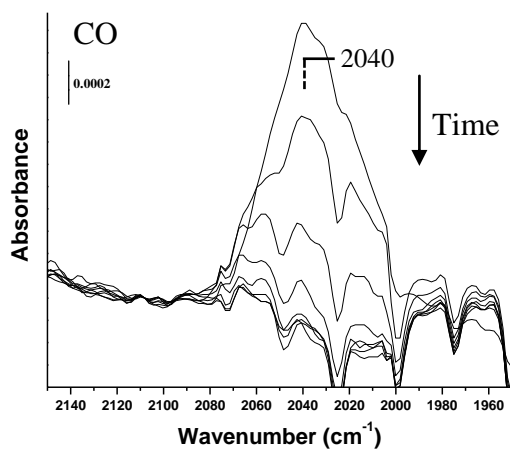


**Figure 5.10.** In-situ ATR-IR spectra of the disappearance of CO after flowing H<sub>2</sub>O saturated with air flowing over Pt/BN for 10 min at 5 bar and 298 K. The water background has been removed.

As mentioned in the previous section, the headspace analysis after ethanol oxidation showed a small amount of methane was produced together with CO<sub>2</sub>. In an attempt to determine whether any carbonaceous species were strongly adsorbed on the Pt surface, a new ATR-IR



background spectrum was recorded after CO was removed with air-saturated water. Then, an aqueous solution saturated with H<sub>2</sub> was pumped over the IRE for 6 h at 1 cm<sup>3</sup> min<sup>-1</sup>. Figure 5.11 shows spectra recorded after 15, 30, 60, 180, and 360 min of flowing H<sub>2</sub> saturated water. The spectrum after 360 min clearly shows two negative peaks at 2920 cm<sup>-1</sup> and 2850 cm<sup>-1</sup>, which are at different positions relative to the C-H stretches of ethanol observed at 2982 cm<sup>-1</sup> and 2904 cm<sup>-1</sup>. We propose that these features are associated with the removal of a carbonaceous species deposited on the catalyst surface. It is difficult to ascertain whether the species was adsorbed on the Pt or on the support, but the inert character of boron nitride and its low surface area and low porosity might preclude it from the strong adsorption of ethanol or its intermediates. These same bands have been associated with adsorbed species on a platinum electrode after ethanol electro-oxidation [13]. The peak at 2920 cm<sup>-1</sup> is likely associated with an asymmetric CH<sub>2</sub> stretch, while the peak at 2850 cm<sup>-1</sup> could either be a symmetric CH<sub>2</sub> stretch or a symmetric CH<sub>3</sub> stretch. However, no associated asymmetric CH<sub>3</sub> stretch was observed around 2960 cm<sup>-1</sup>.

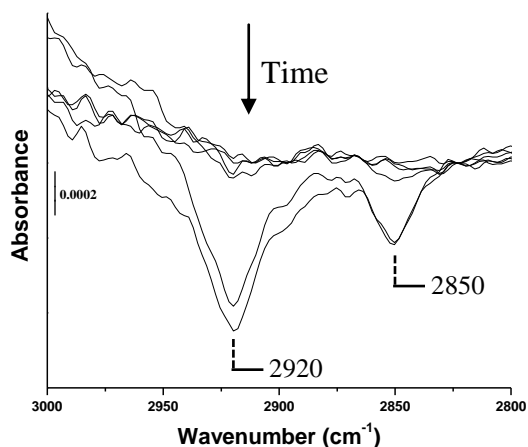


**Figure 5.11.** In-situ ATR-IR spectra of the negative peaks observed after flowing H<sub>2</sub>O saturated with H<sub>2</sub> flowing over Pt/BN for 360 min at 5 bar and 298 K. Spectra obtained at 5, 15, 30, 60, 180, and 360 min. The water background has been removed.

### TGA-MS of ethanol oxidation over Pt/BN

In an attempt to identify if carbonaceous species were strongly adsorbed to the surface, TGA-MS was performed of the Pt/BN catalyst after 24 h of ethanol oxidation in a batch reactor. The Pt/BN catalyst was recovered from solution by centrifugation and then washed with DI water and subsequently recovered ten times to remove loose surface contaminants. The catalyst was then dried overnight at 393 K before being loaded onto the TGA sample platform. Figure 5.12 shows the weight loss profile of fresh (no prior reaction) and the used Pt/BN catalyst. A small amount of weight loss was observed for the fresh and used catalyst prior to 100 °C and this was attributed to weakly adsorbed water after transferring the sample from the oven to the TGA. The used Pt/BN sample clearly shows a large weight loss and corresponding derivative weight peak at 340 °C.

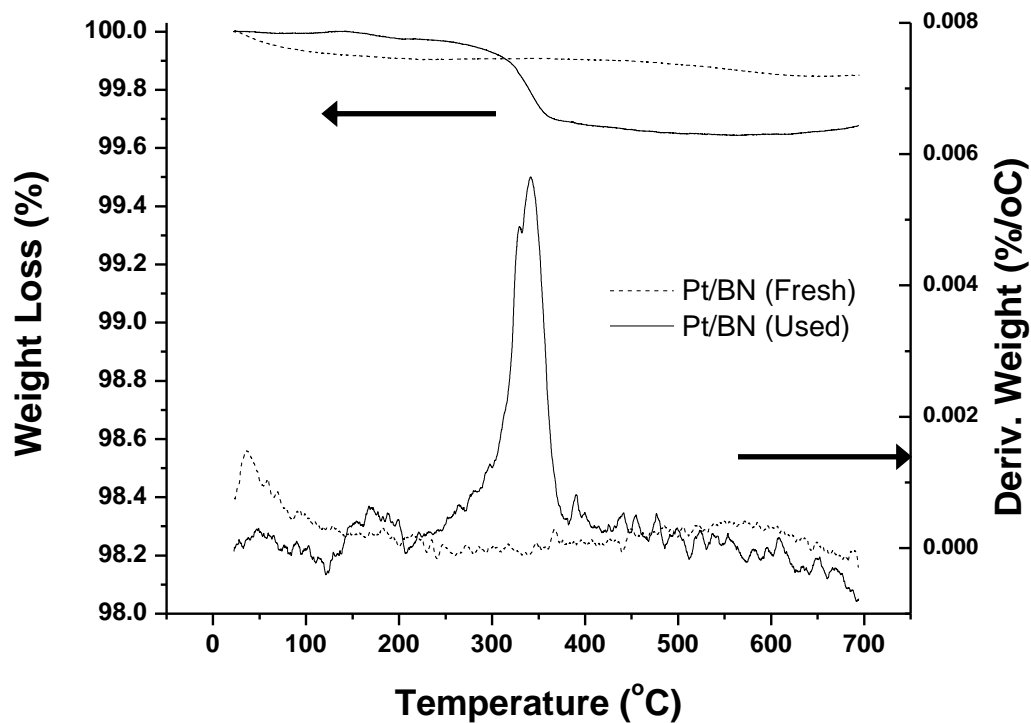


**Figure 5.12.** TGA profile of weight loss (%) and derivative of weight loss (%/°C) of Pt/BN after ethanol oxidation for 24 h.

No significant peaks were observed with mass spectrometry for the fresh Pt/BN catalyst. Figure 5.13 shows the mass spectrum of the TGA profile for the used Pt/BN catalyst. A strong peak was observed at  $m/z = 14$  and a much weaker peak was seen at  $m/z = 16$ . The  $m/z$  of 18 ( $\text{H}_2\text{O}$ ), 31 (Ethanol), 32 ( $\text{O}_2$ ), and 60 (Acetic Acid) had no observable peaks. It is unlikely that the peak at  $m/z$  of 16 originates from water, because the parent peak of water at 18 was not observed. In addition, water would most likely desorb from Pt or the inert boron nitride support at a significantly lower temperature. If the peak MS peak of  $m/z = 14$  is considered the major cause of the loss of weight around  $340\text{ }^\circ\text{C}$ , then a total of  $2.1 \times 10^{-5}$  g or  $1.5 \times 10^{-6}$  moles desorbed from the catalyst and the ratio of the amount of moles desorbed divided by the moles of Pt metal was 0.26. Thus, the desorption of the species observed by MS during TGA could be directly from the Pt surface at high temperature. Given the preponderance of the information in this study, we suggest that a carbon-containing reducible species resides on the Pt during alcohol oxidation and is responsible for a significant fraction of the observed deactivation.

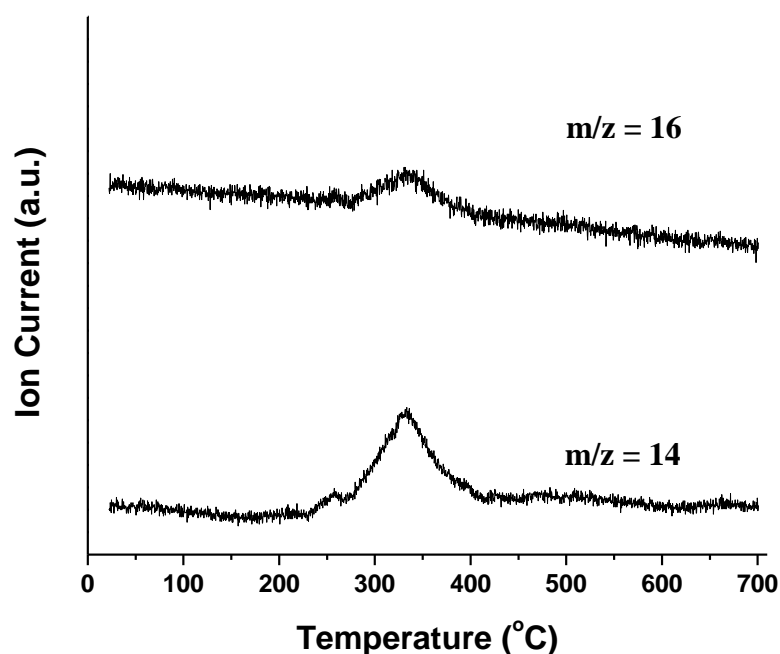


**Figure 5.13.** Mass spectrum corresponding to TGA profile of  $m/z = 14$  and  $16$  after Pt/BN ethanol oxidation for 24 h.

## Conclusions

In-situ ATR-IR spectroscopy observed CO strongly adsorbed to the Pt surface after exposure of the catalyst to benzyl alcohol or ethanol in the presence of water saturated with  $N_2$ . This strongly held CO was rapidly oxidized in the presence of dissolved  $O_2$ . The CO was most likely formed by the decarbonylation of aldehyde intermediates, which would also produce a hydrocarbon remnant species on the Pt surface. Exposure of Pt to  $H_2$  dissolved water was sufficient to remove a species which contained C-H stretches. The TGA-MS of Pt/BN catalyst after ethanol oxidation for 24 h observed a sharp weight loss at 340 °C. The corresponding mass spectrum determined that a species with an  $m/z$  of 14 and/or 16 was most likely the cause of the weight loss. This species was tentatively assigned to a carbonaceous species with a part that is most likely methane adsorbed strongly on the Pt surface.

## Acknowledgements

I thank Derek Falcone for his help with PLD and for teaching me how to use the ATR-IR experimental setup. This material is based upon work supported by the National Science Foundation under Award Nos. EEC-0813570 and OISE 0730277.

## References

- [1] I. Ortiz-Hernandez, In situ investigation of solid-liquid catalytic interfaces by attenuated total reflection infrared spectroscopy. *Langmuir* 19 (2003) 2956-2962.
- [2] N. J. Harrick, *Internal Reflection Spectroscopy*. 1967, New York: Interscience Publishers. pp. 327.
- [3] T. Bürgi, A. Baiker, Attenuated total reflection infrared spectroscopy of solid catalysts functioning in the presence of liquid-phase reactants. *Adv. Catal.* 50 (2006) 227-283.
- [4] D. Ferri, A. Baiker, Advances in infrared spectroscopy of catalytic solid-liquid interfaces: The case of selective alcohol oxidation. *Top. Catal.* 52 (2009) 1323-1333.
- [5] D. Ferri, A. Baiker, Probing boundary sites on a Pt/Al<sub>2</sub>O<sub>3</sub> model catalyst by CO<sub>2</sub> hydrogenation and in situ ATR-IR spectroscopy of catalytic solid-liquid interfaces. *Phys. Chem. Chem. Phys.* 4 (2002) 2667-2672.
- [6] D. Ferri, T. Bürgi, An in situ attenuated total reflection infrared study of a chiral catalytic solid-liquid interface: Cinchonidine adsorption on Pt. *J. Am. Chem. Soc.* 123 (2001) 12074-12084.
- [7] R. He, R. R. Davda, J. A. Dumesic, In situ ATR-IR spectroscopic and reaction kinetics studies of water-gas shift and methanol reforming on Pt/Al<sub>2</sub>O<sub>3</sub> catalysts in vapor and liquid phases. *J. Phys. Chem.-B* 109 (2005) 2810-2820.
- [8] J. Grunwaldt, A. Baiker, In situ spectroscopic investigation of heterogeneous catalysts and reaction media at high pressure. *Phys. Chem. Chem. Phys.* 7 (2005) 3526-3539.
- [9] C. Keresszegi, D. Ferri, T. Mallat, A. Baiker, Unraveling the surface reactions during liquid-phase oxidation of benzyl alcohol on Pd/Al<sub>2</sub>O<sub>3</sub>: an in situ ATR-IR study. *J. Phys. Chem. B* 109 (2005) 958-967.
- [10] C. Mondelli, J. Grunwaldt, D. Ferri, A. Baiker, Role of Bi promotion and solvent in platinum-catalyzed alcohol oxidation probed by in situ X-ray absorption and ATR-IR spectroscopy. *Phys. Chem. Chem. Phys.* 12 (2010) 5307-5316.

- [11] S. D. Ebbesen, B. L. Mojet, L. Lefferts, In situ ATR-IR study of CO adsorption and oxidation over Pt/Al<sub>2</sub>O<sub>3</sub> in gas and aqueous phase: Promotion effects by water and pH. *J. Catal.* 246 (2007) 66-73.
- [12] B. Beden, M. C. Morin, F. Hahn, C. Lamy, "In situ" analysis by infrared reflectance spectroscopy of the adsorbed species resulting from the electrosorption of ethanol on platinum in acid medium. *J. Electroanal. Chem.* 229 (1987) 353-366.
- [13] T. Iwasita, E. Pastor, A Dems and FTIR spectroscopic investigation of adsorbed ethanol on polycrystalline platinum. *Electrochim. Acta.* 39 (1994) 531-537.

## Chapter 6: Bimetallic Nanoparticles for Alcohol Oxidation

### Introduction

Bimetallic nanoparticles often demonstrate significantly different properties when compared to either of the parent metals. When two metals are in close proximity, the interaction between the metals or change in nanoparticle structure can considerably alter the catalytic activity, selectivity, and stability. However, it is not simple to deduce this change prior to catalyst synthesis. In addition, the alloying of two metals on the nano-scale is very different than bulk alloy behavior [1]. Alloys that are immiscible in the bulk, such as Pt and Au, can form bimetallic nanoparticles due to the change in surface free energy at the nanoscale [2]. Phase diagrams that are readily available for bulk alloys of most miscible metals, are not always applicable to nanoparticle alloys and do not accurately predict nanoparticle composition. Because of the high surface to volume ratio and high surface energy, bimetallic nanoparticle formation can happen at much lower temperatures than their bulk phase diagrams predict [3]. PtAu bimetallic nanoparticles have been shown to have a higher activity and/or selectivity for electro-oxidation of alcohols, oxygen reduction reaction, alkane isomerization, aromatic hydrogenation in the presence of sulfur, and nitric acid reduction than platinum alone [2]. However, the addition of Au to Pt has been suggested to be primarily an ensemble (geometric) effect in some applications and a ligand (electronic) effect in others [4].

A major topic of current research for polyol oxidation, such as glycerol, is how to quantify the performance of bimetallic catalysts. It can often be difficult to compare the rate of alcohol oxidation or deactivation behavior of bimetallic catalysts against the monometallic analogues. Ketchie et al. reported that a bimetallic AuPd/C catalyst had a TOF of  $7 \text{ s}^{-1}$ , which is fairly typical of Au catalysts at basic conditions, but with increased selectivity to glyceric acid

[5]. Palladium apparently accelerated the decomposition of  $\text{H}_2\text{O}_2$ , which prevented cleavage of glyceric acid and tartronic acid to two and one carbon products. Other bimetallic AuPd catalysts synthesized with slightly less and more Au were of about the same rate while maintaining the same selectivity at 50% conversion. However, Bianchi et al saw the opposite trend for rate as the AuPd alloy had a faster reaction rate with a TOF of  $1.3 \text{ s}^{-1}$  than just the monometallic Au which had a TOF of  $0.8 \text{ s}^{-1}$  [6]. A bimetallic AuPd catalyst was also synthesized by Dimitratos et al. and showed no significant effect on activity of glycerol oxidation compared to a monometallic catalyst (TOF =  $1.6 \text{ s}^{-1}$ ) [7]. Prati et al. reported that a bimetallic catalyst synthesized by deposition of Ru on the Au/C catalyst (Ru@(Au/C)) using the sol method showed enhanced conversion of glycerol of 99% compared to 73% over the monometallic Au/C catalyst after 1 h, but it is difficult to perform a quantitative rate comparison at such high levels of conversion [8]. An interesting application of bimetallic catalysts was reported by Hirasawa et al., who alloyed Pd and Ag on carbon by co-impregnation [9]. An increase in glycerol conversion from 2.8% for the monometallic Pd/C to 6.7% for the 1:1 PdAg/C catalyst was reported at 353 K and 300 kPa  $\text{O}_2$  in the absence of base. The Ag/C catalyst was inactive at these reaction conditions. In addition, the amount of CO chemisorbed did not vary significantly (<20%) for the monometallic and bimetallic catalysts which led the authors to suggest that the two catalysts have similar metal particle sizes. The researchers speculated that the increase in conversion is due to Ag preventing deactivation of the active Pd catalyst. Similar results have been shown for alloying bismuth with platinum to prevent deactivation during glycerol oxidation at neutral to acidic pH [10-12].

The supported PtAu bimetallic nanoparticle is interesting from both a materials and catalytic viewpoint for the oxidation of alcohols. It has been proposed that the addition of Au to Pt decreases the strength of adsorption of the substrate, products, or byproducts, which in turn



increases the catalytic rate of alcohol oxidation in the presence of base [13]. However, the same research group concluded in different work that the role of Au was to prevent the deactivation of Pt by oxygen or byproducts during alcohol oxidation without base [14]. More recent work by Prati et al. showed the sequential impregnation of Pt on a Au sol to synthesize a 1:1 Pt@Au/C catalyst was twice as active as Pt/C and four times as active as Au/C based on total metal loadings for the oxidation of glycerol in base at 50 °C [15]. However, a detailed characterization of the catalysts was not reported making it difficult to accurately compare monometallic and bimetallic catalysts and the increase in activity was attributed to “strong positive synergistic effects.” Villa et al. used a similar technique to synthesize 1% (6:4) AuPt/C and AuPt/H-Mordenite catalysts, [16] where the AuPt particles were determined to be alloyed by EDS. The catalysts were inactive at 50 °C for glycerol oxidation in the absence of base, but at elevated temperatures (100 °C) an increase in glycerol conversion over the mordenite supported bimetallic was seen when compared to the monometallic Pt/H-Mordenite. However, a decrease in conversion over the PtAu/C catalyst was noted when compared to Pt/C after 2 h of reaction. These results are intriguing because Au is inactive at acidic conditions for alcohol oxidation. However, there is a severe lack of characterization of the catalysts, understanding of the PtAu alloy, and effect of support that needs further investigation to clarify what affect, if any, Au has on Pt for the oxidation of alcohols.

## **Experimental Methods**

### **Catalyst preparation**

A 1% Pt/C, 1% Au/C, 1:1 1% PtAu/C, 3:1 1% PtAu/C, 1% PtPd/C, 3% Pt/SiO<sub>2</sub>, 1% PtAu/SiO<sub>2</sub>, and 1% PtAu/TiO<sub>2</sub> catalyst were synthesized with the sol-immobilization method. For the preparation of all the catalysts, the appropriate amount of H<sub>2</sub>PtCl<sub>4</sub> (Sigma-Aldrich)

and/or  $\text{HAuCl}_4$  (Aldrich) were added to 1.5 L of DI water under constant stirring at 500 RPM. Then polyvinylalcohol (PVA, 75% hydrolyzed, MW=2,000) was added in a ratio of PVA/(Pt+Au) of 1.2 (wt/wt) to stabilize small colloidal nanoparticles. After 15 min, a fresh solution of 0.1 M  $\text{NaBH}_4$  solution was added dropwise over 1 h in a ratio of  $\text{NaBH}_4$ /(Au+Pt) of 5 (mol:mol) to form a sol in aqueous solution. After mixing for an additional 30 min, the solution was acidified by 5 drops of concentrated  $\text{H}_2\text{SO}_4$  followed by the addition of an appropriate amount of support to immobilize the sol. After 2 h of mixing, the slurry was filtered and washed thoroughly with 2.5 L of DI water and dried overnight at 393 K. The catalysts were then reduced under  $100 \text{ cm}^3 \text{ min}^{-1}$  of  $\text{H}_2$  (GT&S 99.999%) for 4 h at 573 K to decompose PVA.

A Pt/C, PtRu/C, PtSn/C, PtCu/C, and PtZn/C catalyst were prepared by incipient wetness co-impregnation of chloroplatinic acid (Sigma-Aldrich) and either ruthenium chloride hydrate, tin tetrachloride, copper nitrate hydrate, or zinc nitrate hexahydrate on an activated charcoal support (Norit, SX ultra). The catalyst was then dried in air for 12 h at 393 K, reduced in  $100 \text{ cm}^3 \text{ min}^{-1}$  of flowing  $\text{H}_2$  for 4 h, cooled, exposed to air, and stored at ambient temperature.

### **Catalyst characterization**

The metal dispersion of the supported Pt and bimetallic Pt catalysts was determined by  $\text{H}_2$  chemisorption using a Micromeritics ASAP 2020 automated adsorption analyzer. The supported Pt catalysts were heated to 473 K at  $4 \text{ K min}^{-1}$  under flowing  $\text{H}_2$  (GT&S 99.999%) and reduced for 2 h. The samples were then evacuated and held for 2 h at 473 K before being cooled to 308 K for analysis in the pressure range of 10-450 Torr. The analysis of the PtPd/C catalyst was carried out at 373 K in the pressure range of 10-450 Torr to avoid formation of the  $\beta$ -phase Pd hydride. The amount of metal on the surface was evaluated by the total amount of  $\text{H}_2$  adsorbed, extrapolated to zero pressure, assuming a stoichiometry ( $\text{H}/\text{M}_{\text{surf.}}$ ) equal to unity.

The elemental analysis of Pt and Au on the catalysts was performed by Galbraith Laboratories (2323 Sycamore Drive, Knoxville, TN 37921) using ICP – AES analysis. The leaching of PtAu/C catalyst after reaction was also measured by ICP of the filtrate for both Pt and Au.

To prepare the 1:1 PtAu/C catalyst for transmission electron microscopy (TEM), ~1 mg of sample was suspended in 2 cm<sup>3</sup> of ethanol by agitating the mixture for 30 minutes in a sonication bath. A copper grid with a holey carbon film was briefly dipped in the solution and the ethanol was evaporated. The imaging of the catalyst was performed on a FEI Titan operating at 180 kV and equipped with a Gatan 794 Multi-scan Camera (EFTEM). The energy-dispersive X-ray spectroscopy (EDS) was performed on the bimetallic PtAu/C catalyst to determine the Pt and Au composition. The EDS of single-particles, a few dozen particles, and several hundred particles were examined to determine the uniformity of Pt and Au deposition on the catalyst support.

The X-ray diffraction (XRD) patterns were recorded on a Scintag automated diffractometer using Cu K $\alpha$  radiation (40 kV, 30 mA) and continuous scanning of  $2\theta$  from 20° to 80° with a step size of 0.05° at a rate of 0.3° min<sup>-1</sup>. The crystalline size of the metal particles was calculated by the Scherrer equation [ $d = K \lambda (\beta_{1/2} \cos (2\theta))^{-1}$ ].

### **Alcohol oxidation**

The semi-batch aqueous alcohol oxidation reactions were performed in a 50 cm<sup>3</sup> Parr Instrument Company 4592 batch reactor with a 30 cm<sup>3</sup> glass liner. The appropriate amounts of substrate, acid (to control pH), and catalyst were added to approximately 10 cm<sup>3</sup> of distilled, deionized water in the glass liner. The glass liner was inserted into the reactor, sealed, purged with He, and heated to 343 K. The reaction was initiated by pressurizing the reactor with 10 bar

absolute O<sub>2</sub> (GT&S, 99.993%). The pressure was maintained at a constant value by continually feeding O<sub>2</sub>. No conversion was observed after 240 min when N<sub>2</sub> was substituted for O<sub>2</sub>. Samples were periodically removed and the catalyst was filtered using 0.2 μm PTFE filters before analyzing in a Waters e2695 high pressure liquid chromatograph (HPLC). The HPLC was equipped with refractive index and UV/Vis detectors. Product separation in the HPLC was carried out with a Aminex HPX-87H column (Bio-Rad) operating at 318 K with 5 mM H<sub>2</sub>SO<sub>4</sub> in water flowing at 5 cm<sup>3</sup> min<sup>-1</sup>. Carbon balances were typically greater than 90%. The retention times and calibration curves were determined by injecting known concentrations of standards. The pH of the samples was determined by a Orien 3-Star Plus pH Portable Meter with a Thermo Orion 9810BN Micro-pH Electrode after the sample had cooled to room temperature.

The initial turnover frequency (TOF) [mol alcohol converted (mol M<sub>surface</sub>)<sup>-1</sup> s<sup>-1</sup>] for alcohol oxidation was calculated from the initial conversion of the alcohol, usually within the first 15 minutes of the reaction. A sample was also taken at 30 minutes to confirm that significant deactivation had not occurred in the initial rate determination. The maximum O<sub>2</sub> transport rate from the gas phase to the aqueous phase in the pressurized reaction system was determined by the sulfite oxidation method [17]. The amount of catalyst added to the reactor was chosen so that the alcohol oxidation rate would not be limited by O<sub>2</sub> mass transfer from the gas to the liquid when determining the TOF. No conversion was found after 240 min in the absence of catalyst. Selectivity to a specific product is defined as moles of that product formed divided by moles of all products produced.

The concentration of hydrogen peroxide formed during the reaction was quantified using a colorimetric method [18]. After removing the catalyst from 1 cm<sup>3</sup> of sample, the hydrogen peroxide was stabilized by the addition of 1 cm<sup>3</sup> of 0.5 M H<sub>2</sub>SO<sub>4</sub>. Then, 0.1 cm<sup>3</sup> of 15 wt%

TiO(SO<sub>4</sub>) in dilute H<sub>2</sub>SO<sub>4</sub> (Aldrich) was added to the sample and the absorbance was measured at 405 nm on a Varian Cary 3E UV-Vis spectrometer. The calibration curve was established by diluting 30 wt% H<sub>2</sub>O<sub>2</sub> (Fisher) with distilled deionized water. The detection limit was determined to be 0.1 mM.

## Results and Discussion

### Catalyst characterization

Table 6.1 summarizes the metal loadings, dispersions, and particle size of the catalysts synthesized by the sol immobilization method. The monometallic Pt/C had a Pt weight loading of 0.73% as determined by ICP-AES analysis. The fraction of platinum metal exposed, or dispersion (d), was determined to be 0.18 by hydrogen chemisorption (H/M) with an estimated particle size (1/d) of 5.6 nm. The crystallite size of the platinum particles by XRD analysis was calculated to be 6.6 nm, which is in good agreement with the particle size estimated by hydrogen chemisorption. The crystallite size of the 1% Au/C catalyst was determined to be 3.5 nm by XRD analysis. The hydrogen chemisorption was not determined because the H/Au<sub>surf</sub> ratio has been shown to be significantly lower than the actual dispersion for monometallic gold catalysts. The dissociation and adsorption of hydrogen only occurs at corner and edge sites [19]. The 3% Pt/SiO<sub>2</sub> had a higher dispersion of 0.47 when compared to Pt/C despite the similar catalyst synthesis with the sol-immobilization technique.

**Table 6.1.** Characterization of catalysts prepared by sol-immobilization.

Catalyst	Metal (wt%)	Atomic Ratio Pt: Au	Dispersion (H/Metal)	Metal Particle Diameter (nm)		
				Chem.	TEM	XRD
Pt/C	0.73	-	0.18	5.6	-	6.6
Au/C	1	-	-	-	-	3.5
Pt-Au/C	1.1	0.86	0.02 (0.04) <sup>a</sup>	-	4.1	3.1
Pt-Au/C	1	3	0.10 (0.13) <sup>a</sup>	-	-	11
Pt/SiO <sub>2</sub>	3	-	0.47	2.1	-	-
Pt-Au/SiO <sub>2</sub>	1	1	(0.49) <sup>a</sup>	-	-	-
Pt-Au/TiO <sub>2</sub>	1	1	(0.11) <sup>a</sup>	-	-	-
Pt-Pd/C	1	1	0.33	-	-	3.6

<sup>a</sup> The dispersion in parenthesis is calculated based on Pt instead of total metal.

The metal weight loading of the 1.1% PtAu/C catalyst was determined by ICP-AES and the atomic ratio of Pt: Au was determined to be 0.86, which is slightly lower than the attempted ratio of 1. The size of the PtAu nanoparticles was determined by analyzing 200 particles from TEM images, which gave an average diameter of  $4.1 \pm 1.6$  nm as shown in Figure 6.1. The crystallite size of the PtAu particles by XRD analysis was calculated to be 3.1 nm with the Scherrer equation. However, the hydrogen chemisorption on the bimetallic catalyst was significantly lower than anticipated with a total metal dispersion of 0.02 or metal dispersion calculated based on just Pt of approximately 0.04. The dispersion measured by analysis of nanoparticles with TEM images (4.1 nm) would be  $(1/D)$  0.24. Thus, approximately 8% of the total exposed metal chemisorbed hydrogen or, if the surface of the nanoparticles was a 50/50 mixture of Pt and Au, one third of the Pt metal ( $0.04 / 0.12$ ) was capable of hydrogen dissociation. These results are similar to those found by Bus et al. where less than 20% of the total exposed metal atoms adsorbed hydrogen for a 1:1 PtAu/SiO<sub>2</sub> catalyst with 1.5 nm particles [20]. The lack of hydrogen adsorption may suggest that the interaction of hydrogen with the PtAu alloy is weaker than that of monometallic Pt. However, the strongly chemisorbed hydrogen

was found to have the same heat of adsorption on Pt/SiO<sub>2</sub> and PtAu/SiO<sub>2</sub> leading the authors to conclude that Au only had a geometric effect on hydrogen adsorption [20].

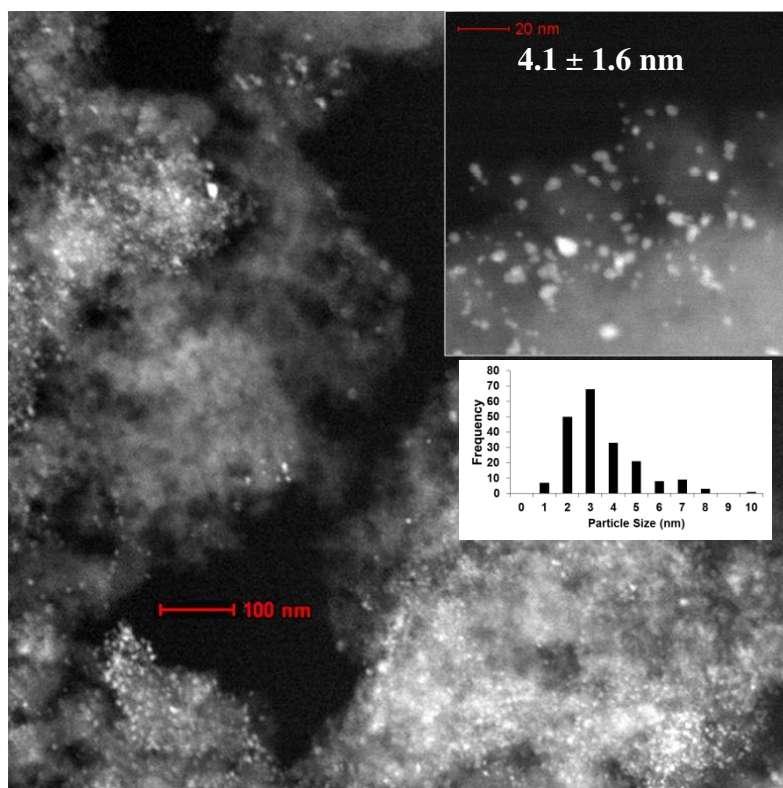


**Figure 6.1.** TEM dark field images of 1.1% PtAu/C.

The energy dispersive X-ray spectroscopy (EDS) of the 1.1% PtAu/C catalyst indicated that all individual particles investigated had both Pt and Au and a sample EDS is shown in Figure 6.2. The orange box in Figure 6.2(a) shows the single nanoparticle that was probed and Figure 6.2(b) is the corresponding EDS spectrum. The focus of the electron beam was on a thin area of the catalyst surface because of the penetrating depth ( $\sim 100$  nm) of the beam. Table 6.2 reports the quantitative elemental composition after averaging several single particle EDS spectrum and finds the bimetallic nanoparticles were approximately 30% Pt and 70% Au. The elemental composition of the nanoparticles was slightly different than that reported by ICP-AES elemental analysis of the catalyst of 46% Pt and 54% Au. Interestingly, the Pt and Au wt% were

fairly consistent across the EDS of 1 particle, 5 particles, 100 particles, and approximately 500 particles as shown in Table 6.2. The limit of detection for EDS is typically around 0.5 wt%, which was approximately the wt% of both Pt and Au in the sample, and may have contributed to the deviation from ICP-AES elemental analysis as well as the large standard deviation [21]. Figure 6.3 shows a used 1.1% PtAu/C catalyst that was recovered after 24 h of 1,6-hexanediol oxidation. The EDS determined that the elemental composition of the used catalyst was within one standard deviation of the fresh catalyst at about 37% Pt and 63% Au when 200 particles were probed. Unfortunately, the EDS of single nanoparticles on the used catalyst was not possible because of species on the catalyst surface that volatilized covering the sample with a film when they were focused on by the electron beam. All EDS elemental analysis results strongly suggest that there are most likely PtAu bimetallic nanoparticles supported on carbon.

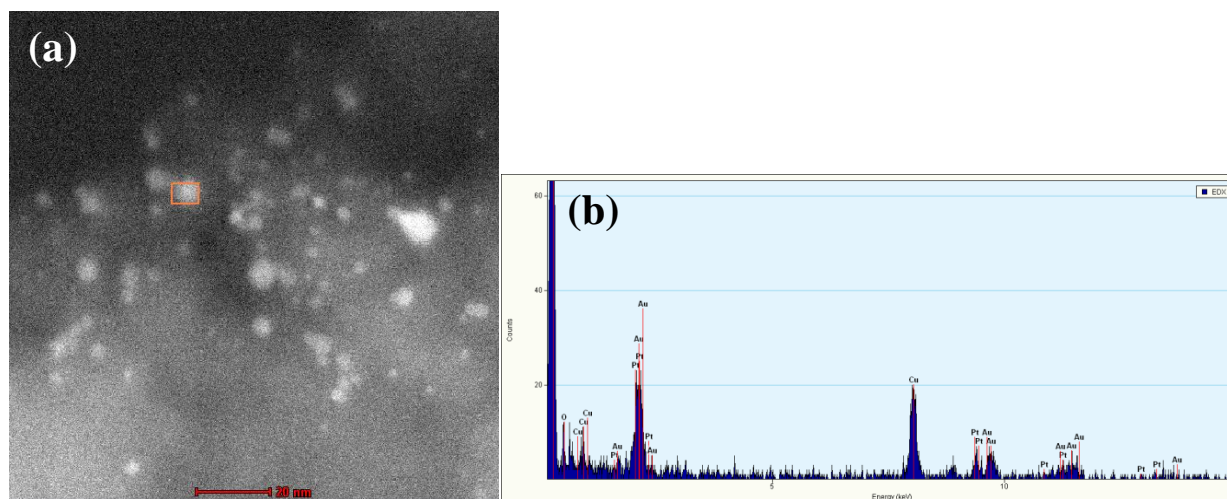


**Figure 6.2.** TEM dark field image (a) and corresponding energy dispersive X-ray spectroscopy (EDS) (b) of a single nanoparticle for the fresh 1.1% PtAu/C catalyst. The orange box identifies the area probed by EDS.



**Table 6.2.** Elemental composition of nanoparticles determined by energy dispersive X-ray spectroscopy.

Number of Nanoparticles	Pt (wt%)	Au (wt%)
Fresh ~ 500 particles	35 ± 3	65 ± 4
Fresh ~ 100 particles	31 ± 6	69 ± 8
Fresh – 5 particles	32 ± 1	68 ± 1
Fresh – 1 particle <sup>a</sup>	30 ± 11	70 ± 14
Used ~ 200 particles	37 ± 4	63 ± 5

<sup>a</sup> Average of several single particle EDS.

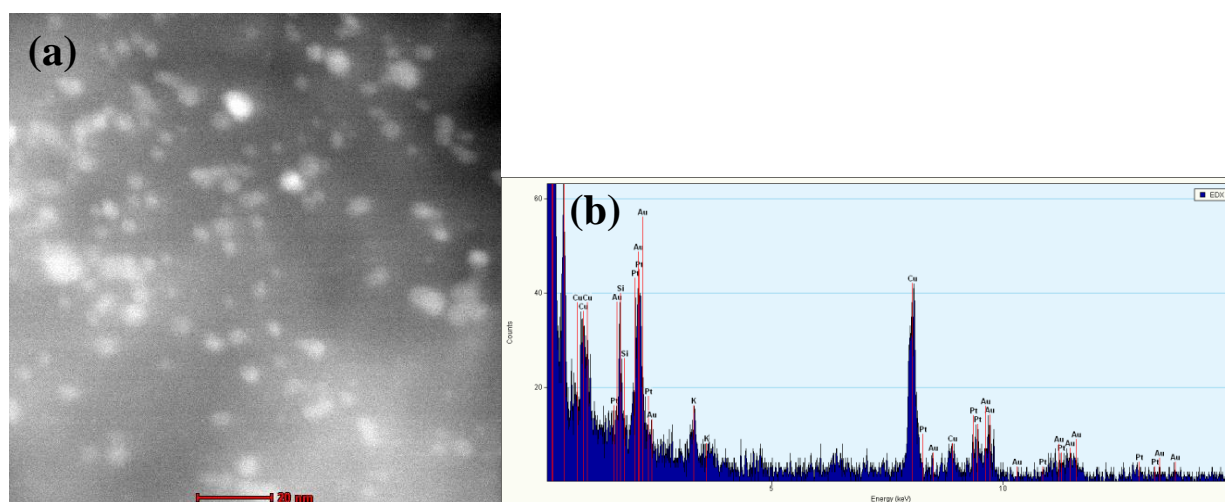


**Figure 6.3.** TEM dark field image (a) and corresponding energy dispersive X-ray spectroscopy (b) of approximately one hundred particles for the used 1.1% PtAu/C catalyst.

The XRD pattern of the three catalysts is shown in Figure 6.4 and the estimation of the crystallite size by the Scherrer equation was reported in Table 6.1. The broad peaks suggest small particle sizes and the crystallite size estimation is within the standard deviation of particle size measured by TEM for the 1:1 PtAu/C catalyst. The diffraction peak of Au(111) for the 1% Au/C sample was found at  $38.2^\circ$  and the 0.73% Pt/C sample had a Pt(111) diffraction peak at  $39.7^\circ$ . The XRD pattern of the Norit Carbon support identified the peaks at approximately  $27^\circ$  and  $44^\circ$  to be structured and amorphous carbon. The diffraction peak of the bimetallic 1:1 PtAu/C catalyst fell between the monometallic peaks at  $38.8^\circ$ , which suggests that a significant

portion of the metals were alloyed [22]. While no peak splitting in the XRD patterns was observed, which would indicate segregation of the metals at the nano-scale, it can be difficult to draw conclusions for such small particles using XRD [23]. However, both the XRD and EDS results suggest that bimetallic nanoparticles were formed during the synthesis of the 1:1 PtAu/C catalyst.

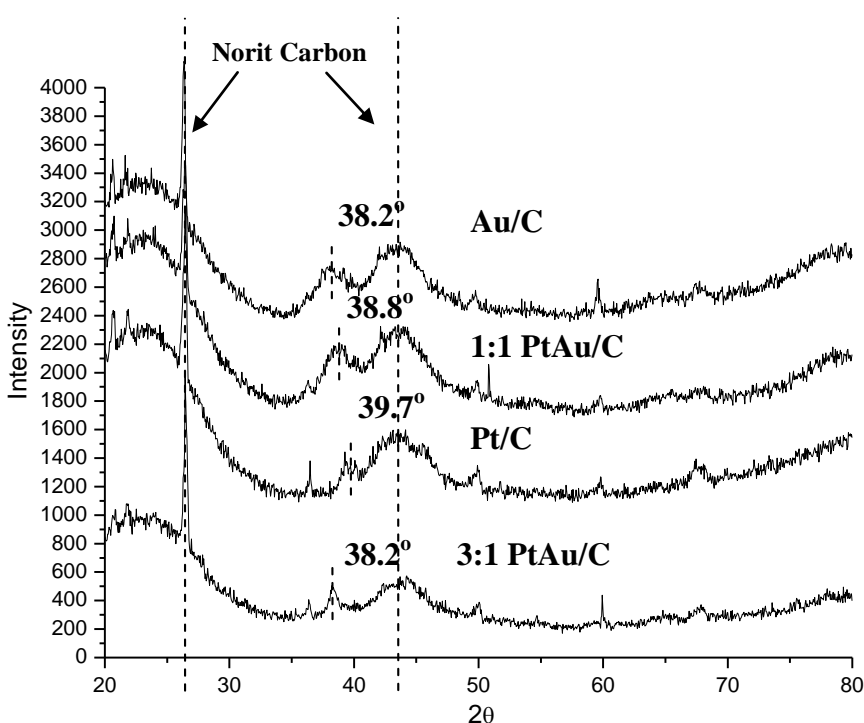


**Figure 6.4.** XRD patterns of Pt/C, Au/C, and PtAu/C Catalysts. The dashed lines represent the (111) faces of the monometallic and bimetallic nanoparticles.

The 3:1 PtAu/C catalyst only had a recognizable diffraction peak of  $38.2^\circ$ , which corresponds to the Au(111) peak as shown in Figure 6.4. The peak for the 1% 3:1 Pt-Au/C catalyst is notably sharper than that of the 1% Au/C catalyst and has a larger crystallite size of 11 nm. The XRD results suggest that segregated Au nanoparticles were formed. The absence of a sharp Pt diffraction peak might indicate that the Pt is well dispersed, however, hydrogen chemisorption determined a dispersion of 0.13 based on just the Pt weight loading (Table 6.2).

The dispersion measured by chemisorption for the 1:1 PtAu/SiO<sub>2</sub> was 0.49 based on just Pt, which was significantly higher than that found in the literature for bimetallic PtAu nanoparticles supported on silica [20]. The 1:1 PtAu/TiO<sub>2</sub>, however, had a dispersion of 0.11, which was similar to that of the 3:1 PtAu/C catalyst. The 1:1 PtPd/C catalyst had a dispersion of 0.33 that corresponds to (1/d) an average particle size of 3 nm.

Table 6.3 summarized the dispersion and XRD crystallite size of the catalysts synthesized by the co-impregnation method. The 3% Pt/C (Norit) catalyst had a dispersion of 0.73 that corresponds to a metal particle diameter (1/d) of 1.4 nm, which was in good agreement with the crystallite size determined by XRD of 2.4 nm. The 3%Pt-1.5%Ru/C catalyst had a dispersion of 0.13 based on the total metal loading, because ruthenium is capable of hydrogen dissociation, while the dispersion of the 3%Pt-1.9%Sn/C that was 0.37 and 3%Pt-1.2%Zn/C that was 0.61 was calculated based on just the Pt weight loading.

**Table 6.3.** Characterization of catalysts prepared by incipient wetness co-impregnation.

Catalyst	H <sub>2</sub> Reduction Temperature (K)	Dispersion (H/Metal)	Metal Particle Diameter (nm)	
			Chem.	XRD
3% Pt/C (Norit)	673	0.73	1.4	2.4
3%Pt-1.5% Ru/C	473	0.13	7.7	5.5
3%Pt-1.9% Sn/C	573	0.37 <sup>a</sup>	2.7	3.1
3%Pt-1.2% Zn/C	673	0.61 <sup>a</sup>	1.6	2.8

<sup>a</sup> The dispersion is calculated based on Pt instead of total metal.

### Alcohol oxidation

The oxidation of 1,6-hexanediol in an aqueous solution with 10 bar dioxygen at 343 K and a pH of 2.5 over the monometallic and bimetallic supported catalysts was investigated and the initial rate of reaction (TOF) was determined. Table 6.4 reports the dispersion and TOF for the catalysts synthesized by the sol-immobilization technique. One concern when using the sol-

immobilization technique is that the polymer stabilizer (PVA) might block a portion of the active sites after catalyst synthesis [23]. Thus, a comparison of the 0.73% Pt/C catalyst was performed before and after thermal decomposition of the polymer with  $100 \text{ cm}^3 \text{ min}^{-1} \text{ H}_2$  flow at 473 K[24]. The 0.73% Pt/C had a TOF for 1,6-hexanediol oxidation of  $0.03 \text{ s}^{-1}$  before a thermal treatment, while after the decomposition of PVA the initial rate of reaction was  $0.20 \text{ s}^{-1}$ . While the decomposition of PVA could leave behind a carbon residue that blocks active catalyst sites, the TOF for Pt/C synthesized by sol-immobilization was similar to the 3% Pt/C (Norit) synthesized by incipient wetness ( $0.19 \text{ s}^{-1}$ ) shown in Table 6.5. The carbon residue could have decreased the hydrogen uptake of the 0.73% Pt/C catalyst and artificially decreased the dispersion, but the good agreement between the average metal particle size determined by dispersion and crystallite size with XRD gives us reasonable certainty that the blocking of active sites was minimal after the thermal decomposition of PVA. The 3% Pt/SiO<sub>2</sub> had a similar TOF of  $0.17 \text{ s}^{-1}$  after thermal treatment to remove PVA, despite the much smaller average particle size as determined by hydrogen chemisorption. The 1% Au/C catalyst was inactive for alcohol oxidation at acidic conditions.

A decrease in initial 1,6-hexanediol oxidation activity was also observed before thermal reduction of the 1.1% 1:1 PtAu/C catalyst. The TOF of  $0.21 \text{ s}^{-1}$  before the thermal treatment was less than one third of the initial rate of reaction of  $0.68 \text{ s}^{-1}$  determined after removal of PVA from the catalyst surface. A similar initial oxidation rate was determined when the ratio of substrate to total metal was increased by four times, which suggests that external mass transfer of oxygen (gas-liquid) was not rate limiting. The bimetallic PtAu/C catalyst had a significantly increased TOF for 1,6-hexanediol oxidation ( $0.68 \text{ s}^{-1}$ ) when compared to the monometallic Pt/C catalyst ( $0.20 \text{ s}^{-1}$ ). In addition, both catalysts had similar average metal particle sizes. The increase in rate

of reaction was particularly interesting because Au was inert for alcohol oxidation at these conditions. Villa et al. observed an increase in glycerol conversion rate when comparing the PtAu/H-mordenite to the Pt/H-mordenite catalyst at 100 °C and a decrease in the oxidation rate of 26% when comparing Pt/C to PtAu/C [16]. This result is a direct contradiction to that in this work. A full characterization of the PtAu/C catalyst was not provided by Villa et al., thus, a significantly different particle size could explain the differences in conversion.

**Table 6.4.** Oxidation activity of 1,6-hexanediol over catalysts synthesized by the sol-immobilization technique.<sup>a</sup>

Catalyst	Dispersion	TOF <sup>b</sup> s <sup>-1</sup>
0.73% Pt/C	0.18	0.20
0.73% Pt/C (Not Reduced)	0.18 <sup>d</sup>	0.03
3% Pt/SiO <sub>2</sub>	0.47	0.17
1% Au/C	0.29	-
0.86:1 1.1% Pt-Au/C	0.24	0.68
0.86:1 1.1% Pt-Au/C (Not Reduced)	0.24 <sup>d</sup>	0.21
0.86:1 1.1% Pt-Au/C <sup>c</sup>	0.24	0.65
3:1 1% Pt-Au/C	0.10	0.17
1:1 1% Pt-Au/SiO <sub>2</sub>	(0.49) <sup>e</sup>	0.13
1:1 1% Pt-Au/TiO <sub>2</sub>	(0.11) <sup>e</sup>	0.16
1:1 1% Pt-Pd/C	0.33	0.12

<sup>a</sup> Reaction Conditions: 0.1 M 1,6-hexanediol (HDO), HDO.:Metal = 500, pO<sub>2</sub> = 10 bar, T = 343 K, 0.35 M Acetic Acid, pH = 2.5.

<sup>b</sup> Turnover frequency is reported at ~10% conversion.

<sup>c</sup> HDO:Met. ~ 2000.

<sup>d</sup> Dispersion assumed identical for reduced and not reduced catalysts in order to compare activity.

<sup>e</sup> The dispersion in parenthesis is calculated based on Pt instead of total metal.

A 1% 3:1 PtAu/C catalyst was synthesized by sol-immobilization and determined to have an initial TOF of 0.17 s<sup>-1</sup> based on a dispersion of 0.10. As mentioned for the 1.1% 1:1 PtAu/C catalyst, the dispersion may not be an accurate representation of the average particle size for bimetallic nanoparticles. The decrease in hydrogen chemisorption on bimetallic nanoparticles would likely result in a much higher actual dispersion, which would in turn decrease the initial

TOF. The 3:1 PtAu/C had a TOF more similar to that of the monometallic 0.73% Pt/C than the bimetallic 1:1 PtAu/C catalyst. This result is surprising because Brett et al. determined that a 3:1 PtAu/MgO catalyst had a faster rate of reaction for glycerol oxidation than the 1:1 PtAu/MgO catalyst based on total metal loading [23]. In our work, however, the XRD pattern of the 3:1 1% PtAu/C catalyst indicated that bimetallic nanoparticles might not have been synthesized and that large Au particles were formed during catalyst synthesis. The TOF of  $0.17 \text{ s}^{-1}$  and XRD results indicate that the 3:1 PtAu/C catalyst may have segregated Pt and Au nanoparticles.

The PtAu bimetallic nanoparticles were also supported on silica and titania and the TOF for 1,6-hexanediol oxidation is shown in Table 6.4. The 1:1 PtAu/SiO<sub>2</sub> had a TOF of  $0.13 \text{ s}^{-1}$ , which was similar to that of the 3% Pt/SiO<sub>2</sub> catalyst, while the 1:1 PtAu/TiO<sub>2</sub> had an initial oxidation rate of  $0.16 \text{ s}^{-1}$ . The PtAu/SiO<sub>2</sub> catalyst had a very high dispersion based on just Pt loading (0.49) compared to the bimetallic 1:1 PtAu/C catalyst (0.04), while the 1:1 PtAu/TiO<sub>2</sub> had a similar dispersion of 0.11. Regardless, the TOF was significantly lower which indicates that the synthesis of the bimetallic PtAu was not replicable on the oxide supports using the same sol-immobilization procedure. The 1:1 PtPd/C had a slightly lower TOF of  $0.12 \text{ s}^{-1}$  when compared to monometallic platinum.

The effect of acetic acid concentration on the TOF of 1,6-hexanediol oxidation is illustrated in Figure 6.5 for the bimetallic 1:1 PtAu/C catalyst. The TOF of oxidation decreased moderately with increasing acetic acid concentration up to about 0.2 M. Then the initial rate of 1,6-hexanediol oxidation stayed relatively constant at 0.35 M and 0.7 M. At an acetic acid concentration of 0.35 M the TOF decreased by 16%. The inhibition of the TOF is of a similar manner to that shown in Chapter 2, however, the percent decrease in the initial oxidation rate was slightly lower than that of Pt/C.

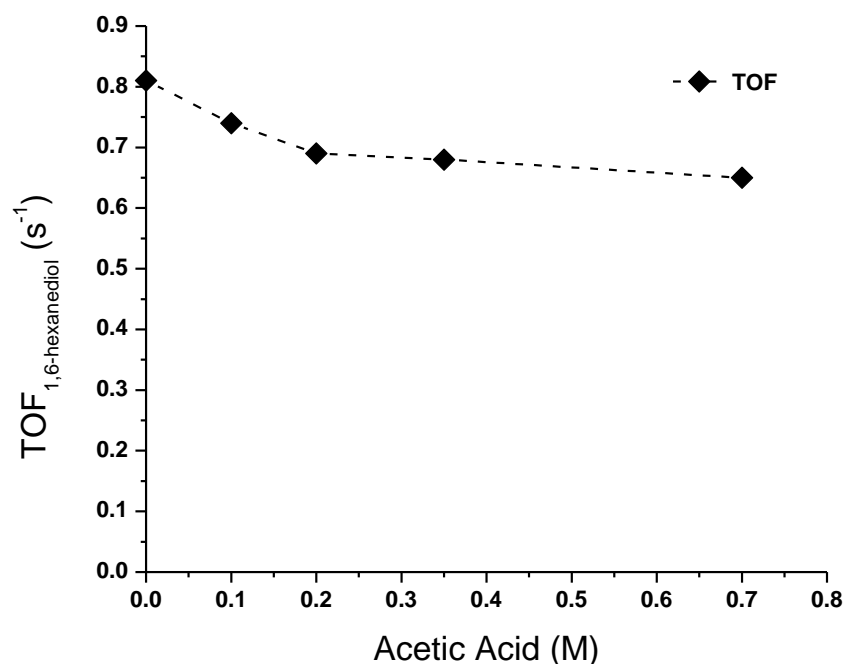


**Figure 6.5.** Influence of acetic acid on the initial turnover frequency (TOF) of 1,6-hexanediol oxidation over 1.1% Pt-Au/C with 0.1 M 1,6-hexanediol at 343 K and 10 bar O<sub>2</sub>.

Figure 6.6 depicts the reaction profile for both the Pt/C and 1:1 PtAu/C catalysts for 1,6-hexanediol oxidation. Despite the increase in initial oxidation rate for 1,6-hexanediol over the Pt-Au/C catalyst compared to that of Pt/C, the bimetallic catalyst deactivated severely after just 5 minutes of reaction. This is different than the rate of 1,6-hexanediol oxidation over Pt/C that was fairly consistent for the first 30 minutes of reaction. To determine if the bimetallic PtAu/C catalyst was leaching into the acidic solution, elemental analysis of the filtrate was measured by ICP-AES after 24 h of 1,6-hexanediol oxidation. No quantifiable leaching of Au or Pt was found in solution, while leaching was observed for the Pt/C catalyst investigated in Chapter 4 in a similar manner. The ultimate selectivity of the 1:1 PtAu/C catalyst was only 34% to adipic acid at 100% conversion of 1,6-hexanediol after 24 h with a 100:1 substrate to catalyst metal molar ratio. Similar experiments in Chapter 4 achieved an adipic acid yield of 86% over Pt/C. The

lower yield of adipic acid over the bimetallic PtAu suggests that the deactivation behavior or structure of the nanoparticles affected the oxidation rate of 6-hydroxyhexanoic acid (alcohol-acid of 1,6-hexanediol oxidation). In addition, the hydrogen peroxide concentration was determined to be approximately 0.1 mM after 4 h of 1,6-hexanediol oxidation over 1:1 Pt-Au/C, similar to that of Pt/C reported in Chapter 3.

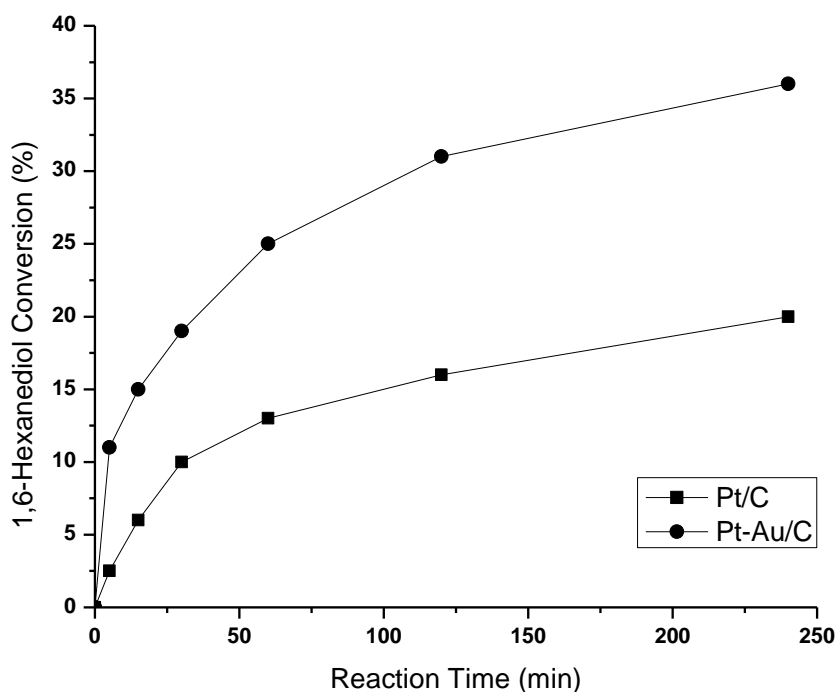


**Figure 6.6.** Reaction profile for the oxidation of 1,6-hexanediol over Pt/C and Pt-Au/C. Reaction conditions: 0.1 M 1,6-hexanediol (HDO), HDO.:Met.  $\sim 500$ ,  $pO_2 = 10$  bar,  $T = 343$  K, 0.35 M Acetic Acid,  $pH = 2.5$ .

Table 6.5 depicts the results of 1,6-hexanediol oxidation over bimetallic catalysts synthesized by the co-precipitation method. The 3% Pt/C catalyst had a TOF of  $0.19 \text{ s}^{-1}$  and a high metal dispersion of 0.73. None of the co-precipitated bimetallic catalysts had an increased initial rate of oxidation or prevented deactivation, however, further characterization of the catalysts is needed to determine if alloyed bimetallic nanoparticles were synthesized. The 3%



Ru/C was not active for 1,6-hexanediol oxidation at these reaction conditions and the Pt-Ru/C catalyst had a very low rate of alcohol oxidation compared to monometallic Pt/C, even though the dispersion was calculated based on the total metal loading. The Pt-Sn/C catalyst also had a low dispersion as measured by hydrogen chemisorption and corresponding low initial rate of alcohol oxidation of  $0.05 \text{ s}^{-1}$ . The co-precipitation of Pt and Zn determined that Zn had no effect on the dispersion or initial rate of 1,6-hexanediol oxidation.

**Table 6.5.** Oxidation activity of 1,6-hexanediol over catalysts synthesized by co-precipitation incipient wetness.

Catalyst	Dispersion	TOF <sup>a</sup> s <sup>-1</sup>
3% Pt/C (Norit)	0.73	0.19
3% Ru/C	0.08	-
3%Pt-1.5%Ru/C	0.13	0.06
3%Pt-1.9%Sn/C	0.37 <sup>b</sup>	0.05
3%Pt-1.2%Zn/C	0.61 <sup>b</sup>	0.20

Reaction Conditions: 0.1 M 1,6-hexanediol (HDO), HDO.:Metal = 500,  $p\text{O}_2 = 10 \text{ bar}$ ,  $T = 343 \text{ K}$ , 0.35 M Acetic Acid,  $\text{pH} = 2.5$ .

<sup>a</sup> The dispersion is calculated based on Pt instead of total metal.

## Conclusions

The rate of 1,6-hexanediol oxidation was evaluated over supported bimetallic nanoparticles that included Pt at acidic conditions and moderate temperature and pressure. To remove catalytic site blocking by the polymer stabilizer, the catalysts synthesized by sol-immobilization were thermally treated. The bimetallic 1:1 PtAu/C catalyst had a TOF three times faster than that of monometallic Pt/C and both had similar particle sizes. Characterization of the 1:1 PtAu/C catalyst by XRD and TEM with EDS determined that even single nanoparticles contained both Pt and Au. The chemisorption of hydrogen showed an inhibition of  $\text{H}_2$  adsorption capacity at room temperature. The synthesis of PtAu supported on both titania and silica showed an increase in hydrogen chemisorption uptake and lower TOF's than PtAu on the carbon support. The support clearly plays a role in the successful synthesis of bimetallic nanoparticles. While no

leaching of Pt or Au was observed by filtrate elemental analysis, the PtAu/C catalyst deactivated at a more rapid rate than Pt/C.

## Acknowledgements

The experiments discussed in this section were partially completed with a summer REU student Jason Bates from the University of Kansas. This material is based upon work supported by the National Science Foundation under Award Nos. EEC-0813570 and OISE 0730277.

## References

- [1] V. Ponc, Alloy catalysts: the concepts. *Appl. Catal. A-Gen.* 222 (2001) 31-45.
- [2] G. C. Bond, The electronic structure of platinum-gold alloy particles. *Platinum Met. Rev.* 51 (2007) 63-68.
- [3] M. Kim, V. N. Phan, K. Lee, Exploiting nanoparticles as precursors for novel nanostructure designs and properties. *Cryst. Eng. Comm.* 14 (2012) 7535-7548.
- [4] E. Bus, J. A. Bokhoven, Electronic and geometric structures of supported platinum, gold, and platinum-gold catalysts. *J. Phys. Chem. C* 111 (2007) 9761-9768.
- [5] W. C. Ketchie, M. Murayama, R. J. Davis, Selective oxidation of glycerol over carbon-supported AuPd catalysts. *J. Catal.* 250 (2007) 264-273.
- [6] C. L. Bianchi, P. Canton, N. Dimitratos, F. Porta, L. Prati, Selective oxidation of glycerol with oxygen using mono and bimetallic catalysts based on Au, Pd and Pt metals. *Catal. Today* 102 (2005) 203-213.
- [7] N. Dimitratos, J. A. Lopez-Sanchez, D. Lennon, F. Porta, L. Prati, A. Villa, Effect of particle size on monometallic and bimetallic (Au, Pd)/C on the liquid phase oxidation of glycerol. *Catal. Lett.* 108 (2006) 147-153.
- [8] L. Prati, F. Porta, D. Wang, A. Villa, Ru modified Au catalysts for the selective oxidation of aliphatic alcohols. *Catal. Sci. Tech.* 1 (2011) 1624-1629.
- [9] S. Hirasawa, Y. Nakagawa, K. Tomishige, Selective oxidation of glycerol to dihydroxyacetone over a Pd-Ag catalyst. *Catal. Sci. Technol.* 2 (2012) 1150-1152.
- [10] A. Brandner, K. Lehnert, A. Bienholz, M. Lucas, P. Claus, Production of biomass-derived chemicals and energy: Chemocatalytic conversions of glycerol. *Top. Catal.* 51 (2009) 278-287.

- [11] W. Hu, D. Knight, B. Lowry, A. Varma, Selective oxidation of glycerol to dihydroxyacetone over Pt– Bi/C catalyst: Optimization of catalyst and reaction conditions. *Ind. Eng. Chem. Res.* 49 (2010) 10876-10882.
- [12] P. Fordham, M. Besson, P. Gallezot, Selective catalytic oxidation of glyceric acid to tartronic and hydroxypyruvic acids. *Appl. Catal. A-Gen.* 133 (1995) 179-184.
- [13] C. L. Bianchi, P. Canton, N. Dimitratos, F. Porta, L. Prati, Selective oxidation of glycerol with oxygen using mono and bimetallic catalysts based on Au, Pd and Pt metals. *Catal. Today* 102 (2005) 203-212.
- [14] N. Dimitratos, A. Villa, D. Wang, F. Porta, D. Su, L. Prati, Pd and Pt catalysts modified by alloying with Au in the selective oxidation of alcohols. *J. Catal.* 244 (2006) 113-121.
- [15] L. Prati, A. Villa, C. Campione, P. Spontoni, Effect of gold addition on Pt and Pd catalysts in liquid phase oxidations. *Top. Catal.* 44 (2007) 319-324.
- [16] A. Villa, G. M. Veith, L. Prati, Selective oxidation of glycerol under acidic conditions using gold catalysts. *Ange. Chem. Int. Ed.* 49 (2010) 4499-4502.
- [17] B. Maier, C. Dietrich, J. Büchs, Correct application of the sulphite oxidation methodology of measuring the volumetric mass transfer coefficient  $k_L a$  under non-pressurized and pressurized conditions. *Food Bioprod. Process.* 79 (2001) 107.
- [18] C.N. Satterfield, A.H. Bonnell, Interferences in titanium sulfate method for hydrogen peroxide. *Anal. Chem.* 27 (1955) 1174.
- [19] E. Bus, J. T. Miller, J. A. van Bokhoven, Hydrogen chemisorption on  $\text{Al}_2\text{O}_3$ -supported gold catalysts. *J. Phys. Chem. B* 109 (2005) 14581-14587.
- [20] E. Bus, J. A. Bokhoven, Hydrogen chemisorption on supported platinum, gold, and platinum–gold-alloy catalysts. *Phys. Chem. Chem. Phys.* 9 (2007) 2894-2902.
- [21] H. Lang, S. Mldonado, K. J. Stevenson, B. D. Chandler, Synthesis and characterization of dendrimer templated supported bimetallic Pt-Au nanoparticles. *J. Am. Chem. Soc.* 126 (2004) 12950-12956.
- [22] Luo, M. M. Maye, V. Petkov, N. N. Kariuki, L. Wang, P. Njoki, D. Mott, Y. Lin, C. Zhong, Phase properties of carbon-supported gold-platinum nanoparticles with different bimetallic compositions. *Chem. Mat.* 17 (2005) 3086-3091.
- [23] G. L. Brett, Q. He, C. Hammond, P. J. Miedziak, N. Dimitratos, M. Sankar, A. A. Herzing, M. Conte, J. A. Lopez-Sanchez, C. J. Kiely, D. W. Knight, S. H. Taylor, G. J. Hutchings, Selective Oxidation of Glycerol by Highly Active Bimetallic Catalysts at Ambient Temperature under Base-Free Conditions. *Angew. Chem. Int. Ed.* 50 (2011) 10136-10139.

[24] J. A. Lopez-Sanchez, N. Dimitratos, C. Hammond, G. L. Brett, L. Kesavan, S. White, P. Miedziak, R. Tiruvalam, R. L. Jenkins, A. F. Carley, D. Knight, C. J. Kiely, G. J. Hutchings, Facile removal of stabilizer-ligands from supported gold nanoparticles. *Nature Chem.* 3 (2011) 551-556.

## Chapter 7: Concluding Remarks

### Conclusions

The oxidation of alcohols and aldehydes is an important reaction in chemical production and is especially relevant in the production of chemicals from biomass resources. While oxidations have long been performed using highly toxic oxidants, the environmental and economic benefits of supported metal catalysts at aqueous conditions and with molecular oxygen as the oxidant are significant. The oxidation of alcohols proceeds through first the oxidation to an aldehyde and second to a carboxylic acid when performed in aqueous conditions. The rapid rate of alcohol oxidation over Pt makes it an attractive catalyst for alcohol oxidation. The oxidation of 1,6-hexanediol was a focus in this work because of the value of its diacid oxidation product, adipic acid.

The oxidation of alcohols was performed over Pt/C, Pd/C, and Au/C at approximately 10 bar O<sub>2</sub> and 343 K in an aqueous solvent at low pH. The addition of an organic acid, in this case acetic acid, allowed reproducible TOFs to be determined for a wide range of alcohols. While the organic acid slightly inhibited the oxidation rate of alcohols, the addition of the acid at the beginning of the reaction allowed us to ignore the inhibition by organic acid products created throughout the reaction. The synthesis of Pt nanoparticles supported on different carbon supports with different Pt particle sizes and the determination of the TOF allowed us to conclude that neither had a measurable effect on the rate of 1,6-hexanediol oxidation. The oxidation of  $\alpha,\omega$ -diols showed an increase in TOF and ultimate selectivity to the diacid with increasing carbon chain length. When the oxidation of various multifunctional alcohol substrates was explored, the proximity of the electron withdrawing group appeared to negatively impact the rate terminal

alcohol oxidation. A high yield of adipic acid was achieved over Pt/C at acidic conditions or over Au/TiO<sub>2</sub> at basic conditions.

Further exploration of the kinetics of 1,6-hexanediol over Pt/C determined that the reaction was nearly zero order with respect to both the dioxygen pressure and substrate concentration at inert startup conditions. In addition, the apparent activation energy was similar regardless of whether 1,3-propanediol, 1,6-hexanediol, ethanol, or 6-hydroxyhexanoic acid were used as the substrate. During an oxidative startup, however, the oxidation of 1,6-hexanediol was first order with respect to substrate concentration. To describe the kinetic results, a two-site mechanism was proposed that explains the rate behavior at both the inert and oxidative startup conditions. At inert startup conditions (reduced Pt), the kinetically relevant step was proposed to be the C-H activation of an adsorbed alkoxide. A kinetic isotope effect was observed when CH<sub>3</sub>CD<sub>2</sub>OH was used as the substrate. This suggested that the apparent activation energy was similar regardless of the substrate because it was measuring the C-H activation barrier. When an oxidative startup was used, the Pt surface was assumed to be covered with adsorbed hydroxyl, which affected the order with respect to substrate, but did not change the order with respect to dioxygen pressure.

The deactivation of supported Pt during alcohol oxidation was also investigated at acidic aqueous conditions. A significant decrease in the rate of terminal alcohol oxidation was observed over Pt/C for all mono-alcohols and multi-functional alcohols. In addition, the deactivation behavior was observed regardless of the Pt support or Pt particle size during 1,6-hexanediol oxidation. The over-oxidation of Pt was easily reversed by treatment with the alcohol reactant in an inert atmosphere. After recycle, however, the deactivated Pt catalyst was not regenerated by a similar procedure. Neither the leaching of Pt into the hot acidic solution nor sintering was

significant enough to account for the severe deactivation. In addition, the aldol condensation activity of the alcohols and intermediates was determined to be negligible at the low pH. The analysis of gas in the headspace of the reactor determined that CO<sub>2</sub> was a byproduct of alcohol oxidation.

To investigate the origin of CO<sub>2</sub> produced during alcohol oxidation, in-situ ATR-IR spectroscopy experiments were performed. The use of either benzyl alcohol with Pt/SiO<sub>2</sub> or ethanol with Pt/BN in the presence of water saturated with N<sub>2</sub> produced strongly adsorbed CO on the Pt surface. This strongly held CO species remained when the alcohol was removed and replaced with neat water. However, the CO was oxidized rapidly in the presence of dissolved O<sub>2</sub>. The CO was likely formed via the decarbonylation of the aldehyde intermediate. A TGA-MS analysis of Pt/BN after ethanol oxidation for 24 h was performed to determine if a fragment was strongly adsorbed to the catalyst surface after decomposition of the alcohol or aldehyde. A sharp weight loss was determined at 613 K and the corresponding mass spectrum revealed that most likely a dehydrogenated carbon species was responsible for catalyst deactivation during alcohol oxidation.

In an attempt to eliminate deactivation and increase the rate of alcohol oxidation, bimetallic heterogeneous catalysts were synthesized. The initial oxidation rate over the catalysts synthesized by sol-immobilization was observed to increase after the removal of PVA stabilizer by a thermal treatment. The polymer stabilizer (PVA) was assumed to be blocking catalytic sites. A bimetallic 1:1 PtAu/C catalyst was found to have a TOF for 1,6-hexanediol oxidation three times that of a monometallic Pt/C prepared in a similar manner. Further characterization of the PtAu/C catalyst by TEM with EDS showed that even single nanoparticles contained significant amounts of Pt and Au. Interestingly, the chemisorption of hydrogen was shown to greatly

underestimate the metal surface area for the PtAu/C catalyst. The synthesis by sol-immobilization of PtAu supported on both titania and silica was not capable of replicating the increased rate of alcohol oxidation found on carbon. While the elemental analysis of the filtrate did not show any leaching of Pt or Au, the bimetallic catalyst did deactivate at a rapid rate.

## **Future Direction**

### **Bimetallic catalyst synthesis**

While our work synthesizing bimetallic nanoparticles composed of Pt and Au was successful when supported on carbon, there clearly was a significant role of the catalyst preparation procedure. The increase in initial TOF reported for PtAu/C was not replicated when the nanoparticles were deposited on silica and titania. The support may have a large effect on the stability of nanoparticles during the thermal treatment of the catalysts, which could have a profound impact on the segregation of PtAu nanoparticles or sintering on the support surface. The ratio of Pt and Au may also be important to the synthesis of homogeneous nanoparticles in solution before deposition on the support. Finally, the synthesis of highly dispersed metals supported on oxides is frequently performed by ion exchange. The exchange of surface species with a charged metal precursor depends on the pH of solution and concentration of precursor in solution. In this work, the metal precursor had already been reduced and nanoparticles had been formed in solution, facilitated and most likely surrounded by a polymer stabilizer (PVA). The interaction of the charged surface species with the PVA polymer stabilizer may greatly affect the interaction between the support and the solution synthesized nanoparticle. Thus, the exploration of bimetallic catalyst synthesis with a particular focus on modifying either the polymer stabilizer or pH of solution may help synthesize truly bimetallic nanoparticles on oxide supports.



### **Influence of solvent on alcohol oxidation rate**

The aqueous phase oxidation of alcohols over Pt presented in this thesis has suggested that water plays a role in the oxidation mechanism. Water is not an inert solvent, but rather an active participant in the catalysis. A summary of the current literature shows that water appears to promote the rate of oxidation over supported Pt, Pd, and Ru as compared to the rate of alcohol oxidation in polar and non-polar organic solvents. Please see Appendix C for a more complete review of the literature. When external mass transfer limitations (ex. O<sub>2</sub> solubility or alcohol solubility) have been removed, there is no obvious reason why water increases the rate of alcohol oxidation or the organic solvent decreases the rate. Water may allow for an alternative mechanism as compared to an organic solvent. Interestingly, water is typically produced as a product of alcohol dehydrogenation when dioxygen is used as the oxidant. A possible explanation for the difference in rate is that the irreversible dissociation of dioxygen to form atomic oxygen may dominate the surface coverage. The high coverage of atomic oxygen might assist in the deprotonation of the alcohol on the platinum metal surface, but also may inhibit the overall rate of reaction because of the ease of dioxygen dissociation on Pt (approximately 30-35 kJ mol<sup>-1</sup>). Thus, a kinetic study on alcohol oxidation in an organic solvent might give insight into the reaction mechanism without water.

### **Oxidation of 1,6-hexanediol in a continuous flow reactor**

While a batch reactor was utilized for this study, the industrial production of diacids would most likely be performed in a continuous flow system. The catalyst would be immobilized in a reactor and liquid could be continuously pumped over the packed bed. The alcohol oxidation behavior of Pt in the flow reactor might be significantly different because of the limited contact time of the substrate with the catalyst. The product selectivities might change and heavily favor

the aldehyde products. The difference in selectivity may affect the deactivation behavior of Pt. In addition, the kinetics of deactivation could be probed and modeled to determine the deactivation kinetic constant with a continuous flow reactor. This would allow us to quantitatively compare the effect of Pt particle size and support on the deactivation of supported Pt catalysts during alcohol oxidation.

## Appendix A: HPLC Analysis

### Sample Chromatograms

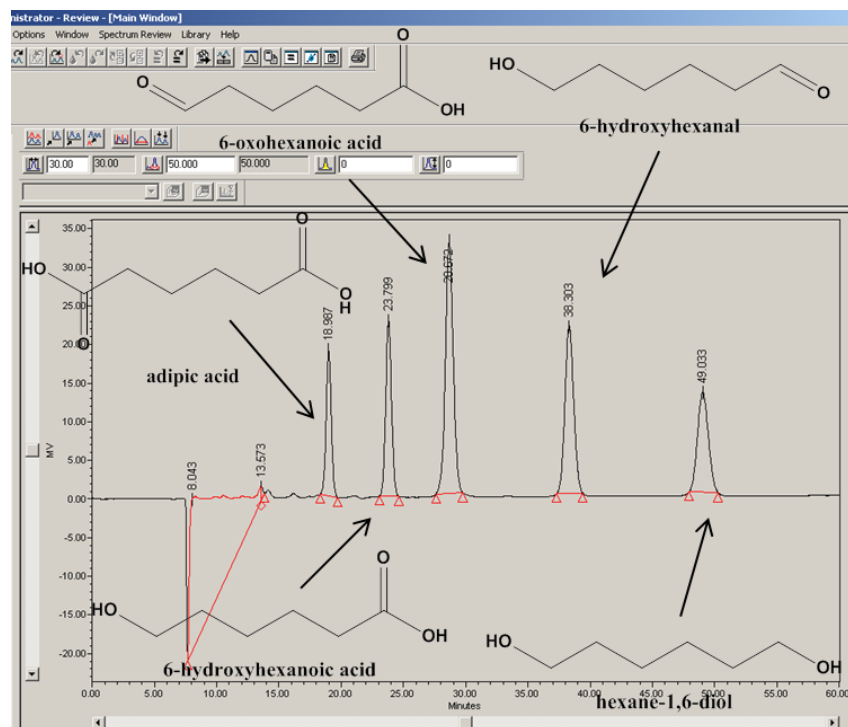


**Figure A.1.** Sample HPLC chromatogram with RI (refractive index) detector for 1,6-hexanediol oxidation using Bio-Rad Aminex column.

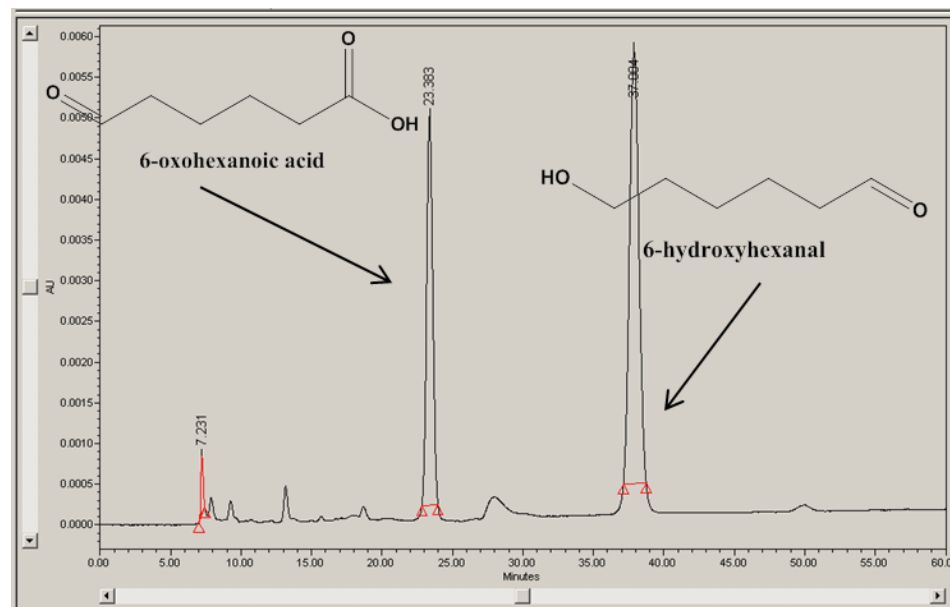


**Figure A.2.** Sample HPLC chromatogram with UV-VIS detector at 290 nm for 1,6-hexanediol oxidation using Bio-Rad Aminex column.

## Sample Calibrations

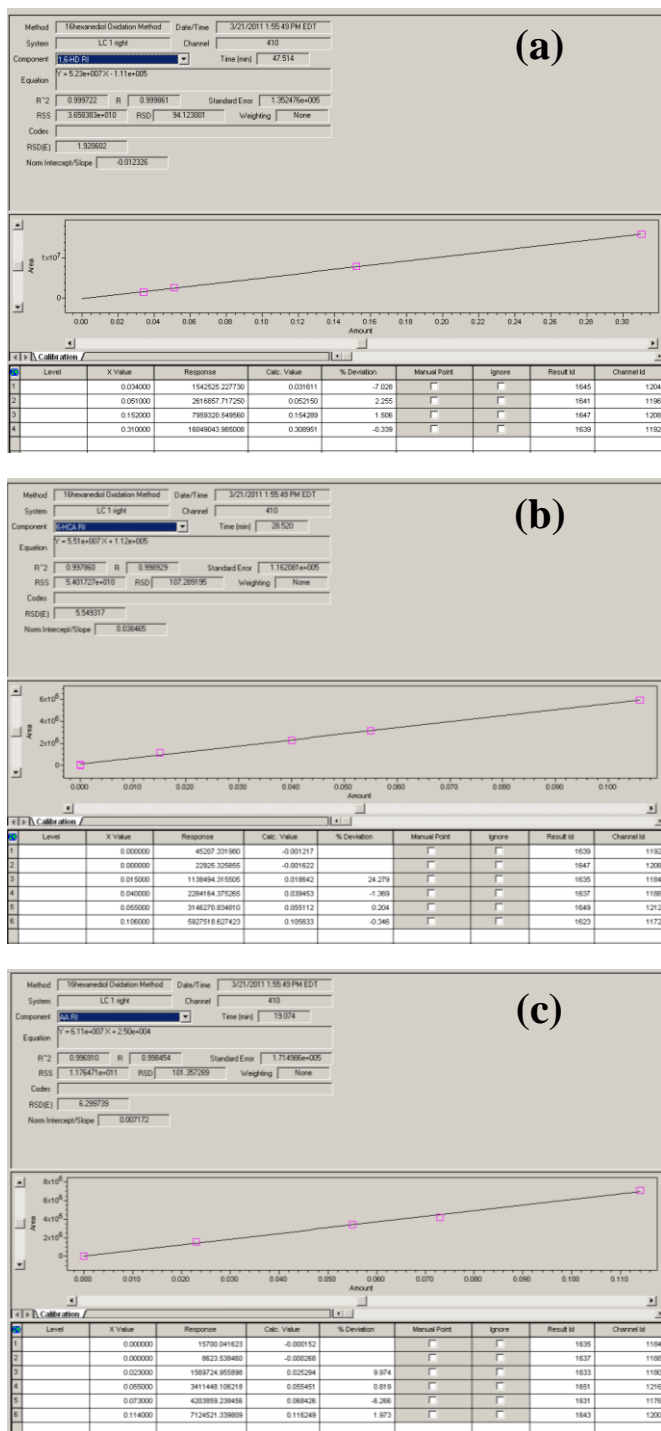


**Figure A.3.** Sample calibration for (a) 1,6-hexanediol, (b) 6-hydroxyhexanoic acid, and (c) adipic acid with the refractive index detector.

## Appendix B: Rate Equation Derivation

### Inert startup

The reaction rate can be described by the proposed kinetic model with the rate of step 2:

$$\text{rate of reaction} = r_2 = k_2 [\text{RCH}_2\text{O}^*] [\text{S}]$$

The equilibrium relationship of step 1 shows:

$$[\text{RCH}_2\text{O}^*] = K_1 [\text{RCH}_2\text{OH}][\text{OH}^*] / [\text{H}_2\text{O}]$$

and the equilibrium relationship of step 4 shows:

$$[\text{OH}^*] = K_4^{1/4} [\text{O}_2]^{1/4} [\text{H}_2\text{O}]^{1/2} [*]$$

The site balance on \* and "S" are:

$$[*]_o = [*] + [\text{RCH}_2\text{O}^*] + [\text{OH}^*] + [\text{RCHO}^*] + \dots \approx [*] + [\text{RCH}_2\text{O}^*]$$

$$[\text{S}]_o = [\text{S}] + [\text{H-S}] \approx [\text{S}]$$

if we assume  $[\text{RCH}_2\text{O}^*]$  is the most abundant species on the \* sites and low hydrogen coverage on the "S" sites.

Thus, the reaction rate can then be described by:

$$r = \frac{K_1 k_2 K_4^{1/4} \frac{[\text{RCH}_2\text{OH}] \text{O}_2^{1/4}}{[\text{H}_2\text{O}]^{1/2}} [*]_o [\text{S}]_o}{\left( 1 + K_1 K_4^{1/4} \frac{[\text{RCH}_2\text{OH}] \text{O}_2^{1/4}}{[\text{H}_2\text{O}]^{1/2}} \right)}$$

If we assume that  $= K_1 K_4^{1/4} [\text{O}_2]^{1/4} [\text{RCH}_2\text{OH}] / [\text{H}_2\text{O}]^{1/2} \gg 1$  then:

$$\text{rate of reaction} = k_2 [*]_o [\text{S}]_o$$

and the rate of reaction would be proportional to  $k_2$ .

## Oxidative startup

The reaction rate for the oxidative startup can be described using the same kinetic model as the inert startup. The major difference is that the site balance on \* is now:

$$[*]_o = [*] + [\text{OH}^*]$$

and the steady state approximation is used to determine [H-S]:

$$r_2 = r_3$$

$$k_2 [\text{RCH}_2\text{O}^*] [\text{S}] = k_3 [\text{OH}^*] [\text{H-S}]$$

$$[\text{H-S}] = k_2 [\text{RCH}_2\text{O}^*] [\text{S}] / k_3 [\text{OH}^*].$$

The rate of reaction can now be determined by the rate of step 3:

$$\text{rate of reaction} = r_3 = k_3 [\text{OH}^*] [\text{H-S}]$$

where (from Step 1)

$$[\text{RCH}_2\text{O}^*] = K_1 [\text{RCH}_2\text{OH}] [\text{OH}^*] / [\text{H}_2\text{O}]$$

And (from Step 4)

$$[\text{OH}^*] = K_4^{1/4} [\text{O}_2]^{1/4} [\text{H}_2\text{O}]^{1/2} [*].$$

Thus, the reaction rate can then be described by:

$$r = \frac{K_1 k_2 K_4^{1/4} \frac{[\text{RCH}_2\text{OH}] [\text{O}_2]^{1/4}}{[\text{H}_2\text{O}]^{1/2}} [*]_o [\text{S}]_o}{\left( 1 + K_4^{1/4} \frac{[\text{O}_2]^{1/4}}{[\text{H}_2\text{O}]^{1/2}} \right)}.$$

If we assume that  $K_4^{1/4} [\text{O}_2]^{1/4} / [\text{H}_2\text{O}]^{1/2} \gg 1$  then:

$$\text{rate of reaction} = K_1 k_2 [\text{RCH}_2\text{OH}] [*]_o [\text{S}]_o$$

and the rate of reaction would be proportional to [RCH<sub>2</sub>OH].

## Appendix C: Promotional Effect of Water on Liquid Phase

### Alcohol Dehydrogenation

#### Literature Review

The influence of water, polar organic solvents, and non-polar organic solvents on the rate and selectivity of alcohol dehydrogenation over supported platinum catalysts has been investigated frequently in the literature. One of the starkest comparisons was observed by Dimitratos et al. when the TOF of alcohol oxidation was compared for water and toluene (non-polar organic). The TOF of cinnamyl alcohol oxidation increased from  $38 \text{ h}^{-1}$  in toluene to  $67 \text{ h}^{-1}$  in water over Pt/C at 333 K and 1.5 atm oxygen. Similarly, the TOF of benzyl alcohol oxidation increased from  $30 \text{ h}^{-1}$  to  $98 \text{ h}^{-1}$  and 1-octanol oxidation increased from  $4 \text{ h}^{-1}$  to  $20 \text{ h}^{-1}$ . [1] The increase in TOF when water was used as the solvent is peculiar because 1-octanol and cinnamyl alcohol have low solubility in water and high solubility in toluene. The same trend in alcohol oxidation activity was observed by Keresszegi et al. for the oxidation of 1-phenylethanol over alumina (a more amphoteric support than activated carbon) supported platinum. The oxidation of 1-phenylethanol achieved a 31% conversion over Pt/Al<sub>2</sub>O<sub>3</sub> after 3 h in cyclohexane at 353 K and 1 atm oxygen, however, a similar conversion of 33% was determined in water at the lower temperature of 328 K after 3 h. [2]

In addition to the comparison of water and non-polar organic solvents, other authors have also compared the influence of water and polar organic solvents. Frassoldati et al. investigated the influence of water and dioxane on the oxidation of 1-octanol and 2-octanol over Pt/C at 373 K and 10 atm air. The conversion of 1-octanol was 36% after 1 h when dioxane was used as the

solvent and the conversion increased to 73% in 90/10 dioxane/water and 67% in 50/50 dioxane/water. The promotional effect of water on the rate of 1-octanol oxidation was also observed at a lower temperature of 333 K as well as after the addition of sodium hydroxide. [3] Similarly, the oxidation of 2-octanol had a conversion of 29% after 6 h in dioxane, whereas 100% conversion was achieved after 6 h in 50/50 dioxane/water. The authors suggest that water acts as a weak base and assists in the deprotonation of the alcohol upon its adsorption on the platinum surface. [3] Follow up work by Frassoldati et al determined that water also promoted the rate of oxidation of 1-phenylethanol and  $\alpha$ -methyl-pyridinemethanol compared to when just dioxane was used as the solvent at 373 K and 10 atm air. [4]

Chibani et al. also observed that water promoted the oxidation of menthol and borneol, both secondary alcohols, over Pt/C at 373 K and 10 atm air. The initial activity of alcohol oxidation was improved with increasing concentration of water from 100% dioxane to 80%/20% dioxane/water (v/v) to 50%/50% dioxane/water. The increase in oxidation rate in the presence of water was determined by a combination of experimental results and DFT calculations to be from the presence of hydroxyl groups formed on the platinum surface by the reaction between water and atomic oxygen. [5] Donze et al. determined the influence of dioxane and water for the oxidation of substituted benzyl alcohol substrates over Pt/C at 373 K and 10 atm air. The oxidation of 2-methylbenzyl alcohol achieved 100% conversion in 6 hours when dioxane was used as the solvent and in 0.7 hours with a 90/10 dioxane/water solvent. [6]

There is also evidence in the literature that supported gold, ruthenium, and palladium catalysts have exhibited similar increases in alcohol oxidation rate in the presence of water. The oxidation of 1-octanol over Au/NiO had a 29% conversion in toluene, 5% conversion in dioxane, 5% conversion in acetonitrile, and 83% conversion in water at 373 K and 5 atm oxygen after 18



h. [7] A similar promotional effect of water was observed by Yang et al. for the oxidation of benzyl alcohol over Au/TiO<sub>2</sub>. The conversion of benzyl alcohol was 12% in p-xylene, 26% in ethanol, and 83% in water at 373 K and 10 atm oxygen after 8 h. The conversion of the ethanol solvent was not discussed. The addition of even a very small amount of water to p-xylene increased the conversion of benzyl alcohol at the same reaction conditions. [8]

The oxidation of benzyl alcohol over Ru/CNT had a 7% conversion in ethanol, 50% in toluene, and 100% conversion in water at 358 K and 1 atm oxygen after 3 h. The main product when ethanol was used as the solvent was ethyl benzoate. [9] Similarly, the TOF of benzyl alcohol oxidation over Pd/C increased from 5 h<sup>-1</sup> in toluene to 30 h<sup>-1</sup> in water at 333 K and 1.5 atm oxygen after 8 h. An even more drastic increase was observed for the TOF of 1-octanol oxidation from 1 h<sup>-1</sup> in toluene to 22 h<sup>-1</sup> in water. [1] The promotional effect of water for benzyl alcohol oxidation was also observed for Pd nanoparticles suspended in an ionic liquid [C<sub>4</sub>mim][BF<sub>4</sub>] solvent. [10]

## References

- [1] N. Dimitratos, A. Villa, D. Wang, F. Porta, D. Su, L. Prati, Pd and Pt catalysts modified by alloying with Au in the selective oxidation of alcohols. *J. Catal.* 244 (2006) 113.
- [2] C. Keresszegi, T. Mallat, J. Grunwaldt, A. Baiker, A simple discrimination of the promoter effect in alcohol oxidation and dehydrogenation over platinum and palladium. *J. Catal.* 225 (2004) 138.
- [3] A. Frassoldati, C. Pinel, M. Besson, Promoting effect of water for aliphatic primary and secondary alcohol oxidation over platinum catalysts in dioxane/aqueous solution media. *Catal. Today* 173 (2011) 81.
- [4] A. Frassoldati, C. Pinel, M. Besson, Aerobic oxidation of secondary pyridine-derivative alcohols in the presence of carbon-supported noble metal catalysts. *Catal. Today* 203 (2013) 133.
- [5] S. Chibani, C. Michel, F. Delbecq, C. Pinel, M. Besson, On the key role of hydroxyl groups in platinum-catalysed alcohol oxidation in aqueous medium. *Catal. Sci. Tech.* 3 (2013) 339.

- [6] C. Donze, P. Korovchenko, P. Gallezot, M. Besson, Aerobic selective oxidation of (hetero)aromatic primary alcohols to aldehydes or carboxylic acids over carbon supported platinum. *Appl. Catal. B Env.* 70 (2007) 621.
- [7] T. Ishida, Y. Ogihara, H. Ohashi, T. Akita, T. Honma, H. Oji, M. Haruta, Base-Free Direct Oxidation of 1-Octanol to Octanoic Acid and its Octyl Ester over Supported Gold Catalysts. *ChemSusChem* 5 (2012) 2243.
- [8] X. Yang, X. Wang, C. Liang, W. Su, C. Wang, Z. Feng, C. Li, J. Qiu, Aerobic oxidation of alcohols over Au/TiO<sub>2</sub>: An insight on the promotion effect of water on the catalytic activity of Au/TiO<sub>2</sub>. *Catal. Comm.* 9 (2008) 2278.
- [9] X. Yang, X. Wang, J. Qiu, Aerobic oxidation of alcohols over carbon nanotube-supported Ru catalysts assembled at the interfaces of emulsion droplets. *Appl. Catal. A-Gen.* 382 (2010) 131.
- [10] K. R. Seddon, A. Stark, Selective catalytic oxidation of benzyl alcohol and alkylbenzenes in ionic liquids. *Green Chem.* 4 (2002) 119.

## Appendix D: The Important Role of Hydroxyl on Oxidation

### Catalysis by Gold

*The work in this appendix was the basis for the publication: M. S. Ide, R. J. Davis, Accounts of Chemical Research, in revisions.*

#### Introduction

Catalysis by gold has attracted the attention of researchers worldwide after the exciting reports by the Haruta group more than two decades ago describing the exceptional performance of Au nanoparticles as catalysts for CO oxidation and H<sub>2</sub> oxidation with molecular oxygen when the particles were supported on titanium dioxide or iron oxide.<sup>1-2</sup> Since Au nanoparticles on silica or alumina were much less catalytically-active for CO oxidation than those supported on titania or iron oxide, the nature of the latter two supports was thought to be a critical factor in the unusual performance of the catalysts.<sup>3</sup> The remarkable activity of gold for CO oxidation at temperatures as low as 203 K was perplexing, because the reaction rate depended on Au particle size yet was nearly independent of the partial pressure of CO and O<sub>2</sub>. In addition, bulk gold metal and small gold particles are inactive for molecular oxygen dissociation at low temperatures, although adsorption of CO still occurs.

Subsequent work by Daté and Haruta involved co-feeding H<sub>2</sub>O with CO and O<sub>2</sub> to explore the effect of moisture on CO oxidation activity over Au/TiO<sub>2</sub>.<sup>4</sup> Great care was taken to remove all moisture from the dry feed gas of CO and O<sub>2</sub>. Interestingly, the rate of CO oxidation increased by an order of magnitude when the water concentration was increased from 0.1 ppm to 3 ppm, and doubled again upon further increasing the concentration to 200 ppm. Despite an

order of magnitude increase in CO oxidation activity by increasing the moisture content from 0.1 to 3 ppm, the apparent activation energy was unaffected by water, which suggests the mechanism was unaltered by the addition of water. Earlier work by Cunningham and Haruta showed a similar promotional effect of water on CO oxidation over Au/Mg(OH)<sub>2</sub>.<sup>5</sup> In that study, the rate of CO oxidation was significantly lowered when the residual moisture level of 10 ppm present in the feed gas was decreased to 0.08 ppm. Both of these studies propose that a water derived species, such as OH, was involved in CO oxidation. Addition of H<sub>2</sub> also accelerates the CO oxidation reaction on Au, presumably by the formation of low levels of water by the oxidation of H<sub>2</sub>.<sup>6</sup>

A measurable promotional effect of water for CO oxidation over gold particles was also observed with supports that were known to be less active than titania. For example, Daté et al. explored the influence of H<sub>2</sub>O on the rate of CO oxidation over Au/Al<sub>2</sub>O<sub>3</sub> and Au/SiO<sub>2</sub> at 273 K.<sup>7</sup> An increase in water concentration from 0.3 ppm to 200 ppm increased the CO oxidation rate by two orders of magnitude for Au/SiO<sub>2</sub> and an order of magnitude for Au/Al<sub>2</sub>O<sub>3</sub>. While Au/TiO<sub>2</sub> always had a rate that was an order of magnitude larger than Au/Al<sub>2</sub>O<sub>3</sub> and Au/SiO<sub>2</sub>, the apparent activation energy was similar regardless of the support. Park et al. observed similar results, with Au/Fe<sub>2</sub>O<sub>3</sub> and Au/TiO<sub>2</sub> being more active than Au/Al<sub>2</sub>O<sub>3</sub> for CO oxidation, regardless of whether the reaction was performed wet or dry.<sup>8</sup> All three supported gold catalysts were promoted upon the addition of water vapor. Daté et al. suggested that water played an important role in the activation of molecular oxygen and that oxide supports with redox properties have higher mobility of adsorbed hydroxyl groups or oxygen atoms at the interface between gold and the support.

Other authors have characterized the promotional effect of water on CO oxidation over Au as the prevention of catalyst deactivation. Costello et al. determined that the rate of CO oxidation over Au/Al<sub>2</sub>O<sub>3</sub> in rigorously dry conditions decreased by an order of magnitude after 30 min at 295 K, but that exposure of the catalyst to 1.5% water vapor completely regenerated the catalyst.<sup>9-10</sup> Kung et al. proposed that not only did hydroxyl groups play a key role in CO oxidation, but that deactivation was due to removal of hydroxyl groups from the support.<sup>11</sup> The activity for CO oxidation and deactivation behavior would therefore depend on both the Au-support interface and on the type of oxide support.

In this Account, we discuss the mechanistic role of the hydroxyl on catalysis by gold nanoparticles for the selective oxidation of both CO and alcohols with molecular oxygen as the oxidant. The importance of water in the vapor and liquid phase for CO oxidation and in the liquid phase for alcohol oxidation is discussed. Finally, a comparison of liquid phase oxidation and electro-oxidation will address the similarities between the two processes over gold supported catalysts.

## **Catalysis by gold and oxidation activity**

The selective oxidation of CO has been studied extensively in both the gas and liquid phase in the presence of water. Remarkably, the rates of reaction for CO oxidation are similar over gold nanoparticles regardless of the phase. Calla et al. investigated the effect of gold loading on the turnover frequency (TOF) of gas phase CO oxidation by leaching Au/Al<sub>2</sub>O<sub>3</sub> with various concentrations of NaCN.<sup>12</sup> The turnover frequency is defined as the number of CO molecules reacted per surface Au atoms in the reactor per time. The TOF of CO oxidation with co-fed water was within a factor of two regardless of the gold loading, between approximately 0.2 and 0.4 s<sup>-1</sup> at 298 K.

The steady-state isotopic transient analysis (SSITKA) of gas phase CO oxidation with water vapor over the same highly-dispersed Au/Al<sub>2</sub>O<sub>3</sub> catalyst revealed a TOF of approximately 0.25 s<sup>-1</sup> at 296 K but an intrinsic TOF of 2.0 s<sup>-1</sup>.<sup>13</sup> While the TOF is based on all surface Au atoms and is a lower bound on the rate, the intrinsic TOF is a maximum turnover rate that is based on the surface concentration of intermediate species that form product. At dry conditions, the TOF was an order of magnitude lower, but because of the low fractional coverage of the carbon intermediate, the intrinsic TOF was still 1.6 s<sup>-1</sup>. Further SSITKA work on Au/TiO<sub>2</sub> and Au/Al<sub>2</sub>O<sub>3</sub> at dry conditions determined that the intrinsic TOF's at 293 K were 3.1 s<sup>-1</sup> and 2.0 s<sup>-1</sup>, respectively, showing that the reaction rate is nearly independent of the support used even without water.<sup>14</sup> However, while the intrinsic TOF might be similar, the overall reaction rate can be quite different if not all of the surface gold is capable of activating molecular oxygen or forming hydroxyl species on the surface in the presence of water. The intrinsic TOF for CO oxidation over gold supported on an oxide can reasonably assumed to be between 2 to 4 s<sup>-1</sup> at room temperature.

Further investigation of the effect of water vapor on the gas phase CO oxidation rate over Au/Al<sub>2</sub>O<sub>3</sub> determined that water affected the orders of reaction with respect to CO and O<sub>2</sub>.<sup>6</sup> The O<sub>2</sub> order increased from 0.36 to 0.48 in the presence of water and the CO order decreased from 0.32 to 0.18. Despite the promotional effect of water, no incorporation of labeled oxygen from H<sub>2</sub><sup>18</sup>O was observed in product CO<sub>2</sub>.<sup>15</sup> However, labeled oxygen was observed in CO<sub>2</sub> during dry CO oxidation with <sup>18</sup>O<sub>2</sub> over both Au/TiO<sub>2</sub> and Au/Al<sub>2</sub>O<sub>3</sub>. While the exact role of both O<sub>2</sub> and H<sub>2</sub>O is not clear, both are required for the high TOF's observed for CO oxidation in the vapor phase.

The rate of CO oxidation in the presence of water vapor can be directly compared to CO oxidation in aqueous solution. The Dumesic group showed gold nanotube membranes catalyzed the oxidation of CO in liquid water.<sup>16</sup> Upon the addition of base to increase the pH of the liquid to 13, the rate increased by a factor of five compared to that in neutral solution. The enhancement of rate at a basic pH suggests that the hydroxyl groups in the solution interacted with the gold surface and either facilitated the activation of O<sub>2</sub> or directly participated in the reaction with CO. Interestingly, the authors mentioned the presence of small quantities of hydrogen peroxide in solution.

The promotional effect of base on aqueous CO oxidation over supported gold catalysts was further investigated by Ketchie et al.<sup>17</sup> The vapor phase oxidation of CO over Au/TiO<sub>2</sub> had a TOF of 0.34 s<sup>-1</sup> at 300 K, similar to that discussed above for other oxide-supported gold catalysts,<sup>6,13-14</sup> while the aqueous phase oxidation had a TOF of 0.11 s<sup>-1</sup> at a pH of 7 at 300 K. The reaction orders with respect to CO and O<sub>2</sub> in the aqueous phase were 0.35 and 0.25, respectively, which are very close to the reaction orders determined in the gas phase in the presence of water vapor over Au/Al<sub>2</sub>O<sub>3</sub>.<sup>6</sup> When the solution was acidic (pH = 0.3), the TOF of CO oxidation was 0.15 s<sup>-1</sup>, which is close to that measured at neutral conditions. However, when the solution was basic (pH = 14), the TOF increased by an order of magnitude to 1.8 s<sup>-1</sup>. Likewise, the TOF's of CO oxidation over Au nanoparticles on two different carbon supports were 5.3 s<sup>-1</sup> and 5.4 s<sup>-1</sup> at a pH of 14, which were an order of magnitude greater than those measured at acidic conditions. Evidently, the role of support was negligible compared to the role of solution pH. The availability of OH<sup>-</sup> in solution greatly accelerated the rate of CO oxidation.

The TOF for aqueous-phase CO oxidation over Au/TiO<sub>2</sub> at high pH (1.8 s<sup>-1</sup> at 300 K) was within a factor of two of the intrinsic turnover rate of CO oxidation over Au/TiO<sub>2</sub> evaluated by

isotopic transient analysis in the vapor phase ( $3.1 \text{ s}^{-1}$  at 293 K). The comparison of the TOF in aqueous solution to the intrinsic TOF in the vapor phase evaluated by SSITKA can be reconciled by assuming all available surface gold sites can adsorb a hydroxyl from solution, while in the vapor phase reaction, water activation to form an adsorbed hydroxyl is promoted only at the gold-oxide interface.

Alcohol oxidation to an acid with molecular oxygen as the oxidant at basic conditions can also be catalyzed by supported gold nanoparticles. Gold particles supported on carbon and alumina were demonstrated to be highly active for liquid phase alcohol oxidation at basic conditions,<sup>18</sup> but were relatively inactive at neutral to acidic conditions at 333 K.<sup>19</sup> Alcohol oxidation over Au occurs at acidic conditions at elevated temperatures ( $> 373 \text{ K}$ ), but the rates were orders of magnitude lower than that at basic conditions. Ketchie et al. also investigated the oxidation of glycerol, a three carbon polyol, at a basic pH, which reacts according to Figure D.1.<sup>17,20</sup> The TOF of glycerol oxidation over Au/TiO<sub>2</sub> at 308 K was  $1.7 \text{ s}^{-1}$  and is quite similar to the TOF of  $1.8 \text{ s}^{-1}$  measured at 300 K for aqueous-phase CO oxidation under basic conditions. It should be emphasized that basic solution alone is not adequate to oxidize alcohols or CO over Au, since neither reaction proceeds without O<sub>2</sub>.



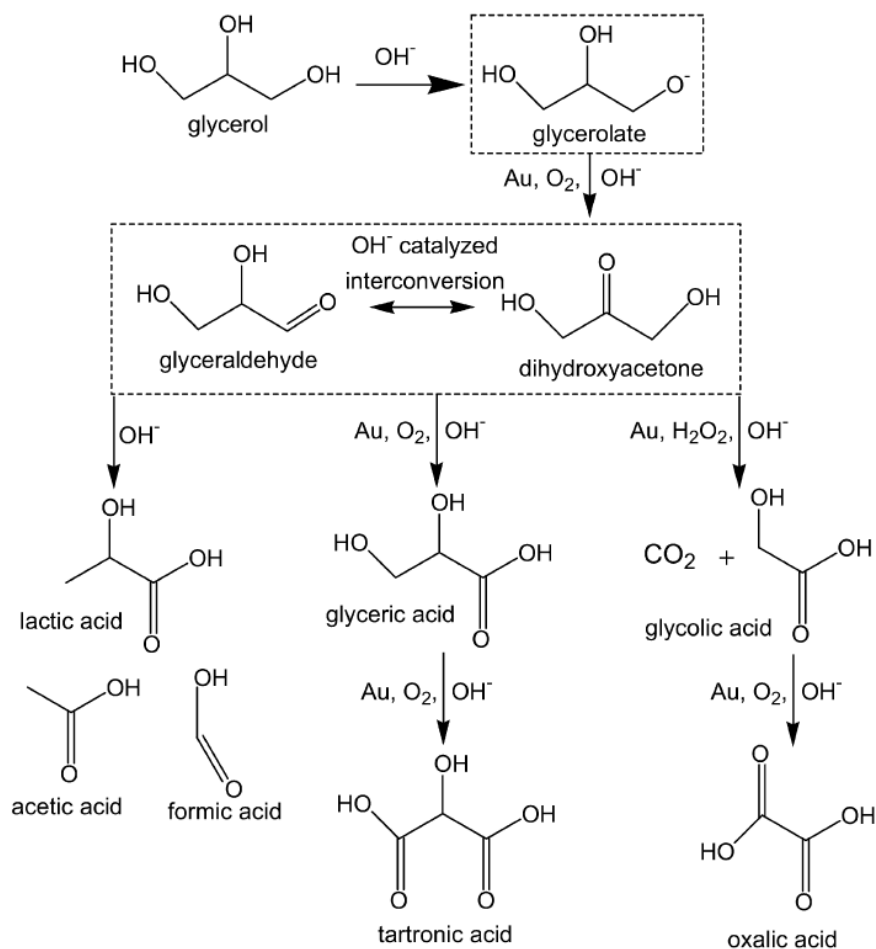


**Figure D.1.** Reaction network for the aqueous-phase oxidation of glycerol over Au catalysts at basic conditions. Proposed intermediates are shown in dotted boxes. Reproduced with permission from ref 20. Copyright 2007 Elsevier Inc.

Whereas small gold nanoparticles are needed to produce an active catalysts for gas phase CO oxidation,<sup>3</sup> the influence of gold particle size on aqueous phase glycerol oxidation at high pH was less significant.<sup>21</sup> The TOF of 5 nm Au particles supported on carbon for CO oxidation was  $5.4 \text{ s}^{-1}$  at a pH of 14, while 45 nm Au nanoparticles on carbon had a TOF an entire magnitude lower at  $0.48 \text{ s}^{-1}$  and even gold powder in solution had a TOF of  $0.36 \text{ s}^{-1}$  at 300 K. Similarly, over dispersed Au/C the TOF of glycerol oxidation was  $17 \text{ s}^{-1}$  and over 20 nm and 45 nm gold nanoparticles on carbon the TOF was  $2.3 \text{ s}^{-1}$  and  $2.2 \text{ s}^{-1}$ , respectively, at 333 K. Even the gold powder in solution had a TOF of  $2.5 \text{ s}^{-1}$ , suggesting that large Au particles ( $> 20 \text{ nm}$ ) behave

similarly to bulk gold. While the rates of CO oxidation and alcohol oxidation appear to moderately depend on particle size, both oxidation reactions require the presence of a basic solution and dioxygen to achieve high rates of reaction in the liquid phase. The hydroxyl group appears to play an important role in the reaction mechanism for both oxidation reactions over gold catalysts.

## **Mechanism of selective oxidation over gold catalysts**

The similar turnover rate for CO and alcohol oxidation over gold supported catalysts based on the total number of surface gold atoms is not likely a coincidence, but is suggestive of common elements in the reaction mechanisms. As mentioned above, hydroxide ions and dioxygen are both required for lower temperature alcohol oxidation in aqueous solution over supported gold. To explore the mechanism of the reaction, isotopic-labeling experiments were performed with glycerol, ethanol, and 5-hydroxymethylfurfural over supported gold catalysts at high pH to determine the source of oxygen inserted into the acid product. When  $^{18}\text{O}_2$  was used as the oxidant for glycerol oxidation in  $\text{H}_2^{16}\text{O}$  solution over Au/C and Au/TiO<sub>2</sub> at 333 K and high pH, no  $^{18}\text{O}$  was observed in the glyceric acid product.<sup>22</sup> Identical experiments carried out over Pt/C and Pd/C catalysts also failed to observe  $^{18}\text{O}$  in the glyceric acid product. In contrast, when  $\text{H}_2^{18}\text{O}$  was used for glycerol oxidation over both Au/C and Au/TiO<sub>2</sub>, up to four  $^{18}\text{O}$  atoms were incorporated into the glyceric acid product. Additional experiments with ethanol oxidation to acetic acid and 5-hydroxymethylfurfural oxidation to 2,5-furandicarboxylic acid over supported gold catalysts also confirmed that oxygen atoms incorporated into the acid products originated exclusively from the water solvent.<sup>16,23</sup>

Although dioxygen was not the source of the oxygen atoms that were incorporated into the acid products, molecular oxygen was required for all of the above-mentioned reactions to

proceed. Kinetic studies revealed that at high enough oxygen pressures ( $> 5$  atm), the rate of 5-hydroxymethylfurfural oxidation over Au/TiO<sub>2</sub> at 295 K was fairly independent of O<sub>2</sub> pressure.<sup>24</sup> To explain the isotopic labeling results during alcohol oxidation, Zope et al. proposed that O<sub>2</sub> played an indirect role in the mechanism by removing electrons from the metal surface generated by alcohol oxidation.<sup>22</sup> The evidence of hydrogen peroxide formation in solution suggests that O<sub>2</sub> is sequentially reduced to a peroxide intermediate and eventually to hydroxide. Thus, O<sub>2</sub> closes the catalytic cycle by serving as an electron scavenger and regenerating hydroxide ions that are consumed in the reaction to produce aldehyde intermediates and acid products. Further work by Zope et al. supports this reaction sequence because the number of OH<sup>-</sup> moles consumed per mole of glycerol oxidized to glyceric acid over Au/TiO<sub>2</sub> was about two, whereas consumption of 4 OH<sup>-</sup> moles is predicted by the electrochemical balance.<sup>25</sup> Evidently, partial regeneration of hydroxide via the reduction of molecular oxygen accounts for the difference.

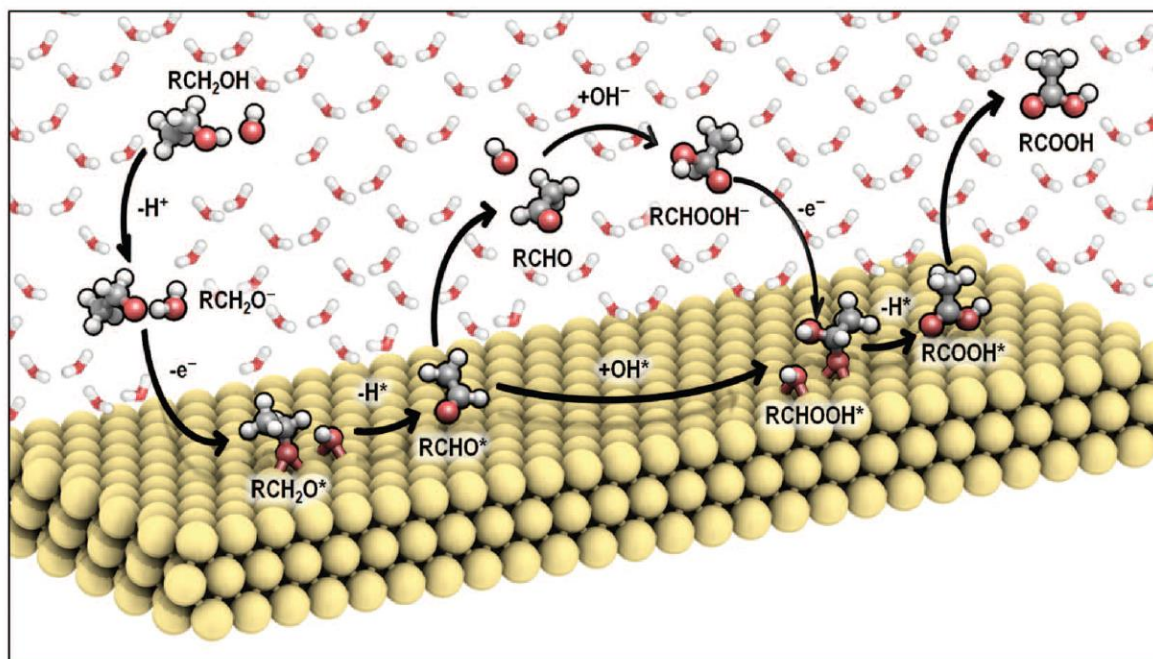


**Figure D.2.** Reaction scheme for the aqueous-phase oxidation of an alcohol to an acid over Au at basic conditions. Reproduced with permission from ref 22. Copyright 2010 Science.

Supporting evidence from density functional theory (DFT) calculations for ethanol oxidation on Au not only confirms that the reduction of dioxygen to hydroxide is energetically feasible, but also suggests an alcohol reaction mechanism over gold, as shown in Figure D.2. The DFT calculations (Table D.1) for the deprotonation of ethanol to form an adsorbed alkoxide on Au(111) in water solvent showed that the presence of a co-adsorbed hydroxide on the surface lowered the activation barrier by an order of magnitude to  $22 \text{ kJ mol}^{-1}$  compared to that associated with a bare gold surface ( $204 \text{ kJ mol}^{-1}$ ).<sup>22</sup> A co-adsorbed hydroxide on the gold surface acts as a Brønsted base to assist in the deprotonation of ethanol to form the adsorbed alkoxide. Another co-adsorbed hydroxide on the gold surface can also participate in the subsequent C-H activation of the adsorbed alkoxide to produce an adsorbed aldehyde, with an activation barrier of  $12 \text{ kJ mol}^{-1}$  compared to the bare surface with a barrier of  $46 \text{ kJ mol}^{-1}$ . Once an aldehyde is formed from the alcohol, subsequent base-catalyzed formation of a gem-diol and

dehydrogenation results in the formation of an acid product. Thus, the hydroxide is involved in alcohol deprotonation, dehydrogenation to the aldehyde, hydration of the aldehyde, and dehydrogenation of the diol to the acid. The critical role of O<sub>2</sub> is to remove the electrons that must be deposited into the metal throughout the oxidation of alcohol, thus partially regenerating hydroxide.

It should be noted that supported Au catalysts for glycerol oxidation in high pH solution slowly deactivate.<sup>26</sup> Although carboxylic acids do not strongly compete with the substrate, products of secondary reactions that produce ketones or enones adsorb strongly to the Au surface.

**Table D.1.** DFT results for reaction energies (kJ mol<sup>-1</sup>) and activation energies (kJ mol<sup>-1</sup>) for the oxidation of ethanol and reduction of oxygen on Au(111) in a water solvent.<sup>22</sup>

Reaction	Au(111) w/ H <sub>2</sub> O	
	$\Delta H_{\text{RXN}}$	$E_{\text{ACT}}$
CH <sub>3</sub> CH <sub>2</sub> OH* + * → CH <sub>3</sub> CH <sub>2</sub> O* + H*	196	204
CH <sub>3</sub> CH <sub>2</sub> OH* + OH* → CH <sub>3</sub> CH <sub>2</sub> O* + H <sub>2</sub> O*	13	22
CH <sub>3</sub> CH <sub>2</sub> O* + * → CH <sub>3</sub> CHO* + H*	-40	46
CH <sub>3</sub> CH <sub>2</sub> O* + OH* → CH <sub>3</sub> CHO* + H <sub>2</sub> O*	-222	12
CH <sub>3</sub> CHO* + OH* → CH <sub>3</sub> CH(OH)O* + *	-33	5
CH <sub>3</sub> CH(OH)O* + * → CH <sub>3</sub> COOH* + H*	-151	21
OH* + H* → H <sub>2</sub> O* + *	-183	39
O <sub>2</sub> * + * → O* + O*	41	105
O <sub>2</sub> * + H* → OOH* + *	-161	25
O <sub>2</sub> * + H <sub>2</sub> O* → OOH* + OH*	-4	16
OOH* + H* → HOOH* + *	-146	19
OOH* + H <sub>2</sub> O* → HOOH* + OH*	37	48
HOOH* + * → OH* + OH*	-86	71

A kinetic model for CO oxidation also suggests that the role of hydroxide is vital to the mechanism. Figure D.3 illustrates a suggested reaction path for CO oxidation over gold supported catalysts as proposed by Kung et al. involving a cationic gold species.<sup>27</sup> The importance of water is highlighted because an initial hydroxide on a cationic gold species in close proximity to the support reacts with weakly adsorbed carbon monoxide on a neighboring

gold atom. The reaction forms a hydroxycarbonyl that eventually decomposes to the products  $\text{CO}_2$  and  $\text{OH}$ . For vapor phase  $\text{CO}$  oxidation with  $\text{Au}$ , the origin of the adsorbed hydroxide and involvement of  $\text{H}_2\text{O}$  and  $\text{O}_2$  in the reaction mechanism has been further investigated by kinetic modeling and isotopic labeling studies.

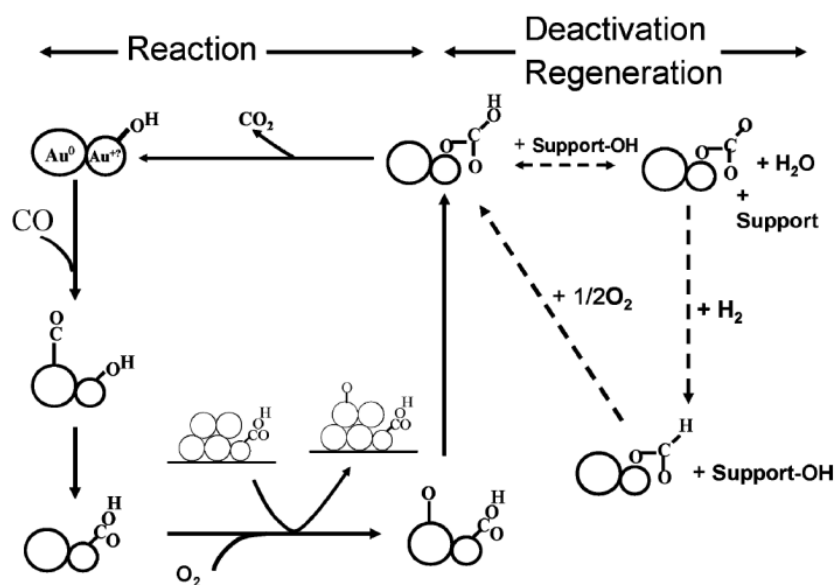


**Figure D.3.** Proposed reaction and regeneration/deactivation pathway for  $\text{CO}$  oxidation involving cationic gold. Reproduced with permission from ref 27. Copyright 2007 American Chemical Society.

A detailed kinetic study of  $\text{CO}$  oxidation in the presence of water was undertaken by Ojeda and Iglesia over  $\text{Au}/\text{Al}_2\text{O}_3$  at room temperature in an attempt to further elucidate the mechanism.<sup>28</sup> One kinetic model that fit their experimental observations involved an equilibrium reaction between dioxygen and water to produce adsorbed hydroxide and a hydroperoxy ( $\text{OOH}$ ) species. The peroxide can then react with  $\text{CO}$  to produce  $\text{CO}_2$  and  $\text{OH}$  in a kinetically-relevant step. An isotopic study comparing  $\text{H}_2\text{O}$  and  $\text{D}_2\text{O}$  measured a kinetic isotope effect of 1.21 at room temperature, which is a relatively small effect. Evidently, activation of the  $\text{O-H}$  bond was not kinetically-relevant. Since exchange between  $^{16}\text{O}_2$  and  $^{18}\text{O}_2$  and between  $\text{H}_2^{18}\text{O}$  and  $^{16}\text{O}_2$  was

not observed over the Au/Al<sub>2</sub>O<sub>3</sub> catalyst at 300 K, the researchers concluded that the direct dissociation of O<sub>2</sub> was not involved in the mechanism of CO oxidation.<sup>28</sup>

Surface science experiments performed by Kim et al. for CO oxidation on Au(111) at 77 K determined that there was exchange of atomic oxygen in the presence of co-adsorbed water.<sup>29</sup> More specifically, when a Au surface that was pre-covered in <sup>16</sup>O and H<sub>2</sub><sup>18</sup>O was exposed to CO, both CO<sup>16</sup>O and CO<sup>18</sup>O were produced. While slightly more CO<sup>18</sup>O was produced, the authors also showed scrambling between the atomic oxygen and water, complicating the final analysis. Apparently, if there is a mechanism for the production of atomic oxygen on Au, the resulting oxygen is reactive with both CO and H<sub>2</sub>O. However, Schubert et al. determined that for CO oxidation with <sup>18</sup>O<sub>2</sub> over an iron oxide supported gold catalyst that only CO<sup>18</sup>O was observed.<sup>30-</sup>

31

In summary, the adsorbed hydroxide appears to participate in the fast reaction path for CO oxidation. Thus, one might suspect that supported gold catalysts modified with alkali metals might also promote the rate of CO oxidation. Qian et al. showed that the addition of NaOH to a Au/SiO<sub>2</sub> catalyst improved its catalytic oxidation activity.<sup>32</sup> While the Au/SiO<sub>2</sub> catalyst was inert at room temperature, the addition of a 6 to 1 sodium to gold molar ratio increased the rate of gas phase CO oxidation to 0.0866 mol g<sup>-1</sup> h<sup>-1</sup> without the presence of added water. Similarly, Gluhio et al. observed that the addition of Rb<sub>2</sub>O and BaO to a Au/Al<sub>2</sub>O<sub>3</sub> catalyst decreased the temperature that achieved 95% conversion of CO from 385 K to 351 K and 298 K, respectively, at dry conditions.<sup>33</sup> The recent patent literature also contains a few examples of base promotion of CO oxidation by gold supported catalysts. For example, Brey et al. determined that the addition of Ba(NO<sub>3</sub>)<sub>2</sub> to a Au/Al<sub>2</sub>O<sub>3</sub> increased the amount of CO converted from 800 ppm to 1500 ppm at 85% relative humidity and room temperature.<sup>34</sup> Similarly, Brady et al. determined

that the addition of KOH to a Au/TiO<sub>2</sub> catalyst slightly increased CO conversion at 90% relative humidity and approximately 303 K.<sup>35</sup>

## **Analogy to electrochemistry**

Electro-catalysis simply divides the oxidation and reduction reactions into two different reaction zones, whereas both reactions happen simultaneously at the same location in heterogeneous catalysis. For example, in electrocatalysis, oxidation of substrates such as H<sub>2</sub>, CO, or alcohols generates electrons at the anode, whereas reduction of O<sub>2</sub> consumes the electrons at the cathode. For heterogeneous catalysis by gold nanoparticles, the oxidation of substrate and reduction of O<sub>2</sub> occur on a single gold particle. Whereas the electrical potential in an electrochemical cell provides the major driving force for reaction, the chemical potential is important in catalysis. The analogy between electrochemical oxidation and catalytic oxidation is quite informative and has been reviewed recently by Wieckowski and Neurock.<sup>36</sup> The implications of the electrochemical analogy for CO oxidation and alcohol oxidation are discussed briefly below.

The electro-catalytic oxidation of CO over Au electrodes is thought to proceed similarly to that of the vapor and liquid phase catalytic oxidation. Figure D.4 shows the reaction scheme for catalytic CO oxidation in basic aqueous solution on a bulk Au(111) surface.<sup>36</sup> The reaction proceeds via the coupling of adsorbed CO and OH species whereby the cleavage of the formed adsorbed bicarbonate produces CO<sub>2</sub> and H<sub>3</sub>O<sup>+</sup>. The reaction pathway depicted in Figure 4 has been shown to be energetically reasonable by DFT theory calculations with an overall reaction energy of -231 kJ mol<sup>-1</sup>.<sup>36</sup> While CO oxidation can proceed in acidic media, higher potentials are required to produce adsorbed hydroxide on the gold surface and the rate of oxidation is much greater in alkaline media. Hayden et al. observed that small Au particles supported on a TiO<sub>x</sub>



electrode oxidized CO to CO<sub>2</sub> at much lower potentials than a polycrystalline Au electrode suggesting a strong influence of gold particle size on the rate of reaction, which is consistent with results in gas phase CO oxidation over Au/TiO<sub>2</sub>.<sup>37</sup>

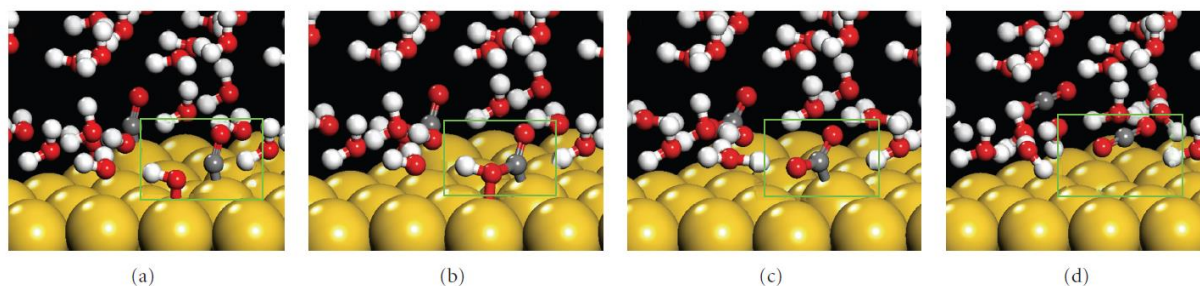


**Figure D.4.** DFT calculations for the reaction coordination of CO oxidation. The reaction scheme is (a) adsorption of CO\* and OH\*, (b) nucleophilic addition of OH\* to CO\* to form COOH\*\*, (c) cleavage of O-H bond, and (d) formation of CO<sub>2</sub> and H<sub>3</sub>O<sup>+</sup>. Reproduced with permission from ref 36.

Similar to the electro-oxidation of CO over Au, oxidation of alcohols occurs in acidic media but requires very high potentials to generate adsorbed hydroxyl on the surface and the rate is greatly enhanced in alkaline conditions. The mechanism of alcohol electro-oxidation is believed to proceed either by a four or six electron process. For example, the four electron path for alcohol electro-oxidation is selective to the acid product whereas the six electron path over-oxidizes the alcohol to produce CO and CO<sub>2</sub>. Although the latter path is desired for maximum production of electrons in a fuel cell, it is difficult to completely oxidize ethanol and larger alcohols because of the high activation barrier of C-C bond breaking over Au.<sup>38</sup> The mechanism for selective electrochemical oxidation of ethanol to acetic acid involves activation of the O-H and C-H bonds by adsorbed hydroxide on the gold surface, which is identical to that proposed for the selective catalytic oxidation of ethanol.

Kwon et al. studied the electro-oxidation of glycerol and other alcohols in basic solution and proposed that a significant portion of the chemistry was carried out in the alkaline solution.<sup>39</sup>

They suggest that the initial deprotonation of glycerol (or other alcohols) was base-catalyzed, but the subsequent dehydrogenation of the alkoxide to form glyceraldehyde occurred on the Au electrode. The researchers then argued that the final products of selective glycerol oxidation were primarily those resulting from the decomposition of glyceraldehyde in basic solution, without the need for the Au. It should be noted that glyceraldehyde decomposition at high pH also produced lactic acid and glyceraldehyde dimers, which are not frequently observed in the presence of a gold catalyst.

Although gold is generally inert toward  $O_2$ , it becomes an active electrode for the  $O_2$  reduction reaction (ORR) in alkaline media.<sup>40</sup> The reduction of molecular oxygen in water by four electrons generates four hydroxide ions, similar to that suggested for the mechanism of dioxygen reduction during Au-catalyzed selective oxidation of alcohols, as discussed above. The incomplete electro-reduction of dioxygen at acidic conditions on Au electrodes produces a peroxide intermediate, which explains why small quantities of peroxide were observed during catalytic alcohol oxidation reactions over gold.<sup>41</sup> Ab initio quantum chemical calculations show that the reaction of molecular oxygen and water as well as the reduction of OOH is energetically feasible on Au(111) surface.<sup>38</sup>

These examples illustrate the useful analogy between selective oxidation reactions on supported Au nanoparticles and electro-oxidation reactions on Au electrodes. In both cases, the role of hydroxyl is critical for rapid oxidation rates on Au surface at modest temperatures.

## **Conclusions and outlook**

In conclusion, the important mechanistic role that adsorbed hydroxyl plays in the catalysis by gold nanoparticles for both CO and alcohol oxidation with molecular oxygen and water has been described. The intrinsic turnover frequency of gas phase CO oxidation over titania supported

gold nanoparticles determined by an isotopic transient method was similar to both CO and glycerol oxidation rates in aqueous solution. Evidently, the role of the hydroxyl is important for oxidizing both substrates, whereby during alcohol oxidation an adsorbed hydroxyl activates C-H and O-H bonds, while during CO oxidation the adsorbed hydroxyl can directly add to CO to form COOH, which decomposes to CO<sub>2</sub>. The observed particle size dependence for gas-phase oxidation reactions over gold nanoparticles is most likely related to the optimum number of metal-support interfacial atoms that allow interactions with support hydroxyl groups. If hydroxyl groups are supplied through the solution medium, the metal-support interface is much less important so that even bulk gold becomes an active catalyst. Since selective oxidation reactions in the liquid phase can also be performed in an electrochemical cell, results from electrochemistry have provided important mechanistic insights on the role of hydroxyl. As the demand by the chemical community for environmentally-benign reaction conditions and so called “green” solvents increases, researchers must pay careful attention to water as an active participant in catalysis.

## Acknowledgements

This material is based upon work supported by the National Science Foundation under Award Nos. EEC-0813570 and OISE 0730277. Helpful discussions with Professor Matthew Neurock are also acknowledged.

## References

1. Haruta, M.; Yamada, N.; Kobayashi, T.; Iijima S. Gold Catalysts Prepared by Coprecipitation for Low-Temperature Oxidation of Hydrogen and Carbon Monoxide. *J. Catal.* **1989**, *115*, 301-309.
2. Haruta, M.; Yamada, N.; Sano, H.; Yamada, N. Novel Gold Catalysts for the Oxidation of Carbon Monoxide at a Temperature far Below 0 °C. *Chem. Lett.* **1987**, *16*, 405-408.

3. Haruta, M.; Tsubota, S.; Kobayashi, T.; Kageyama, H.; Genet, M.J.; Delmon, B. Low-Temperature Oxidation of CO over Gold Supported on TiO<sub>2</sub>, α-Fe<sub>2</sub>O<sub>3</sub>, and CO<sub>3</sub>O<sub>4</sub>. *J. Catal.* **1993**, *144*, 175-192.
4. Daté, M.; Haruta, M. Moisture Effect on CO Oxidation over Au/TiO<sub>2</sub> Catalyst. *J. Catal.* **2001**, *201*, 221-224.
5. Cunningham, D. A. H.; Vogel, W.; Haruta, M. Negative Activation Energies in CO Oxidation over an Icosahedral Au/Mg(OH)<sub>2</sub> Catalyst. *Catal. Lett.* **1999**, *63*, 43-47.
6. Calla, J. T.; Davis, R. J. Influence of Dihydrogen and Water Vapor on the Kinetics of CO Oxidation over Au/Al<sub>2</sub>O<sub>3</sub>. *Ind. Eng. Chem. Res.* **2005**, *44*, 5403-5410.
7. Daté, M.; Okumura, M.; Tsubota, S.; Haruta, M. Vital Role of Moisture in the Catalytic Activity of Supported Gold Nanoparticles. *Angew. Chem. Int. Ed.* **2004**, *43*, 2129-2132.
8. Park E. D.; Lee J. S. Effects of Pretreatment Conditions on CO Oxidation over Supported Au Catalysts. *J. Catal.* **1999**, *186*, 1-11.
9. Costello, C. K.; Kung, M. C.; Oh, H. S.; Wang, Y.; Kung, H. H. Nature of the Active Site for CO Oxidation on Highly Active Au/γ-Al<sub>2</sub>O<sub>3</sub>. *Appl. Catal. A-Gen.* **2002**, *232*, 159-168.
10. Costello, C. K.; Yang, J. H.; Law, H.Y.; Wang, Y.; Lin, J. N.; Marks, L.D.; Kung, M.C.; Kung, H.H. On the Potential Role of Hydroxyl Groups in CO Oxidation over Au/Al<sub>2</sub>O<sub>3</sub>. *Appl. Catal. A-Gen.* **2003**, *242*, 15-24.
11. Kung, H. H.; Kung, M. C.; Costello, C. K. Supported Au Catalysts for Low Temperature CO Oxidation. *J. Catal.* **2003**, *216*, 425-432.
12. Calla, J. T.; Davis, R. J. X-ray Absorption Spectroscopy and CO Oxidation Activity of Au/Al<sub>2</sub>O<sub>3</sub> Treated with NaCN. *Catal. Lett.* **2005**, *99*, 21-26.
13. Calla, J. T.; Davis, R. J. Investigation of Alumina-Supported Au Catalyst for CO Oxidation by Isotopic Transient Analysis and X-ray Absorption Spectroscopy. *J. Phys. Chem.* **2005**, *109*, 2307-2314.
14. Calla, J. T.; Bore, M. T.; Datye, A. K.; Davis, R. J. Effect of Alumina and Titania on the Oxidation of CO over Au Nanoparticles Evaluated by <sup>13</sup>C Isotopic Transient Analysis. *J. Catal.* **2006**, *238*, 458-467.
15. Call, J. T.; Davis, R. J. Oxygen-Exchange Reactions During CO Oxidation over Titania- and Alumina-Supported Au Nanoparticles. *J. Catal.* **2006**, *241*, 407-416.
16. Sanchez-Castillo, M. A.; Couto, C.; Kim, W. B.; Dumesic, J. A. Gold-Nanotube Membranes for the Oxidation of CO at Gas-Water Interfaces. *Angew. Chem. Int. Ed.* **2004**, *43*, 1140-1142.

17. Ketchie, W. C.; Murayama, M.; Davis, R. J. Promotional Effect of Hydroxyl on the Aqueous Phase Oxidation of Carbon Monoxide and Glycerol over Supported Au Catalysts. *Top. Catal.* **2007**, *44*, 307-317.
18. Prati, L.; Rossi, M. Gold on Carbon as a New Catalyst for Selective Liquid Phase Oxidation of Diols. *J. Catal.* **1998**, *176*, 552-560.
19. Carrettin, S.; McMorn, P.; Johnston, P.; Griffin, K.; Hutchings, G. J. Selective Oxidation of Glycerol to Glyceric Acid using a Gold Catalyst in Aqueous Sodium Hydroxide. *Chem. Comm.* **2002**, 696-697.
20. Ketchie, W. C.; Murayama, M.; Davis, R. J. Selective Oxidation of Glycerol over Carbon-Supported AuPd Catalysts. *J. Catal.* **2007**, *250*, 264-273.
21. Ketchie, W. C.; Fang, Y.; Wong, M.; Murayama, M.; Davis, R. J. Influence of Gold Particle Size on the Aqueous-Phase Oxidation of Carbon Monoxide and Glycerol. *J. Catal.* **2007**, *250*, 94-101.
22. Zope, B. N.; Hibbitts, D. D.; Neurock, M.; Davis, R. J. Reactivity of the Gold/Water Interface During Selective Oxidation Catalysis. *Science*. **2010**, *330*, 74-78.
23. Davis, S. E.; Zope, B. N.; Davis, R. J. On the Mechanism of Selective Oxidation of 5-Hydroxymethylfurfural to 2,5-Furandicarboxylic Acid over Supported Pt and Au Catalysts. *Green Chem.* **2012**, *14*, 143-147.
24. Davis, S. E.; Houk, L. R.; Tamargo, E. C.; Datsy, A. K.; Davis, R. J. Oxidation of 5-Hydroxymethylfurfural over Supported Pt, Pd and Au Catalysts. *Catal. Today*. **2011**, *160*, 55-60.
25. Zope, B. N.; Davis, S. E.; Davis, R. J. Influence of Reaction Conditions on Diacid Formation During Au-Catalyzed Oxidation of Glycerol and Hydroxymethylfurfural. *Top. Catal.* **2012**, *55*, 24-32.
26. Zope, B. N.; Davis, R. J. Inhibition of Gold and Platinum Catalysts by Reactive Intermediates Produced in the Selective Oxidation of Alcohols in Liquid Water. *Green Chem.* **2011**, *13*, 3484-3491.
27. Kung, M. C.; Davis, R. J.; Kung, H. H. Understanding Au-Catalyzed Low-Temperature CO Oxidation. *J. Phys. Chem. C* **2007**, *111*, 11767-11775.
28. Ojeda, M.; Zhan, B.; Iglesia, E. Mechanistic Interpretation of CO Oxidation Turnover Rates on Supported Au Clusters. *J. Catal.* **2012**, *285*, 92-102.
29. Kim, T. S.; Gong, J.; Ojifinni, R. A.; White, J. M.; Mullins, C. B. Water Activated by Atomic Oxygen on Au(111) to Oxidize CO at Low Temperatures. *J. Am. Chem. Soc.* **2006**, *128*, 6282-6283.

30. Schubert, M. M.; Hackenberg, S.; van Veen, A. C.; Muhler, M.; Plzak, V.; Behm, R. J. CO Oxidation over Supported Gold Catalysts—"Inert" and "Active" Support Materials and Their Role for the Oxygen Supply During Reaction. *J. Catal.* **2001**, *197*, 113-122.
31. Schubert, M. M.; Venugopal, A.; Kahlich, M. J.; Plzak, V.; Behm, R. J. Influence of H<sub>2</sub>O and CO<sub>2</sub> on the Selective CO Oxidation in H<sub>2</sub>-Rich Gases over Au/ $\alpha$ -Fe<sub>2</sub>O<sub>3</sub>. *J. Catal.* **2004**, *222*, 32-40.
32. Qian, K.; Zhang, W.; Sun, H.; Fang, J.; He, B.; Ma, Y.; Jiang, Z.; Wei, S.; Yang, J.; Huang, W. Hydroxyls-Induced Oxygen Activation on "Inert" Au Nanoparticles for Low-Temperature CO Oxidation. *J. Catal.* **2011**, *277*, 95-103.
33. Gluhio, A. C.; Tang, X.; Marginean, P.; Nieuwenhus, B. E. Characterization and Catalytic Activity of Unpromoted and Alkali(earth)-Promoted Au/Al<sub>2</sub>O<sub>3</sub> Catalysts for Low-Temperature CO Oxidation. *Top. Catal.* **2006**, *39*, 101-110.
34. Brey, L. A.; Wood, T. E.; Buccellato, G. M.; Jones, M. E.; Chamberlain, C. S.; Siedle, A. R. Catalysts, Activating Agents, Support Media, and Related Methodologies Useful for Making Catalyst Systems Especially When the Catalyst is Deposited onto the Support Media Using Physical Vapor Deposition. U.S. Patent 8,314,048, Nov. 20, 2012.
35. Brady, J. T.; Jones, M. E.; Brey, L. A.; Buccellato, G. M.; Chamberlain, C. S.; Huberty, J. S.; Siedle, A. R.; Wood, T. E.; Veeraraghavan, B.; Fansler, D. D. Heterogeneous, Composite, Carbonaceous Catalyst System and Methods that use Catalytically Active Gold. U.S. Patent 8,058,202, Nov. 15, 2011.
36. Wieckowski, A.; Neurock, M. Contrast and Synergy between Electrocatalysis and Heterogeneous Catalysis. *Adv. Phys. Chem.* **2011**, *2011*, 907129.
37. Hayden, B. E.; Pletcher, D.; Suschland, J. P. Enhanced Activity for Electrocatalytic Oxidation of Carbon Monoxide on Titania-Supported Gold Nanoparticles. *Angew. Chem. Int. Ed.* **2007**, *46*, 3530-3532.
38. Lai, S. C. S.; Kleijn, S. E. F.; Ozturk, F. T. Z.; van Rees Vellinga, V. C.; Koning, J.; Rodriguez, P.; Koper, M. T. M. Effects of Electrolyte pH and Composition on the Ethanol Electro-Oxidation Reaction. *Catal. Today* **2010**, *154*, 92-104.
39. Kwon, Y.; Lai, S. C. S.; Rodriguez, P.; Koper, M. T. M. Electrocatalytic Oxidation of Alcohols on Gold in Alkaline Media: Base or Gold Catalysis? *J. Am. Chem. Soc.* **2011**, *133*, 69114-6917.
40. Braunschweig, B.; Hibbitts, D.; Neurock, M.; Wieckowski, A. Electrocatalysis: A Direct Alcohol Fuel Cell and Surface Science Perspective. *Catal. Today* **2013**, *202*, 197-209.
41. Yeager, E. Electrocatalysts for O<sub>2</sub> Reduction. *Electrochim. Acta* **1984**, *29*, 1527-1537.

## Appendix E: Effect of Oxygen Pressure

### TOF of 1,6-Hexanediol at Low Oxygen Pressure

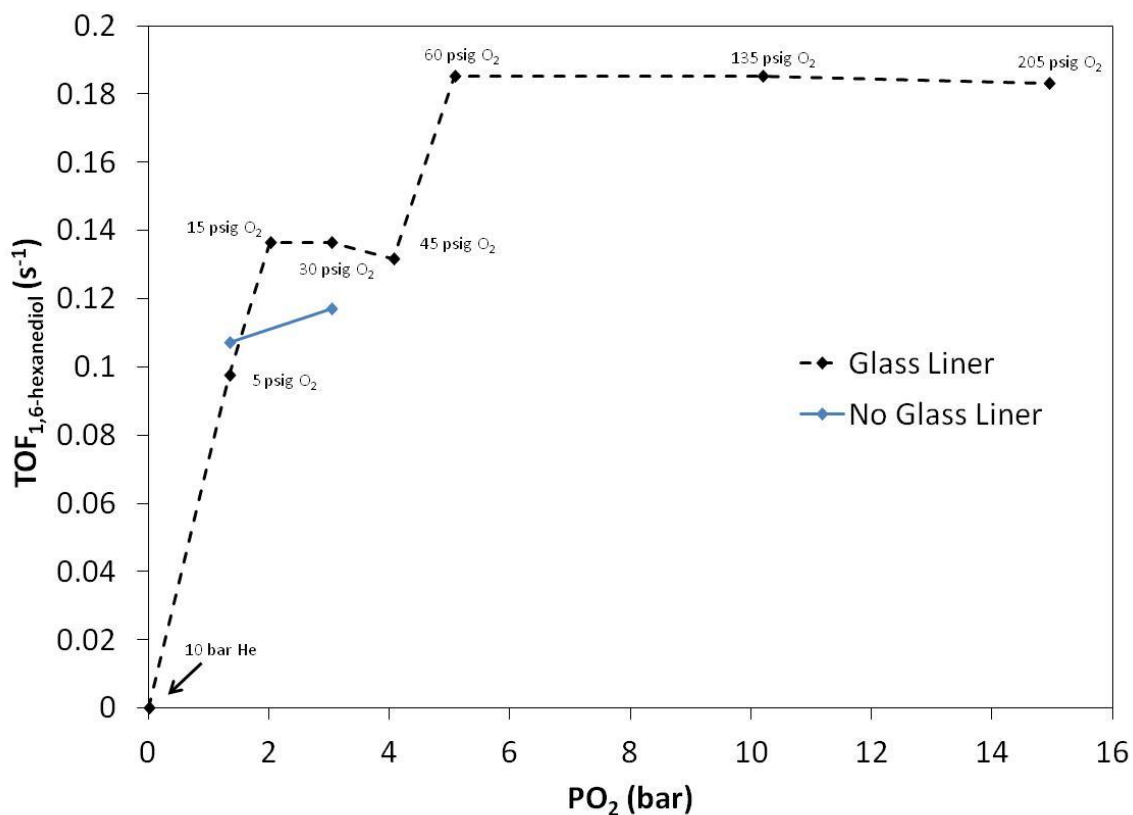


**Figure E.1.** TOF of 1,6-hexanediol oxidation at low oxygen pressure.